2022

# Decentralized Digital Fabrication of Flexible Micro/Nano Devices Using a Laserjet Printer

Arshya Bamshad
*University of Central Florida*

# DECENTRALIZED DIGITAL FABRICATION OF FLEXIBLE MICRO/NANO DEVICES USING A LASERJET PRINTER

by

ARSHYA BAMSHAD

B.Sc. Islamic Azad University Central Tehran Branch, 2012
M.Sc. University of Tehran, 2015

A dissertation submitted in partial fulfillment of the requirements
for the degree of Doctor of Philosophy
in the Department of Mechanical and Aerospace Engineering
in the College of Engineering and Computer Science
at the University of Central Florida
Orlando, Florida

Spring Term
2022

Major Professor: Hyoung Jin Cho

# ABSTRACT

The fabrication of traditional micro/nano devices requires access to cleanrooms, complex and expensive tools, and highly-skilled labor. A facile and digital do-it-yourself (DIY) technique for the fabrication of low-cost devices on flexible substrates (paper, cloth, and plastic films) is presented in this work. A set of office-grade equipment (i.e., laserjet printer, thermal laminator, computer-aided paper cutter), and commercially available supplies (i.e., baking wax paper, furniture restoration metal-leaf) are utilized. The presented technology enables community-embedded production by removing a high technological barrier. The validity of the proposed technology was proved by designing three levels of experiments, i.e., patterns, devices, and systems. The performance was evaluated at each level to cover various application domains in environmental monitoring and biomedical diagnostics utilizing conductometric, colorimetric, biochemical, and chemoresistive detection principles. Devices with features of varying sizes, from nanometers to centimeters, were fabricated and characterized. Expanding the concept further, a copper oxide (CuO) nano-sorbent cloth-based filter was designed, fabricated, and tested to demonstrate the application in the fabrication of a water filtration system. An inexpensive and robust filtration system for real-time arsenic removal from polluted water, which could easily be embedded into the existing water pipes, showed the effective removal rate without requiring any power source for operation. To demonstrate the pervasiveness of the laserjet printing-based fabrication, a novel print-and-release method to produce color-tagged microplastics was presented. A lack of reliable methods to replicate the microplastic samples is one of the main challenges in the design of experiments for systematic studies. The newly developed fabrication techniques in this

work provide an alternative route to decentralized production of low-cost flexible sensors and functional devices, with minimal steps, time, cost, and facilities. The operation of such devices is simple and can be further empowered by ubiquitous smartphones for data analysis and transmission.

To my family.

# ACKNOWLEDGMENTS

I am grateful to all who supported me in accomplishing my research to complete this dissertation. I would like to begin by expressing my greatest appreciation to my Ph.D. advisor, Prof. Hyoung Jin Cho, for giving me this opportunity to pursue my doctorate program under his supervision, to grow as a researcher, and to expand my knowledge. The experience that I have earned in his laboratory will guide me for many years and I am extremely appreciative of the guidance and mentorship that I have received. He was more than an advisor to me, and ever since I began my doctorate program, he has provided invaluable assistance and support to me, and I feel lucky to be among his students. I hope our scientific collaborations will continue throughout my career.

I would also like to express my gratitude to the rest of my committee members, Dr. Jihua Gou, Dr. Kawai Kwok, and Dr. Woo Hyoung Lee for their time to evaluate my research and for their constructive comments and discussions. Besides, I must appreciate Dr. Melanie Beazley and Dr. Lei Zhai for their help in the completion of my research.

My appreciation is also given to my previous and current lab mates Dr. Xiaochen Wang, Dr. Alireza Karbalaei, Dr. Pawan Pathak, and Dr. Sanghoon Park for their constructive feedbacks on my research and above all for their friendship. Finally, I must express my appreciation to my parents, my sister, my brothers, and my friends for their support and help. Special thanks to my best friend Mohsen Vaziri for encouraging and supporting me all the time and my appreciation to Sadaf Firoz for her unconditional help and support.

# TABLE OF CONTENTS

# LIST OF FIGURES

# LIST OF TABLES

# LIST OF ABBREVIATIONS AND ACRONYMS

| | |
|---|---|
| µPAD | Microfluidic Paper-Based Analytical Device |
| APTES | (3-Aminopropyl) Triethoxysilane |
| FTIR | Fourier Transform Infrared Spectroscopy |
| ICP-MS | Inductively Coupled Plasma – Mass Spectrometry |
| IDE | Interdigitated Electrode |
| LSPR | Localized Surface Plasmon Resonance |
| MEMS | Micro Electro-Mechanical System |
| MOS | Metal Oxide Semiconductor |
| NEMS | Nano Electro-Mechanical System |
| OPC | Organic Photoconductor |
| PCR | Primary Charge Roller |
| RIE | Reactive Ion Etching |
| SEM | Scanning Electron Microscopy |
| VOC | Volatile Organic Compounds |
| XPS | X-ray Photoelectron Spectroscopy |

# CHAPTER 1: INTRODUCTION

A micro/nano device can be defined as a device with at least one micro/nano scale feature size [1]. These devices with applications in various aspects of daily life such as environmental monitoring, industrial measurements, and biological testing and healthcare are becoming an important part of the modern world [2-7]. Fabricating processes associated with MEMS/NEMS devices (lithography, RIE, etching, plasma treatment, etc.) generally require well-equipped laboratories, with expensive and specialized instruments [8-13]. Additionally, these processes are dependent on cleanroom environment as well [14-20]. These restrictions not only increase the fabrication cost, but also limit production of micro/nano devices only under well-developed infrastructure, which are mainly located in developed countries. Removing these limitations may democratize the production of inexpensive devices with no requirement for costly and sophisticated instruments and processes. All these features finally can potentially induce rapid user-base growth in the micro/nano technologies.

To overcome this dependency, this research work has explored novel fabrication techniques to manufacture micro/nano sensors/devices only by using the traditional office equipment such as laserjet printers. Achieving a simple technology to print circuits and micro/nano sensors/devices on flexible substrates (paper, cloth, and plastic films) merely with office equipment without requiring centralized fabrication facilities and complex instruments can be considered as a fundamental improvement toward low-cost micro/nano device fabrication, suitable for both prototyping and mass production. These devices may be manufactured on site directly from the digital files instead of relying on

traditional manufacturing processes that require cleanrooms and other facilities. Unquestionably, utilizing such devices that can monitor critical parameters for medical conditions, environmental protection, and food safety within a few minutes can help expedite decision making and remedy emergency situations.

The uneven regional distribution of resources in different parts of the world presents a noticeable socio-economic gap between individuals and communities across the globe [21, 22]. These challenges can be encountered in the areas of medical testing and treatment as well as environmental monitoring and remedy. In the field of medical testing and treatment, a shortage of healthcare workers, an increase of counterfeit medicines, a rapid spreading of endemic infectious diseases, and vulnerable infrastructure pose a unique threat to today's world [23, 24]. In the field of environmental monitoring and remedy, a lack of accessibility to test facilities and sensors imposes a severe limitation on timely warning and remedy necessary when unexpected polluting events take place [25, 26].

From the perspective of manufacturing inexpensive sensors and devices for the aforementioned applications, the traditional, centralized manufacturing process has exposed its weakness in the face of a pandemic when the supply chain was severely disrupted recently [27, 28]. Being predicted by many experts and accelerated by the recent COVID-19 pandemic, it is inevitable to witness the rapid transformation of current manufacturing practices into a more robust decentralized operation [28, 29]. The focus of our work is the utilization of a decentralized production routine for fabricating inexpensive detection devices. Easily discernible, fast diagnostic assays that can be run on low-cost devices are attractive to the areas where access to test facilities and equipment is limited

[30, 31]. Various types of such inexpensive devices can be designed, custom-fabricated, and implemented in different aspects of daily life [32, 33]. Researchers have demonstrated such low-cost devices for various applications [3, 9, 34-38]. However, the centralized fabrication process of these devices is still a prevalent limitation.

From the perspective of manufacturing and distribution, the 4$^{th}$ industrial revolution characterized by the synergistic technological breakthrough in artificial intelligence, robotics, internet of things, bio/nanotechnology, 3D printing, etc., is replacing the traditional supply chain model where the centralized operation has dominated [39-42]. Therefore, decentralized production of light, flexible, and low-cost devices made available at home and office without the need for dedicated large-scale factories will bring many benefits and address the current challenges. A bigger impact can be expected in underdeveloped countries where reliable transportation systems are not in place, which are considered crucial to centralized production and distribution [43, 44]. Decentralized low-cost manufacturing tools will enable the production of customized devices that uniquely meet the needs of communities they belong to. In this usage scenario, these devices manufactured on-site directly from digital files instead of relying on traditional manufacturing processes will be customized to monitor critical parameters for medical conditions, environmental protection, and food safety, for example, to help communities.

This dissertation explores a facile, digital, rapid, and do-it-yourself (DIY) fabrication technology for ultra-cheap chemical, environmental, and biological macro/micro-sensors by expanding the concept of low-cost devices on flexible substrates, i.e., paper, cloth, and plastic films, to the domain of democratized and fabless production. Using a set of commercially available office equipment, i.e., a laserjet printer, a paper cutter, and a

thermal laminator, at a total capital investment cost of less than $250, different types of sensors are created and tested to demonstrate the validity of this method of fabrication.

Figure 1.1 shows an overview on the next chapters in this dissertation. In the continuation of this dissertation, first the printing process in a laserjet printer and the printer`s components are introduced. Then, the proposed technology and its working principle are explained. Finally, the application of the introduced decentralized digital technology in fabrication of micro/nano sensors, nano-sorbent filters, and microplastic fabrication is presented. This demonstrates the applicability of this technology to a wide range of devices in various fields.

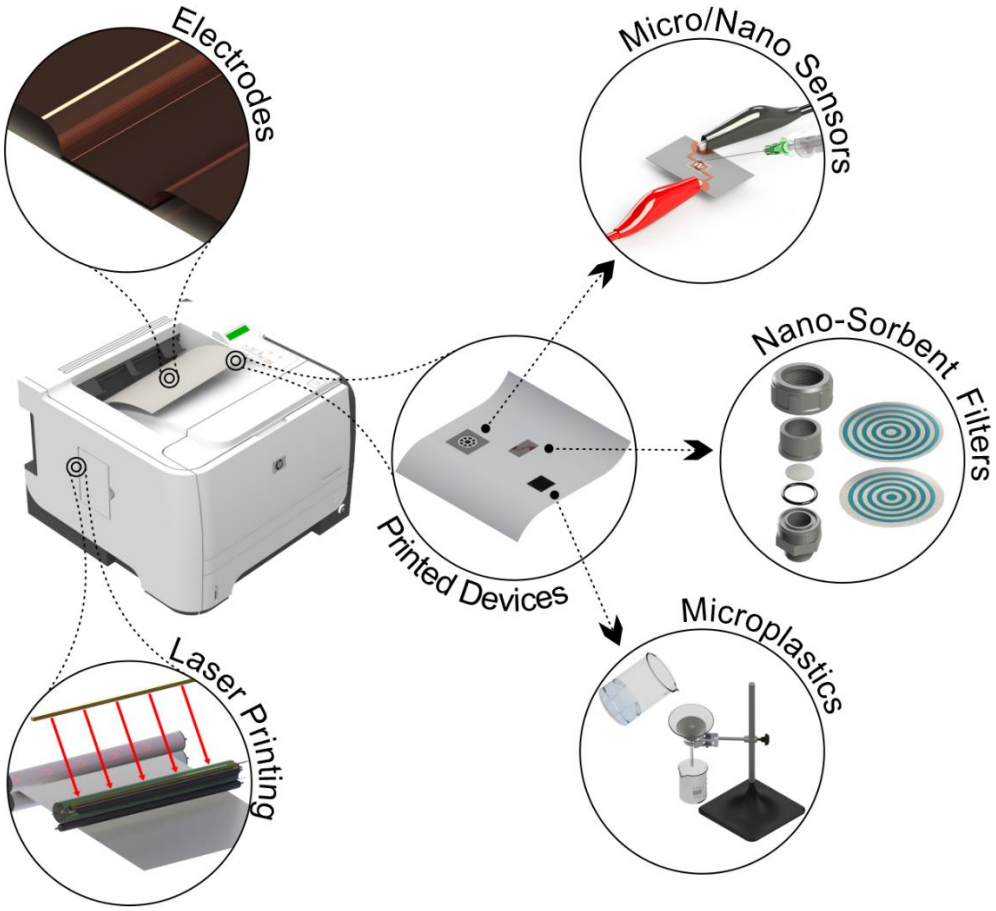


Figure 1.1: Laserjet printer components and printed devices.

This simplified technology would not require a high labor skill level, which will enable community-embedded production without a high technological barrier. The devices in the form of digital computer-aided design (CAD) files can simply be transferred, modified, and used for printing out patterns to form sensor devices. Besides, the operation procedure is simple and empowered by the smartphone which can further facilitate data analysis and transmission. This technology can be utilized pervasively in various regions, including homes, offices, remote access areas, space bases, etc. Devices with conduits to transport fluids (by hydrophobic/hydrophilic contrast definition) and electrodes for electrical detection (by metal transferring) can be fabricated on flexible substrates through this technique. Fewer fabrication steps, faster manufacturing time, no need for customized specialty equipment/mask, and compatibility with a wider range of substrates are the main advantages in comparison with the existing methods [45-55]. Due to the simplicity of the proposed method, secondary benefits of lower cost and better accessibility can be expected [56-75].

# CHAPTER 2: MAIN CONCEPT AND FABRICATION METHOD

Some of the materials used in this chapter have been previously published by Wiley:

A. Bamshad and H. J. Cho, "Laserjet Printed Micro/Nano Sensors and Microfluidic Systems: A Simple and Facile Digital Platform for Inexpensive, Flexible, and Low-Volume Devices." Advanced Materials Technologies 6.12 (2021): 2100401.

## 2.1 Working Principle

Understanding the working principle and components of laserjet printers is essential to identifying potentials of this fabrication method. A CAD software (to design the desired pattern) and an office-grade laserjet printer are the requirement for fabrication of devices, as the first step. Figure 2.1 demonstrates the components of a regular laserjet printer. The PCR (Primary Charge Roller) roller first positively charge the OPC (Organic Photo-Conductor) drum. Then, the laser scanning unit emits the laser beam in the pattern of the printable file to selectively reverse the electric charge on the surface of the OPC drum. The agitator transfers toner powder (contains a small amount of magnetic material) on the magnetic roller – specific thickness controlled by the doctor blade, and the magnetic roller transfers toner to the negatively charged areas on the OPC drum. The OPC drum transfers the toner to a positively charged paper to form desirable text/shape on the paper. The wiper blade removes toner residues on the OPC drum and makes it ready for rest of printing. Finally, the paper passes through the fuser/pressure unit, which melts the toner on paper to print. The fuser/pressure unit has a similar working principle as thermal laminators; however, the contact time is less compared to the thermal laminators.

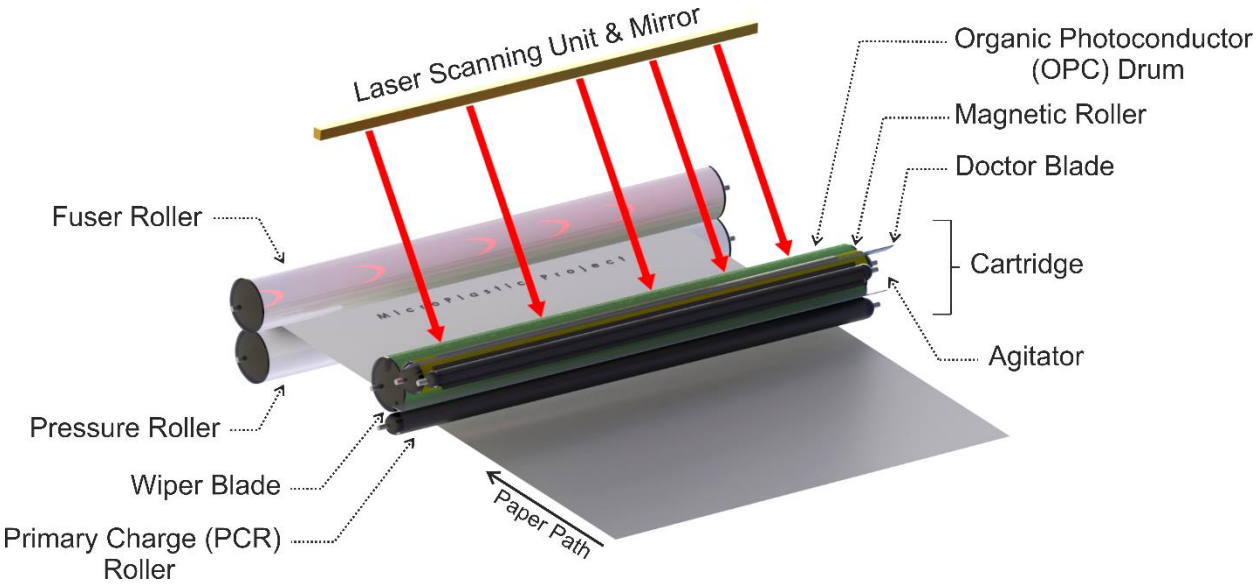


Figure 2.1: A detailed view of laserjet printer components and printing process.

## 2.2 Fabrication Method

To fabricate microfluidic systems and micro/nano sensors and devices a set of office equipment and supplies such as a laserjet printer, a craft cutter machine, a thermal laminator (for heat treatment), commercial wax paper sheets, and metal leaf sheets (for furniture restoration) are required. Depending on the desired goal and application, different substrates (paper, cloth, plastic sheet) may be chosen and the fabrication of a device through this method can have one or two steps. To demonstrate details of this method, fabrication steps of a microfluidic paper-based analytical device (µPAD) – which requires both steps – are demonstrated in figure 2.2.

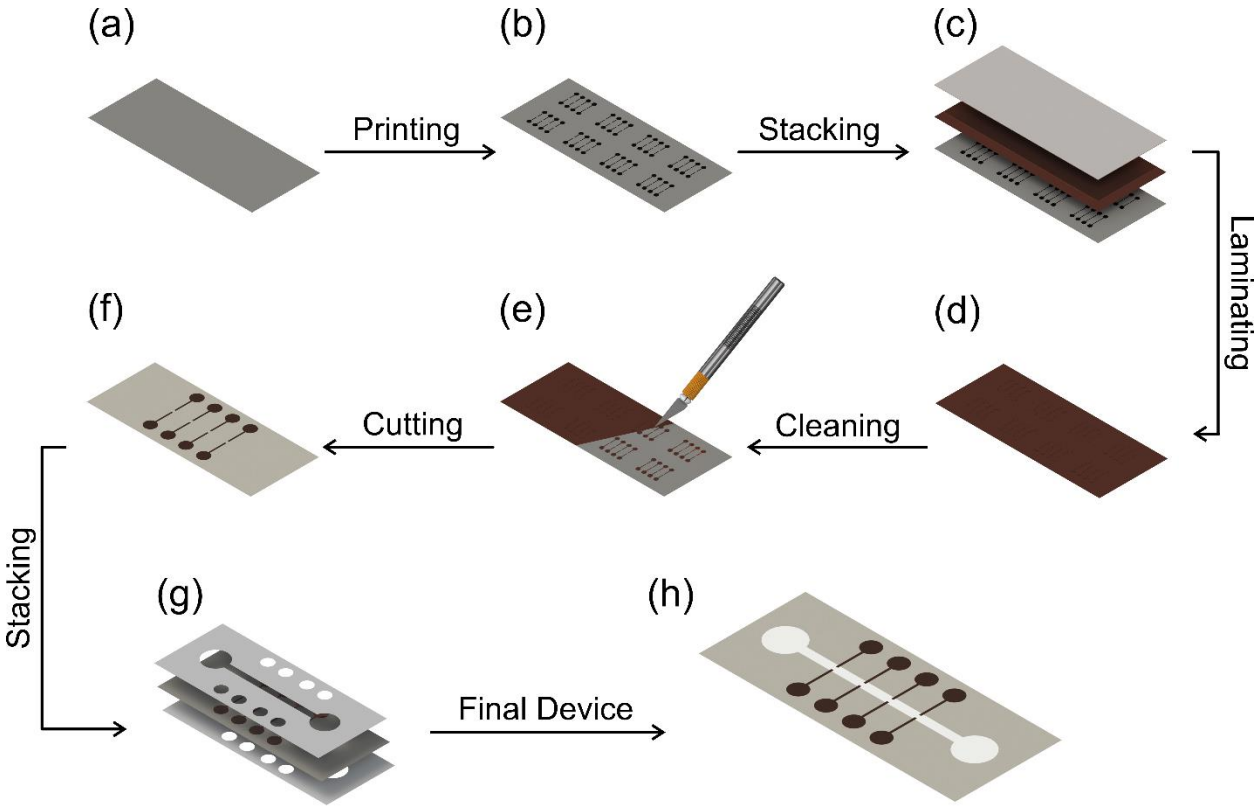


Figure 2.2: Fabrication steps of a paper-based microfluidic device with interdigitated electrodes: (a-f) metal transferring step, and (g-h) wax transferring step.

The presented µPAD consisted of a channel medium to transport fluid and electrodes for electrical detection. Step-1 (metal transferring) is to fabricate electrodes (or a base for growing metal oxide) on the desired substrate, figure 2.2(a-e). This step is carried out by: using a laserjet printer to print the electrode pattern which is designed using a CAD software; covering the printed pattern with copper leaf; layering paper on top to confine copper to printed pattern and prevent the unwanted transfer to the thermal laminator's rollers; heating the treatment under moderate pressure by the thermal laminator, and wiping the surface with a brush (or tip of a razor) to remove residue, respectively. Step-2 (wax transferring) is to define hydrophobic/hydrophilic regions to create channels on the desired permeable substrate, figure 2.2(g-h). This step is achieved

through the following steps: designing a pattern to define hydrophobic/hydrophilic regions using CAD software, covering one side of the wax paper with scotch tape to improve cutting quality, cutting the CAD pattern on to the taped wax paper with an electronic craft cutter, sandwiching the filter paper between wax papers (two similar layers on top and bottom), using a thermal laminator to transfer wax, and detaching the layers, respectively.

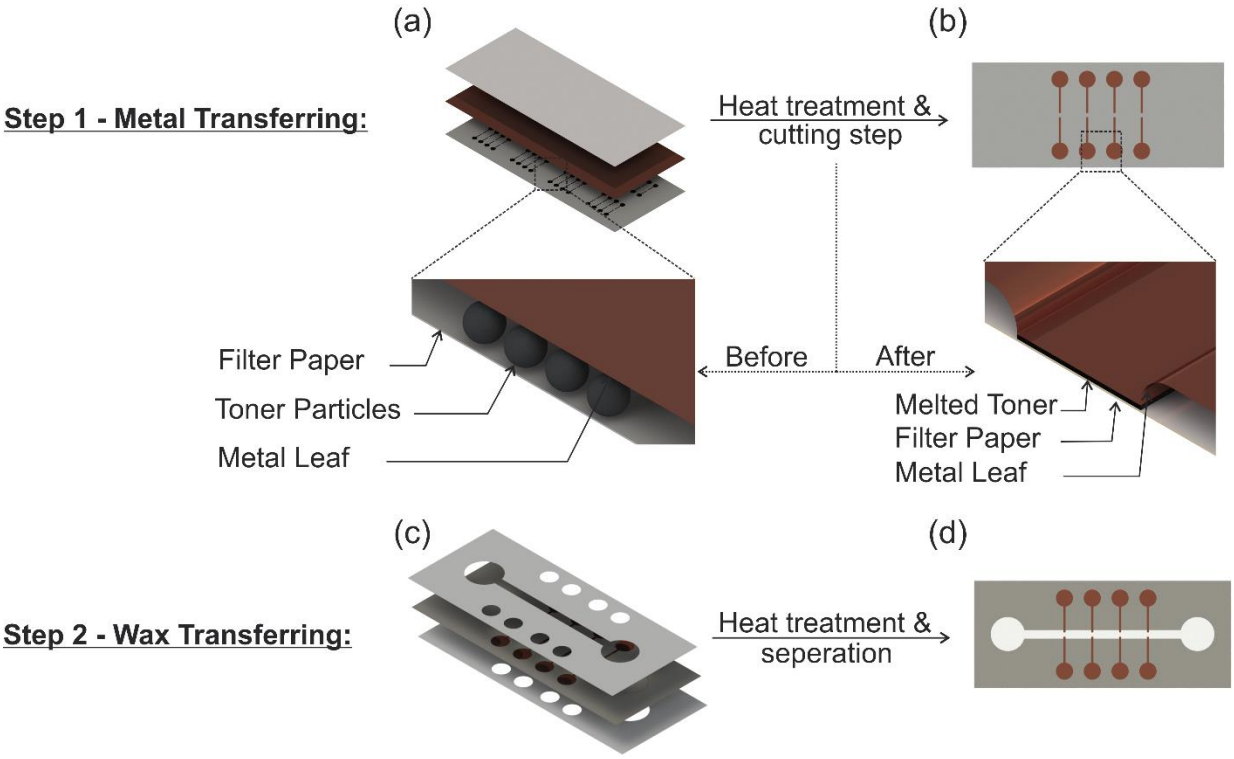


Figure 2.3: A detailed view of fabrication steps of a paper-based microfluidic device with interdigitated electrodes: (a-b) metal transferring step (toner particle melting step), and (c-d) wax transferring step.

The metal transferring step takes advantage of the strong adhesion property of the laserjet toner particles (polystyrene particles [76]) on printed patterns under heating to transfer a thin metal film. Melting and re-drying of the laserjet toner during heat treatment and then lamination is the working principle to transfer metal leaf to the substrate, figure 2.3(a-b). The transferred metal may be used as interdigitated electrodes (IDEs) or a

functionalized surface for other applications. The chemical stability of polystyrene in contact with acids, solvents, chemical reagents, and bio-samples, makes the fabricated devices suitable for various applications [77]. Whereas the wax transferring step defines hydrophobic regions by transferring wax through heat treatment from a commercial wax paper that is cut by a craft cutter machine, figure 2.3(c-d). The obtained hydrophilic area may be used as a confinement region for chemical and biochemical samples.

# CHAPTER 3: SENSOR FABRICATION

Some of the materials used in this chapter have been previously published by Wiley and IEEE:

A. Bamshad and H. J. Cho, "Laserjet Printed Micro/Nano Sensors and Microfluidic Systems: A Simple and Facile Digital Platform for Inexpensive, Flexible, and Low-Volume Devices." Advanced Materials Technologies 6.12 (2021): 2100401.

A. Bamshad and H. J. Cho, "Disposable Sensor Devices Fabricated by Paper Crafting Tools." 2020 IEEE Sensors Applications Symposium (SAS). IEEE, 2020.

A. Bamshad and H. J. Cho, "Digital microfabrication on paper and cloth For heavy metal detection and remediation." 2019 20th International Conference on Solid-State Sensors, Actuators and Microsystems & Eurosensors XXXIII (TRANSDUCERS & EUROSENSORS XXXIII). IEEE, 2019.

## 3.1 Introduction

Fabrication technologies should be capable of creating a wide array of different micro/nano devices to be accepted as a standard alternative to traditional cleanroom-based micro/nano fabrication methods. The application of the proposed technology was demonstrated by defining three levels of experiments. These levels were designed to assess the comprehensiveness and responsiveness of the proposed method to the needs of existing research fields. The performance of the fabricated devices was evaluated at each level to cover various application domains in environmental monitoring and

biomedical diagnostics utilizing conductometric, colorimetric, biochemical, and chemoresistive detection principles. Devices with varying size of features, from nanometers to centimeters, were fabricated and characterized.

## 3.2 Design of Experiments

Figure 3.1 shows three levels of experiments that were conducted to investigate and reveal all aspects and capabilities of the proposed fabrication method. Level-1 (patterns) was designed to ensure the performance of each component of a typical µPAD to investigate the optimum conditions for fabrication. Level-2 (devices) was designed to determine the fabrication ability of complex connecting devices, including, multi-layer and 3D devices. Level-3 (systems) was designed to demonstrate the applicability of this technology to the fabrication of various sensors and systems with a variety of applications, feature sizes, and different detection principles.

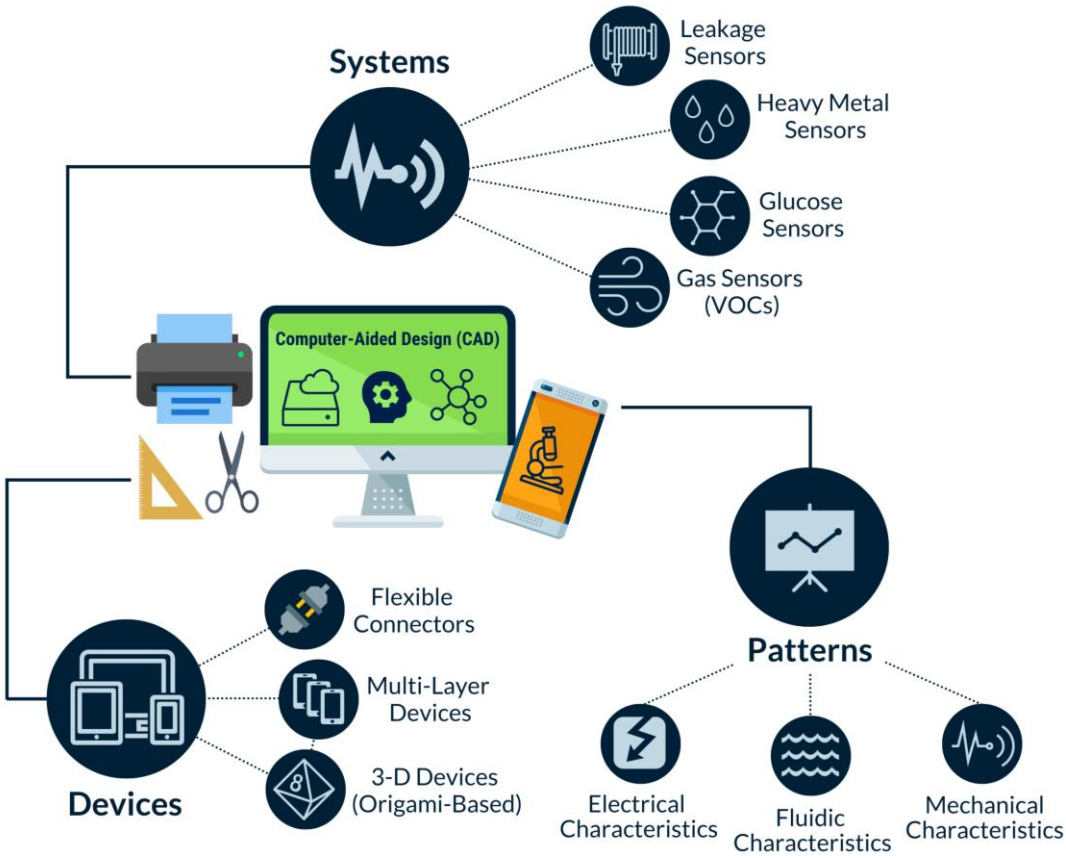


Figure 3.1: Comprehensive experiments designed to investigate validity of the proposed technology for a wide range of applications.

The performance of each element in a micro electro-mechanical system (MEMS) fabricated by the proposed fabrication method was individually investigated through the level I of experiments. Applicability of performing simultaneous and complex measurements was demonstrated in the level II by fabricating flexible connectors, multilayer devices, and three dimensional (3D) components. The level III of experiments was designed to investigate the applicability of fabricating complex systems and sensors in the most prevalent aspects of commercial sensors. Four various types of sensors in the fields of environmental, biomedical, and industrial monitoring, were selected for this purpose. The derivative fabrication techniques combining the proposed method with the

known chemical/physical processes were demonstrated. Experiments were conducted at controlled room temperature (21 °C) and were repeated three times to minimize errors – the average results are reported.

## 3.3 Level I – Patterns

Utilizing unaltered office-grade equipment limits variable parameters to only heating time and printing resolution. Heating time affects both steps; hence, it was inevitable to investigate its impact individually. The metal leaf adhesion quality to the substrate was investigated to evaluate this criterion for the first step. The contrast between hydrophobic and hydrophilic regions was investigated to find out the optimum laminating time for the wax transferring step. It was observed that a minimum of 10 seconds of thermal laminating was necessary to completely transfer metal leaf to paper, cloth, and plastic film, and exactly 5 seconds (sandwiched substrate configuration) was necessary to transfer wax from commercial wax papers to the porous substrates. A negative effect on the quality of the transferred wax was observed by increasing heating time. Also, 600 dpi (dots per inch) minimum printing resolution was required to achieve interdigitated electrodes (IDES) with a 200 µm feature size.

### 3.3.1 Electrical Characteristics

The electrical characteristics study was conducted to investigate repeatability. The electrical resistance and its dependency on heating time, and the functionality of electrodes were characterized during the metal transferring step. To maintain the low-cost and investigate the possibility of using different leaves, in addition to the genuine copper leaf, imitations of gold and silver leaves have been tested as well. The transfer of

different materials with various compositions is ultimately translated into the ability to build sensors with different electronic specifications which result in different sensitivities.

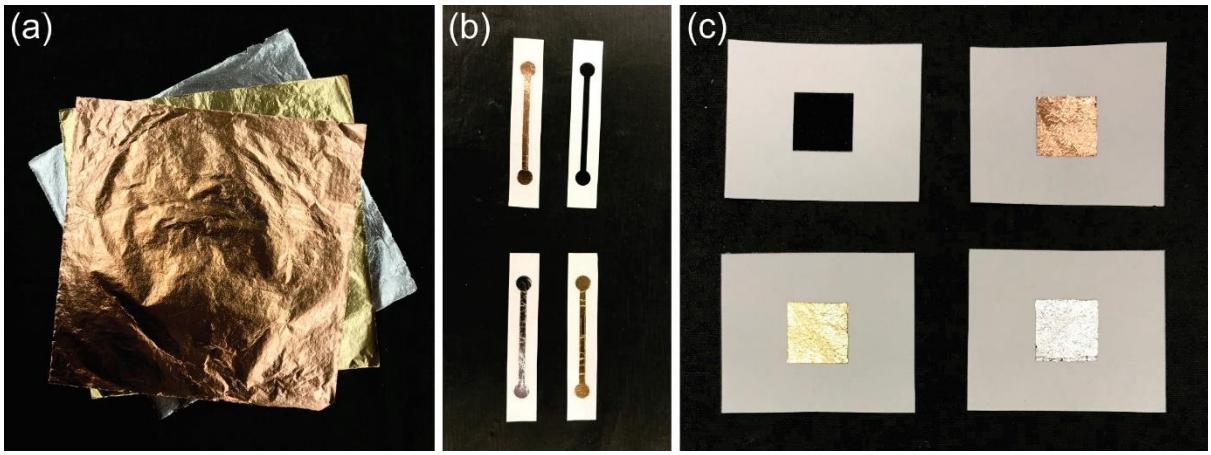


Figure 3.2: Samples prepared for electrical characterization before and after metal transferring step: (a) metal leaves; (b) repeatability study samples, and (c) sheet resistance study samples.

Figure 3.2(a) shows three different metal leaves with a thickness of 4 μm that were used for this study. The repeatability of the electrical performance of a transferred metal leaf was measured to be 98 %. This value was calculated with repeated measurements of electrical resistance of identical samples (10 cm length) made of different metal leaves, figure 3.2(b). Four-point probe resistivity measurement was carried out to determine the resistivity of square shape samples, figure 3.2(c).

The sheet resistance of samples (1 $cm^2$) before and after transferring on the paper substrate was measured (table 3.1). A slight increase in sheet resistance due to sheet curvature was observed after transferring metals on filter paper. No dependency between electrical resistance and heating time was observed.

Table 3.1: Sheet resistance before and after metal transferring step.

| Type | Sheet Resistance Not Transferred Metals ($m\Omega\ sq^{-1}$) | Sheet Resistance Transferred Metals ($m\Omega\ sq^{-1}$) |
|---|---|---|
| Genuine copper samples | 43 ± 2 | 48 ± 2 |
| Silver imitation samples | 57 ± 2 | 62 ± 2 |
| Gold imitation samples | 72 ± 3 | 80 ± 3 |

Figure 3.3(a) shows a fully hydrophobized paper-based sensor made of filter paper that was used for electrode functionality study. To obtain various levels of ions in an aqueous solution, different concentrations of sodium chloride (NaCl) solutions (5 mM-150 mM) were prepared by dissolving NaCl in deionized (DI) water. Figure 3.3(b) shows the fully hydrophobized sample's measured electrical resistance using identical IDEs with 350 µm gap size. A decrease in the impedance readout of the IDEs with increasing concentrations was observed – with a 3.1% variation in the electrical resistance measurements.

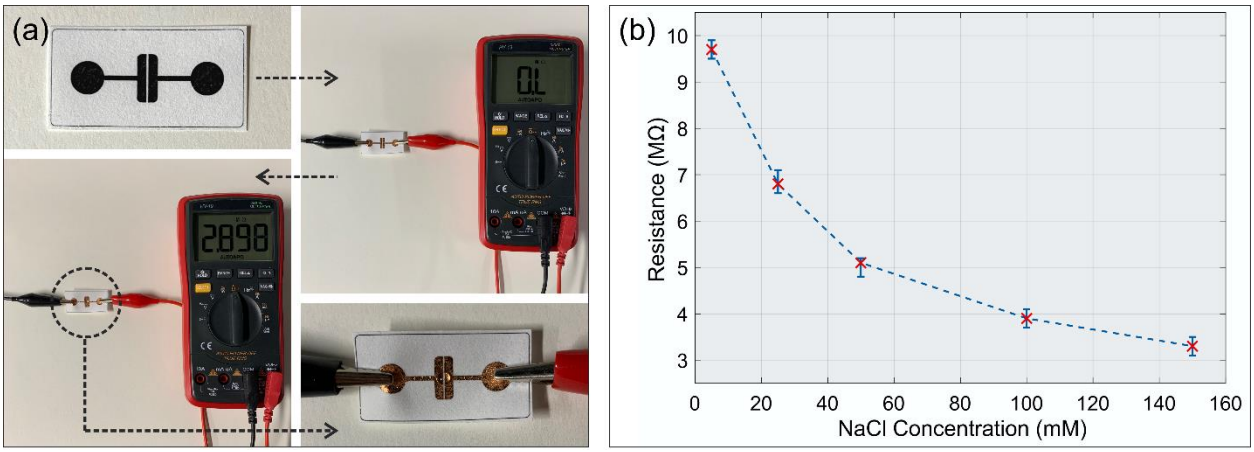


Figure 3.3: (a) electrode performance study experimental setup and (b) electrode performance study results in the form of electrical resistance changes as a function of NaCl concentration.

### 3.3.2 Fluidic Characteristics

A fluidic characteristics study was conducted to investigate possible changes in the physical properties of cellulose fibers during the metal transferring step, which may cause variation in governing behaviors for capillary flow in µPADs. The presence of wax, a wicking substrate, direct contact at high temperatures, and the toner`s components can be factors that cause such changes. A closer look at the laserjet toner components reveals the presence of polystyrene, polypropylene (pp) wax, carbon, iron oxide, and silicon dioxide. The pp wax is utilized to prevent polystyrene particles from sticking to each other. This substance is capable of interfering with the transferred wax that was used to define hydrophobic/hydrophilic contrast during heat treatment steps. Hence, it is crucial to investigate the wicking of pp wax and its impact on cellulose fibers' wettability while forming electrodes at a higher temperature.

Two different samples with identical channels were prepared through wax transferring on filter paper as follows: sample-1, as an analytical device with a 4-point electrode detection system and printed border, and sample-2, as a plain sample without any printed toner. Figure 3.4(a) shows sample-1 with a 32 mm length of channel and 2 mm width of the channel. Channel dimensions were selected based on the average dimensions of common paper-based analytical devices. The location of the deionized (DI) water meniscus overtime was used as the indicator to investigate the impact of pp wax on the governing capillarity actions. A 240-fps camera mounted on top of a microscale labeled lens is utilized to capture these data. Figure 3.4(b) shows the result of this study. Insignificant changes in the fluid behavior of the channels were observed. This result can demonstrate that no changes in capillary action/fluid behavior in analytical devices were

made by the filter paper using the proposed method. Besides, the DI water contact angle was studied. It was observed the contact angle was increased from 15.4° ± 1.4 (untreated filter paper) to 128.4° ± 1.0 (double-layer treated filter paper) during the lamination step. Instability in contact angle is observed for the samples treated only with one layer of wax paper.

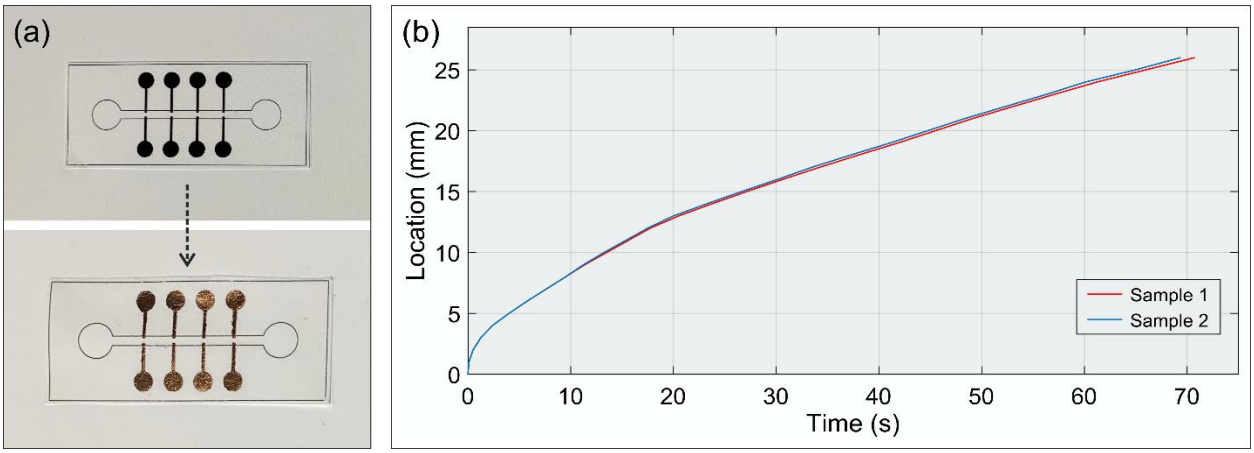


Figure 3.4: (a) 4-point electrodes paper-based analytical device utilized for fluidic characteristics study and (b) meniscus location overtime measured in fluidic characteristics study.

### 3.3.3 Mechanical Characteristics

A mechanical characteristics study was conducted to investigate mechanical properties such as swelling effect, reliability, and flexibility of the fabricated sensors/devices on different substrates. The fabrication of the electrodes on a thin film of polymer prevented the electrodes from direct contact with the paper substrate and subsequently the cellulose fibers. This mitigated the unwanted noise from the known swelling phenomenon of paper-based sensors [78]. In addition, the utilization of fully automated instruments (a craft cutting machine and a laserjet printer) reduces variability

caused by human error for fabrication devices. The error of the utilized instruments has been reported to be < 5 % for features with > 200 µm dimension, in previous studies [76, 79]. Hence, fabrication of sensors/devices with acceptable repeatability and performance can be achieved consistently.

The flexibility study was conducted to explore the effect of bending on the electrode's response, the durability, and the maximum number of bending cycles before the sensor`s failure. A cyclic bending test was performed to determine the number of bending cycles before the failure of the sensor/device. In this test, the separation of the electrode from the substrate or the termination of the electronic connection in the electrodes was considered as a sign of the component failure. Identical electrodes made on different materials (paper, fabric, and plastic film) were cyclically bent using a slider-crank mechanism with a 1.5 mm radius in the smallest part. The allowable number of cycles for electrodes fabricated on plastic film, paper, and cloth were measured at minimum 15,000, 12,000, and 10,000 cycles, respectively. The effect of bending on the electrode`s response was investigated by monitoring the electrical resistance of the electrodes during the bending process. Cyclic bending test indicates recovery of the initial response signal upon shape restoration, figure 3.5(a). This demonstrates the high durability and acceptable performance of the electrode`s signal during bending. A test of 10,000 cyclic bends revealed fluctuation in relative resistance by about 7% for every 1,000 cycles, figure 3.5(b). This amount of change in electrical resistance is similar to the previously introduced highly conductive flexible nanocomposites [80]. In addition, doubling of the electrical resistance of the electrodes was observed after ten thousand cycles. Similar results were obtained for all studied substrates.

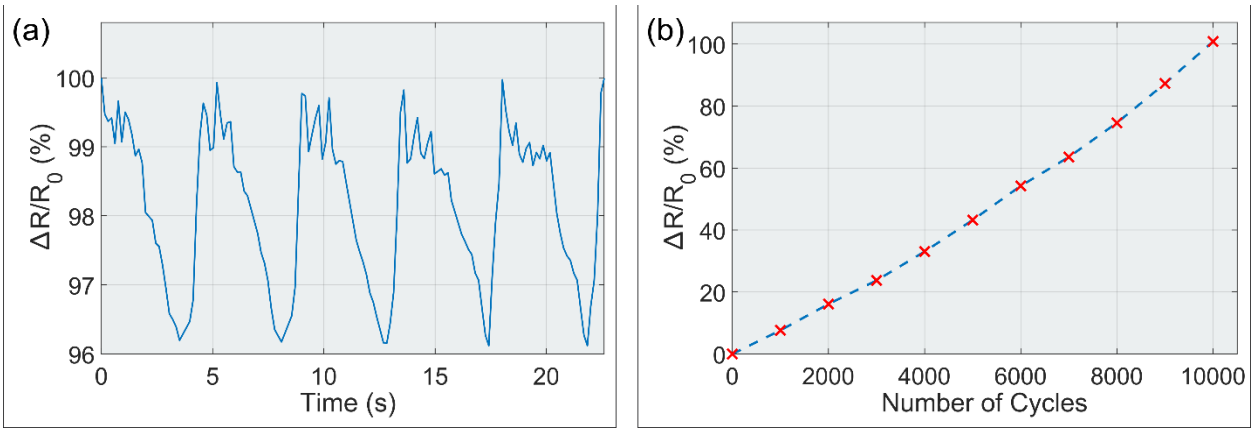


Figure 3.5: (a) cyclic response of the electrodes during bending and (b) fluctuation in the relative electrical resistance during 10,000 bending cycles.

## 3.4 Level II – Devices

### 3.4.1 Flexible Connectors

Flexible connectors play a key role to demonstrate the capability to fabricate systems by connecting individual components. Here, a print-and-transfer scotch tape method using a plain cloth (to minimize transferring fibers of the support layer) as the support layer was utilized to fabricate a flexible connector, figure 3.6.

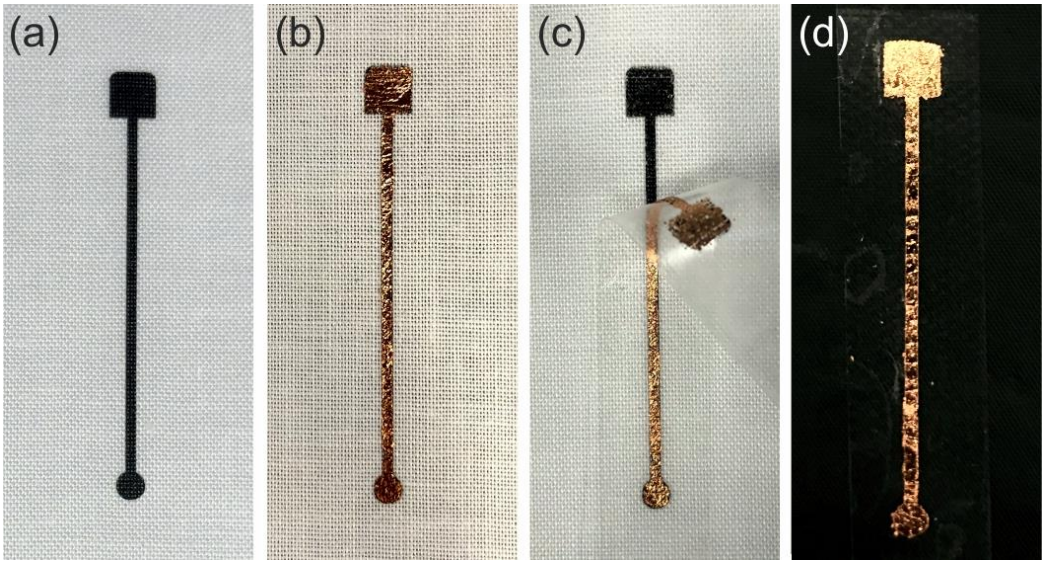


Figure 3.6: (a) Printed connector pattern on the cloth; (b) copper leaf selectively transfers to the printed area; (c) stick-and-peel step by the scotch tape, and (d) final thin film copper-made flexible connector on scotch tape.

### 3.4.2 Multilayer Devices

Multilayer devices could benefit from high detection efficiency, simultaneous detection, minimized volume/weight required for sensors due to stacking the components in a smaller space. Figure 3.7 shows the experimental configuration to investigate electrodes and fluidic independence and performances of multilayer devices. Two identical µPADs, with color indicator bars, were connected back-to-back together via a double-sided tape. In addition, PBS, flexible connector, and commercial multimeters were used for this study. Color indicators with different dyes were used to evaluate the penetration of liquids between layers. The non-interrupted performance of electrodes in the multilayer configuration was successfully observed through electrical resistance changes before and after dropping the solution (on each layer). Also, no dye leakage overtime was observed that can demonstrate a suitable fluidic performance of multilayer

configurations. No-interference of different layers' functionality in both impedance and colorimetry studies was observed. The same results for samples with more than two-layers were obtained.

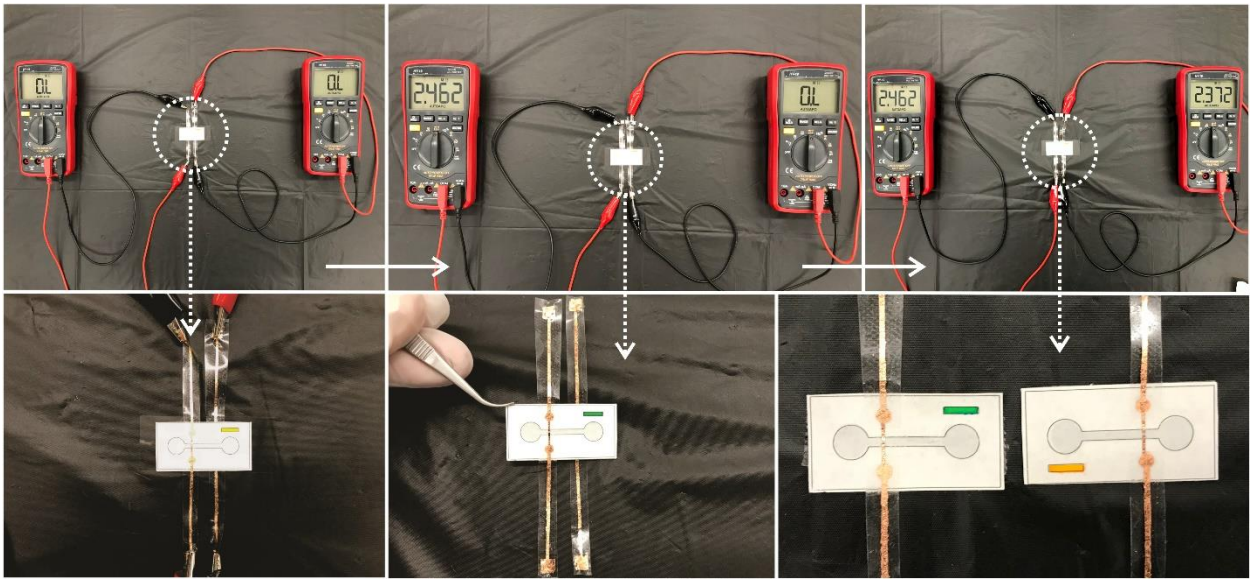

Figure 3.7: Experimental results of a multilayer paper-based analytical device, figures are in order of experimental setup, electrical resistance change of top layer, electrical resistance change of both layers, flexible connections on top layer, flexible connections on bottom layer, and transferred wax quality indicator.

### 3.4.3 3D Devices

Origami method was used recently to create three dimensional (3D) analytical devices by folding a single sheet of paper [81]. Such devices uniquely provide different controllable reaction zones with completely separate electrical and fluid components that can result in complex devices for simultaneous measurements [82]. The proposed method is capable of fabricating such 3D devices as well. Figure 3.8(a) shows a foldable 3D device that was prepared by transferring wax by a thermal laminator and was cut by a craft cutter machine. This chip was sandwiched between two transparent acrylic sheets with five holes by two paper clamps, figure 3.8(b). To investigate the performance and

quality of hydrophobic borders and wax transferring step, the ability of this 3D chip for penetrating a dyed sample solution through different layers was studied. Four different colors were drop-casted in the side confinement areas of the 3D disposable device to investigate and demonstrate the ability to transfer and selectively move fluids (reagents) between different layers. To complete this study and investigate the impermeability of the fluid to other parts, the fluorescent dye that has a higher penetration power than other fluids was drop-casted in the central hole, figure 3.8(c). Color indicators successfully were confined when folded and showed 90° clockwise rotation when unfolded, without any leakage through the first and subsequent layers, figure 3.8(d). The leakage of fluorescent dye was investigated under UV lamp as a supplementary experiment. No observable leakage from both regular and fluorescent dyes was found.

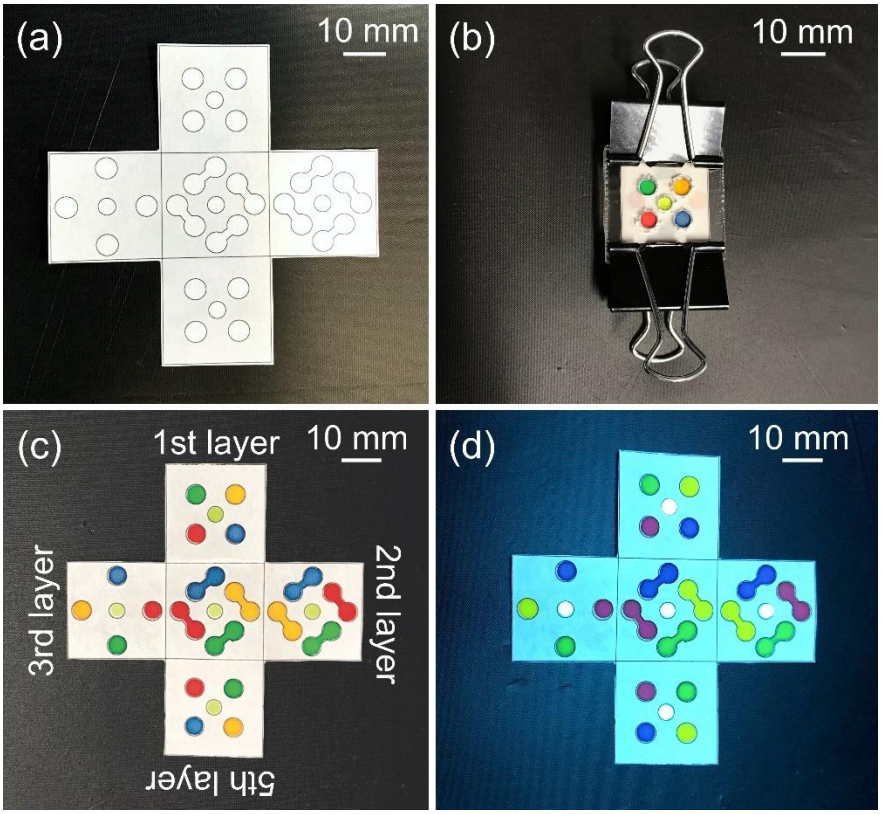


Figure 3.8: Experimental results of a 3D analytical device, figures, in order, are the wax transferred unfolded 3D device, dyed solution dropped on the folded device, color indicators rotated (90°) from the 1st layer to the 5th layer, and fluorescent dye studied under UV radiation.

## 3.5 Level III – Systems

The last level of experiments was designed to investigate the applicability of fabricating complex systems and sensors in the most prevalent aspects of commercial sensors. Four various types of sensors in the fields of environmental, biomedical, and industrial monitoring, were selected for this purpose. The derivative fabrication techniques combining the proposed method with the known chemical/physical processes were demonstrated.

### 3.5.1 Leakage Sensors

Monitoring and detecting a leakage is one of the key parameters to prevent pressure drop in the fluid transfer process. Leakage sensors have a wide range of applications in various industries such as medical sciences, oil drilling, mining, and water piping [83, 84]. Manufacturing a low-cost, on-demand, and disposable leakage sensor is quite desirable. Figure 3.9 shows an inexpensive paper-based one-dimensional leakage sensor to investigate the validity of the fabrication method for the environmental sensor application. Colorimetry and impedance changes were used as detection parameters in this sensor. Four tiny holes were made deliberately on a commercial PVC pipe to indicate leaks in different locations. The leakage sensor consisted of four separate zones (work as parallel resistances) that were created on a piece of office-grade paper by metal and wax transfer, respectively. Each zone consisted of two electrodes with a small gap in between. The edges on the sensor`s back-side were covered with a water-based acrylic paste and dried at room temperature to be attached to the surface of the pipe. For colorimetry and impedance studies, solutions with different colors were prepared by mixing food dye in tap water.

To demonstrate leaks in the pipe artificially, syringes with tubes were used. Leakage of water into each hydrophilic zone causes changes in electrical impedance, in which each zone works as a resistor. The zones were arranged in a similar configuration of identical parallel resistors to identify the number of leaks on a pipe. Finite values of electrical impedance could be observed after the first leakage and constantly measured via a multimeter. This value decreased intermittently as the leak progresses ($R_0$, $\frac{R_0}{2}$, $\frac{R_0}{3}$,

$\frac{R_0}{4}$). The same leakage progress was confirmed through the color changes as shown in figure 3.9. Additionally, these results confirm the ability to build two-dimensional paper-based leakage sensors capable of covering pipes entirely. Leakages in pipes cause changes in the read overall electrical resistance of the sensor (using a wireless readout), and based on this, the location and size of the crack can be detected approximately.

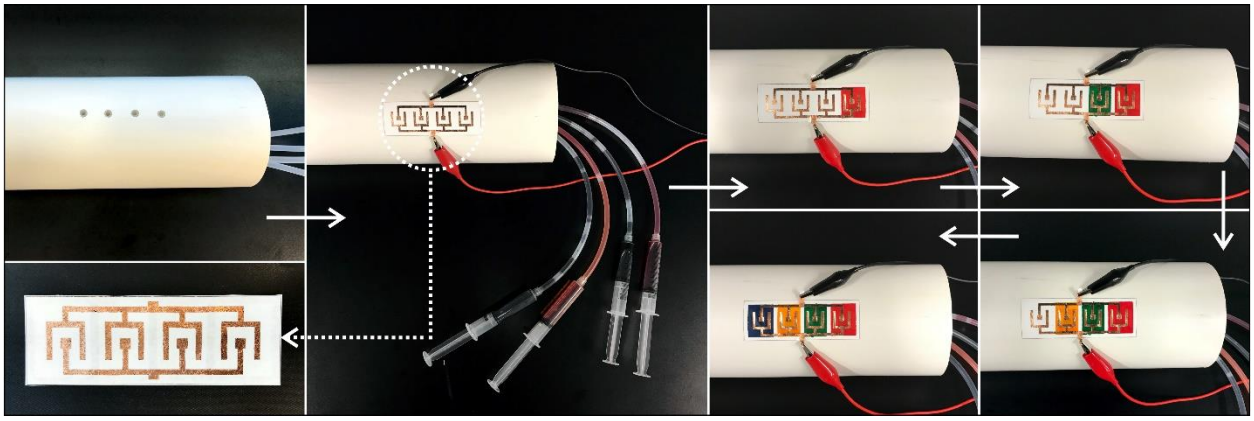

Figure 3.9: Experimental results of a paper-based leakage sensor and the experimental configuration with colorimetry and impedance detection.

### 3.5.2 Heavy Metal Sensors

Pollution in water resources typically occurs naturally (through soil erosion) and unnaturally (through mining and industrial activities) [25, 85]. This phenomenon causes irreparable health problems and numerous environmental difficulties [26]. Among common water pollutants, cobalt (II) recently gained notoriety for the wide-spread exploitation of this element to satisfy a high demand for electric vehicle batteries [26]. An inexpensive paper-based sensor with colorimetric detection using the proposed fabrication method was designed and fabricated for cobalt (II) detection.

Figure 3.10 shows the fabrication and operation steps of this cobalt (II) sensor. A confinement area for drop-casting was defined by printing toner via a laserjet printer followed by wax transferring to define the hydrophobic region on a filter paper that was previously cut via a craft cutter machine. (3-aminopropyl) triethoxysilane (APTES) was drop-casted in the confined areas and was kept in a sealed environment until the experiment.

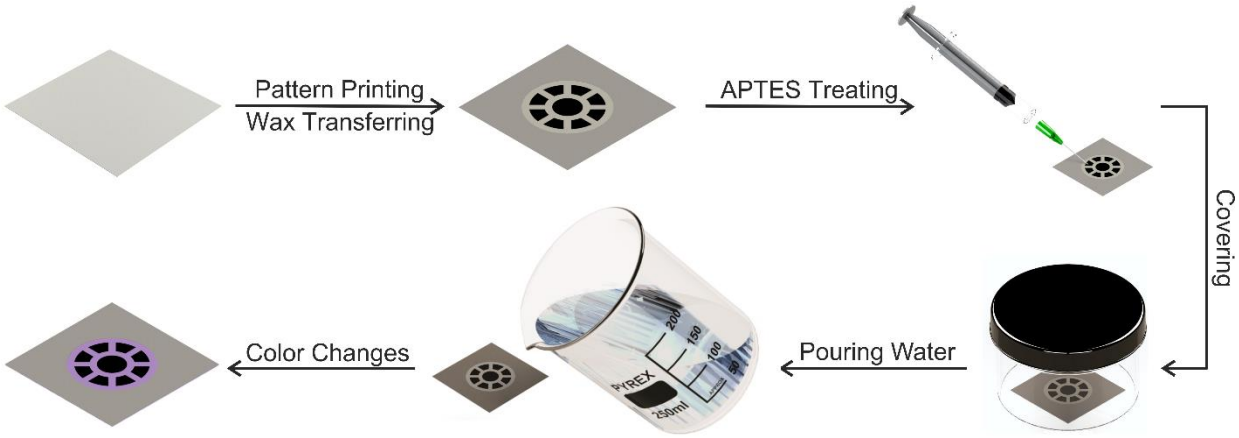


Figure 3.10: Fabrication and operation steps of a colorimetric sensor to detect cobalt (II), the steps in order are paper cutting, pattern printing and wax transferring, APTES drop-casting, sealing, water pouring, and observing the color change.

Researchers have previously reported color changes of aqueous solutions containing heavy metals in contact with APTES [86]. These color changes are caused by the localized surface plasmon resonance (LSPR) phenomenon [3, 87]. In fact, amine groups of APTES drop-casted in the paper-based device have high affinity to bivalent cobalt ions [3, 87]. It can form a metal-amine complex, and consequently the cobalt nanoparticles by self-seed generation with silanization [3, 87]. The nanoparticles formed have LSPR properties, which can be used for colorimetric detection of the target ion

without necessity to immobilize the target on supporting material, unlike the common methods introduced earlier [3, 87]. This color change is unique and varies depending on the contaminant [86]. Good selectivity of APTES for detection of cobalt (II) has been reported [86]. Adding contaminated water to the detection zone led to a color change within a few seconds where the intensity of the observed color change represents different concentrations of the pollutant.

Various concentrations of cobalt (II) solutions (5-1500 ppm) were prepared by dissolving cobalt sulfate in distilled water. High concentrations of spiked cobalt (II) samples were intentionally used for the initial validation in this study. A commercial smartphone (iPhone X) was used to take photos and open-source software (ImageJ) was utilized to process captured images and analyze data. Normalizing of the captured images was performed to remove ambient noises and swelling effect, by considering the brightest and darkest spots as the pure white and black, respectively, in each photo. Figure 3.11 shows the paper-based sensor utilized to detect cobalt (II) in the aqueous phase and the colorimetric changes (color code) of the detection region as a function of the pollutant concentration. The color code is a unique number that is assigned to each specific color during image processing. This number was obtained by analyzing the detection zone through RGB color model via ImageJ software. Linear behavior in the sensor response was observed in the concentrations of 5-150 ppm and 200-1500 ppm. The minimum detectable concentration of cobalt (II) was 5 ppm in the presented colorimetry sensor.

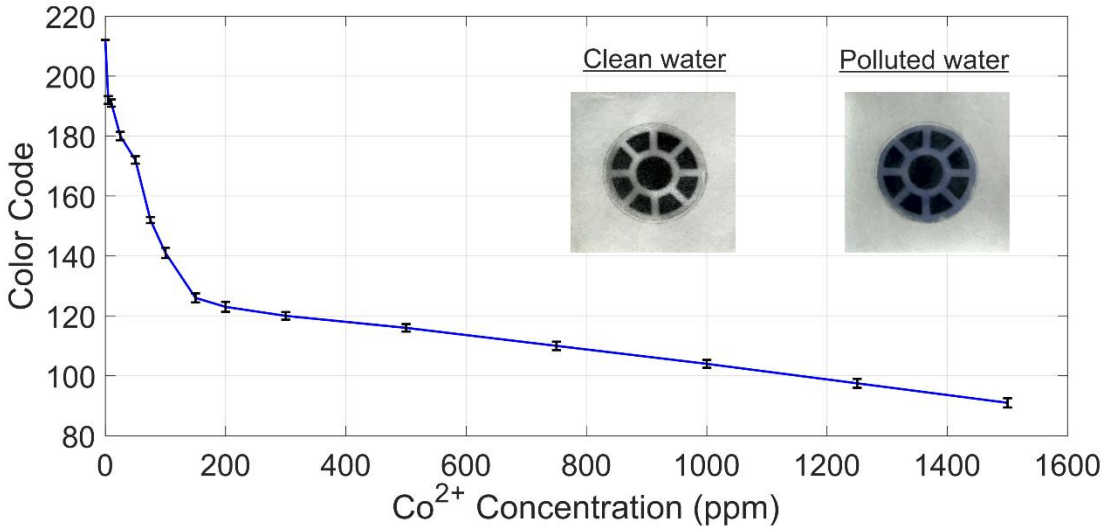


Figure 3.11: Sensors` responses of a colorimetric sensor for cobalt (II) detection, color code as a function of pollutant concentration in water.

### 3.5.3 Glucose Sensors

Nowadays, about 18% of the worldwide population suffers from diabetes [88]. Patients with this disease sometimes have to measure their blood sugar up to 5 times a day, which indicates the need for inexpensive and affordable devices [88, 89]. The requirement for test strips and dependency on centralized manufacturing of such devices can be considered a drawback. Figure 3.12 demonstrates the fabrication and operation steps of an on-demand paper-based glucose assay.

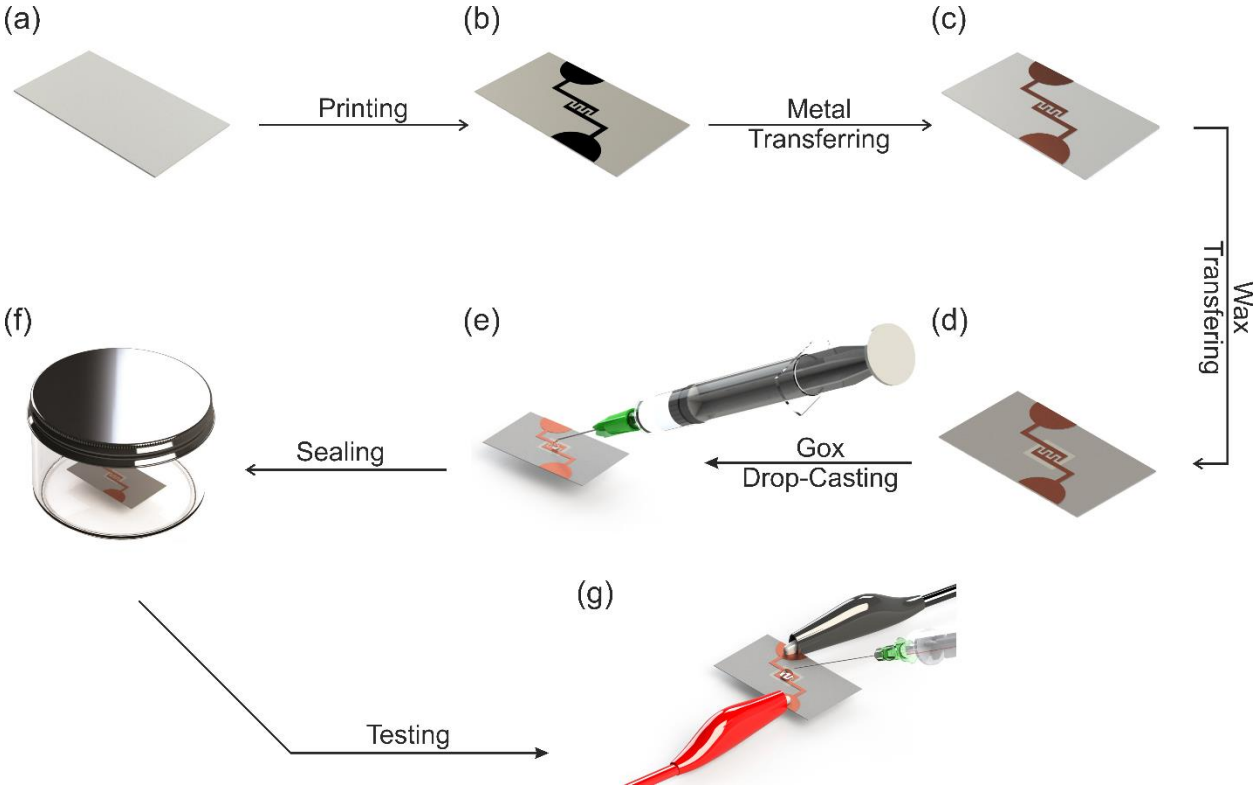


Figure 3.12: Fabrication and operation steps of a glucose disposable assay, the steps in order are paper cutting, pattern printing, leaf transferring, wax transferring, GOx drop-casting, sensor sealing, and glucose concentration measuring.

A filter paper was cut by a craft cutter machine followed by electrode pattern printing. Electrodes and confinement regions were formed by transferring copper leaf and wax, respectively. Two drops of 100 kU/L glucose oxidase (GOx) were drop-casted in the confinement zone, and the finalized analytical device was sealed and stored at a refrigerator (4 °C) prior to the experiment. GOx is a well-known standard enzyme utilized to detect glucose in enzymatic biosensors [90]. High selectivity of GOx for this purpose has been reported [90, 91]. The completed device was utilized to measure glucose concentration by measuring the impedance change after dropping the sample using a source meter. The impedance change was caused due to the formation of gluconate ions

that were produced by the gluconic acid in an aqueous solution at neutral pH [92]. This organic component and hydrogen peroxide were produced by oxidizing glucose in the presence of glucose oxidase [93]:

$$\text{D-Glucose} + H_2O + O_2 \xrightarrow{\text{Glucose Oxidase}} \text{D-Gluconic Acid} + H_2O_2$$

Various concentrations of glucose aqueous solution in the range of 1-150 mg/dL were prepared by dissolving D-glucose in distilled water, which is similar to the range of human blood glucose level. The sensor's electrical resistance was measured in specific time intervals (1-, 2-, 3-, and 4-minutes) after dropping the solution on the measurement zone. The time intervals between placing the solution and measuring the resistances were determined considering the time required for the reaction to reach completion and form gluconic acid. Inconsistencies were observed in sensor responses before 2-minutes, which is approximately the time required to complete the formation of gluconate ions and after 3-minutes, due to the initialization of surface evaporation from cellulose fibers. Figure 16 demonstrates the sensor's normalized response with an interdigitated electrode structure with 1.4 mm fingers length and 350 µm gaps width.

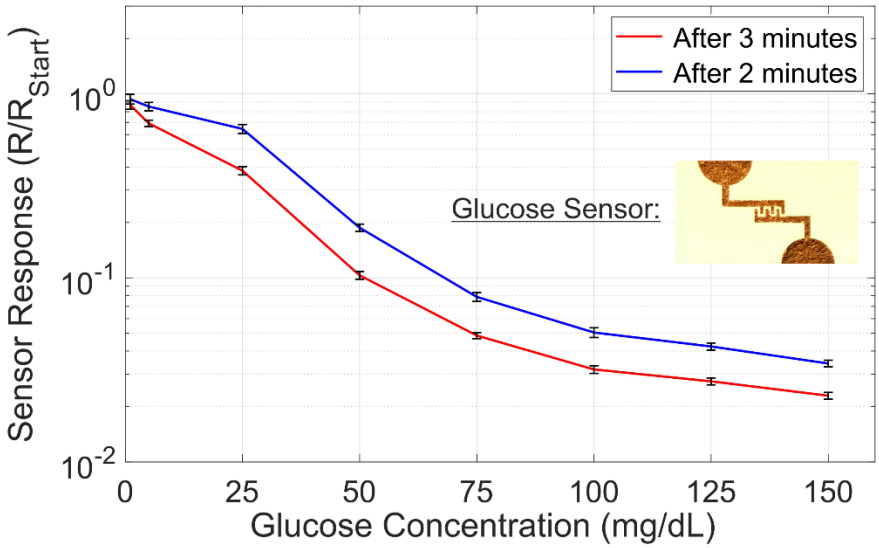


Figure 3.13: Sensors` responses of a glucose disposable assays measured after 2 and 3 minutes of placing glucose samples.

This sensor was capable of measuring the concentration of glucose in the predetermined concentration range with less than 3% error on average. Linear behavior in the sensor response was observed in the ranges of 5-50 mg/dL and 75-150 mg/dL. The presented biosensor showed a detection limit of 1 mg/dL in glucose detection. The sensor performance was in line with previously reported enzymatic studies [91].

### 3.5.4 Gas Sensors

Gas sensors are critical components in the modern world with a broad range of applications in environmental sciences, indoor/outdoor air quality monitoring, healthcare/biological testing, oil refining, etc. [94] Among different gases, volatile organic compounds (VOCs) are a popular target due to their abundance in the environment and frequently encountered in many human activities [95]. Gas sensors can be classified into different categories, such as electrochemical, infrared absorption, solid electrolyte, metal oxide semiconductor (MOS), catalytic combustion, and thermal conductive sensors [96].

MOS gas sensors are widely used due to their high sensitivity and selectivity, low material cost, and easy fabrication process [97]. Electrical resistance change due to adsorption/desorption of oxygen on the metal oxide surface in contact with the gas is the working principle of MOS gas sensors [98]. Zinc, copper, tin, indium, cerium oxides are the most common metal oxides that are used to fabricate MOS gas sensors [99].

To show the applicability of the proposed method to fabricate micro/nanometer feature sized sensors, a flexible gas sensor with confined interdigitated electrodes (125 µm electrode gap size) and a nanostructured sensing layer and was designed, fabricated, and tested. Figure 3.14 shows the fabrication steps of this flexible copper oxide gas sensor to monitor the concentration of VOC gases.

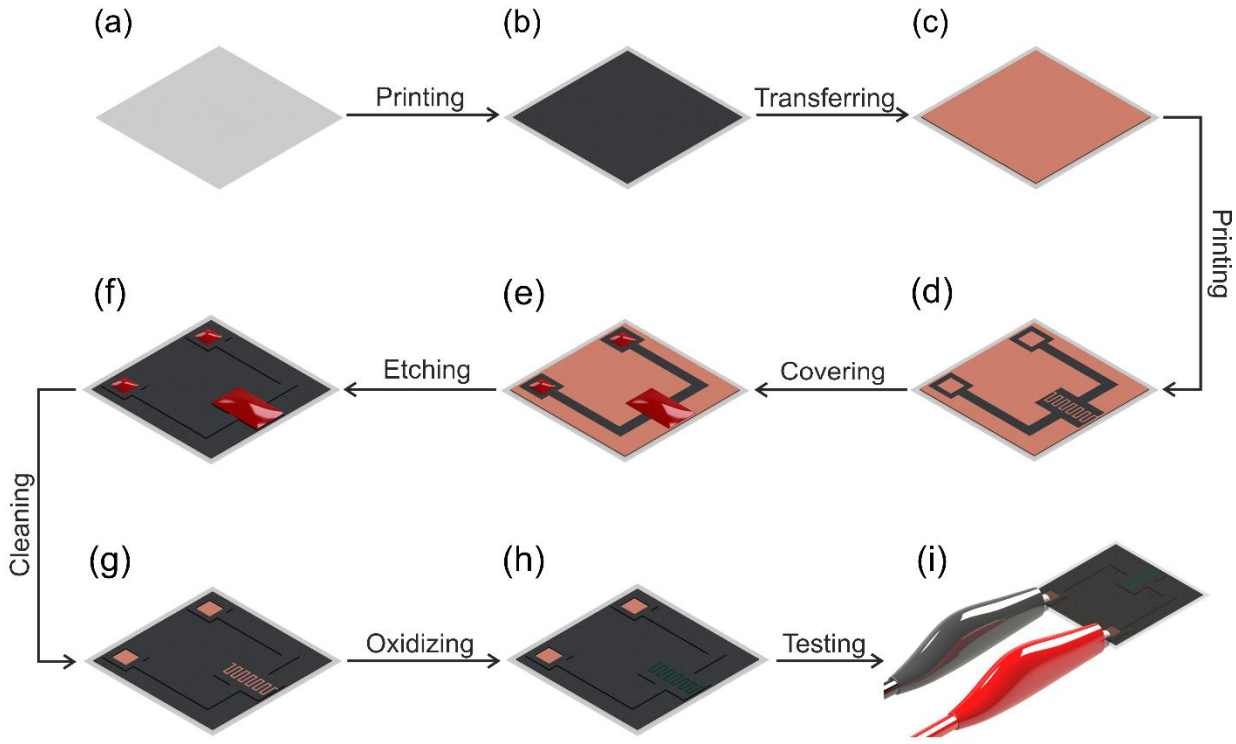


Figure 3.14: a VOC flexible gas sensor, the steps in order are plastic cutting, base printing, copper transferring, IDEs pattern printing, pad/electrodes covering, copper etching, Shipley removing, and copper oxidizing.

An office-grade transparency printable film was completely covered with toner through a printing step followed by a thermal lamination step to transfer copper leaf on top of it. The transferred copper then was treated by an atmospheric plasma surface treater for 30 seconds to clean out the organic pollutants and improve the printing quality on top of copper. This was followed by the sensor pattern printing step using the laserjet printer. The device was washed with 4 M hydrochloric acid (HCl) and rinsed with DI water to remove the copper oxide layer on top of the copper leaf. Connection pads and electrodes were manually covered with a few drops of a positive photoresist (S1813) and dried at room temperature. The difference in the contact angle of the photoresist on top of the toner and the copper leaf prevents the droplets from spreading to other parts. The copper etchant solution was used to dissolve the copper residues within 5 seconds, followed by washing off the photoresist and the sensor with acetone and DI water. Finally, a nanostructured copper oxide layer, used as the sensing material, was grown at room temperature in the gap between electrodes over the transferred copper layer by soaking the electrodes in a solution of 1 M sodium hydroxide and 35 mM ammonium persulfate, following oxidation reaction, for a certain time duration [26]:

$$Cu + 4NaOH + (NH_4)2S_2O_8 \longrightarrow CuO + 2Na_2SO_4 + 2NH_4OH + H_2O$$

The minimum required time to fully oxidize the copper leaf under this chemical reaction was measured to be 45 minutes. Various oxidation duration times (45 minutes, 60 minutes, 90 minutes, and 120 minutes) were utilized to form different nanostructured morphologies. The sensing performance was investigated by repeated exposure to 250 ppm ethanol vapor, at room temperature and atmospheric pressure, figure 3.15. Different

oxidation times, respectively, resulted in single-nanowires, binary-nanowires, multiple-nanowires, and nanoflowers, figure 3.16.

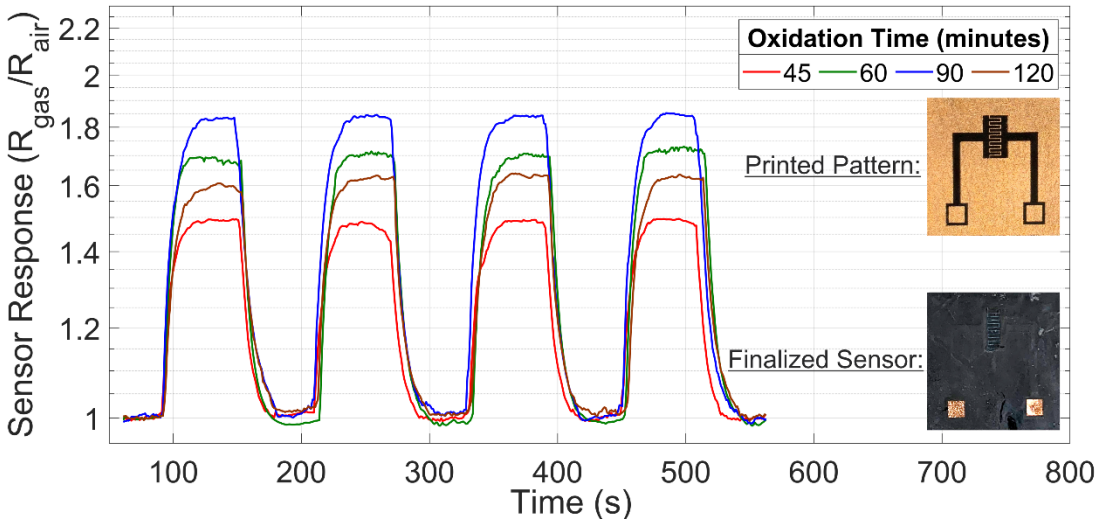


Figure 3.15: Sensors` responses of a VOC flexible gas sensors, electrical resistance changes by repeated exposure to 250 ppm ethanol vapor, with different copper oxide nanostructured morphologies, fabricated under: 45 minutes, 60 minutes, 90 minutes, and 120 minutes oxidation times.

The response times ($t_{Response,\ 90\%}$) were measured, respectively, to be 8 s, 9 s, 10 s, and 11 s. The recovery times ($t_{Recovery,\ 90\%}$) were measured, respectively, 10 s, 11 s, 13 s, and 14 s. The sensors` sensitivities ($S = \frac{R_{gas}-R_{air}}{R_{air}} \times 100$) were calculated, to be 50 %, 70 %, 85 %, 60 %, respectively. The obtained response/recovery times are faster than both microstructured CuO gas sensors that operate at higher temperature (≈400 °C) and room temperature nanostructured CuO gas sensors [100, 101]. The highest sensitivity of 85 % was observed in the sensor with a multiple-nanowire sensing layer, which is a slightly better sensing performance in comparison with previously reported CuO flexible gas sensors fabricated through the inkjet printing method [101]. Although higher sensitivities and similar response/recovery times have been reported in some of nanostructured CuO

gas sensors, their values were measured at elevated temperatures (above 200 °C) [100, 102]. The sensitivity was not improved any further beyond the 90 minutes oxidation time. This can be explained by the reduced number of active sites due to the decreasing surface to volume ratio of nanostructured copper oxide.

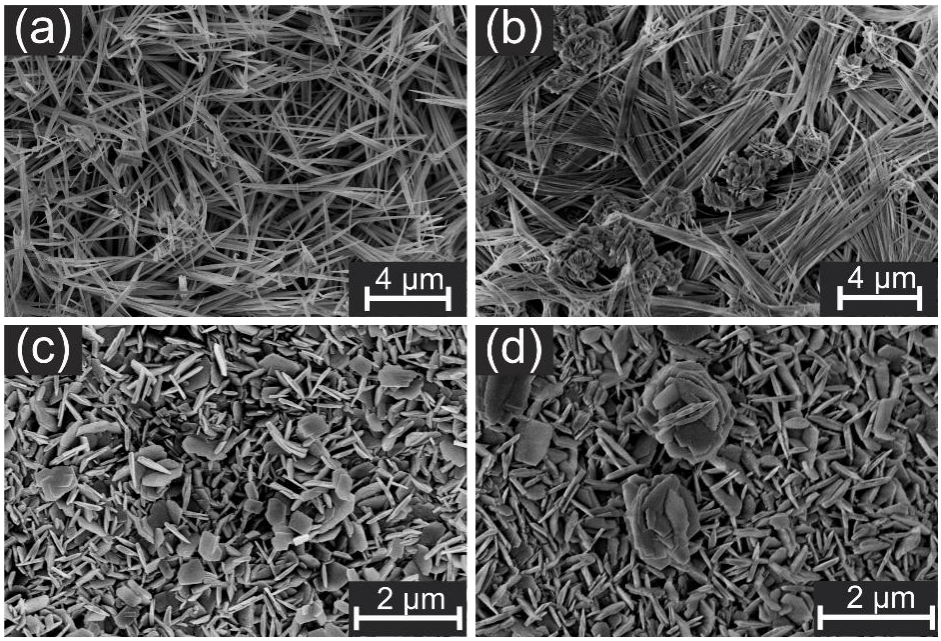


Figure 3.16: SEM images of copper oxide nanostructured morphologies after: (a) 15 minutes; (b) 120 minutes; (c) 180 minutes, and (d) 240 minutes.

The gas concentration used in this study was selected only for validation; however, different intensities in response to various concentrations of ethanol were observed. The detection limit and selectivity of this sensor were not studied; however, the detection limit and high selectivity of nanostructured CuO to VOCs with similar morphologies have been reported [102, 103]. The proposed sensor was capable of sensing ethanol vapor with high sensitivity at low operating temperature.

## 3.6 Summary

A decentralized production routine based on office-grade equipment to fabricate disposable sensors/devices on flexible substrates (i.e., paper, cloth, and plastic) was proposed. Functional units ranging from several nanometers to several centimeters can be fabricated by the proposed method. The fabrication of a typical sensor by this method mostly requires two major steps (wax and metal transferring) to define hydrophobic/hydrophilic contrast and form electrodes. The minimum channel width achieved in the wax transferring step and the minimum feature size in direct metal transferring were 200 µm, defined by the resolution of cutting or printing rendered by the office equipment. The minimum achievable gap size in IDEs was 100 µm, and the smallest feature of nanorods synthesized by a subsequent oxidation step was 80-10 nm diameter. The time duration to fabricate the components presented in this study (excluding the oxidation step for the gas sensor) varies between 1 and 3 minutes. The proposed method can be compared with other previously introduced methods from the perspective of, (1) electrode fabrication, and (2) hydrophobic/hydrophilic definition.

Researchers reported five prevalent techniques to fabricate electrodes on flexible substrates, including, screen printing, stencil printing, inkjet printing, micro-wire placement, and pen-on-paper [53]. Compared to these methods, the presented electrode fabrication step (metal transferring) has the following advantages: (1) lower cost [45, 46, 48-52, 55]; (2) simpler and faster steps [45, 46, 48-52, 55]; (3) better reproducibility [47, 54]; (4) ease of scale-up [47, 50, 54, 55]; (5) better consistency in electrode conductivity [45, 47, 49, 51, 52, 54]; (6) better stability under varying temperature and humidity conditions [45, 46, 48, 49, 51, 52]; (7) no substrate deformation (for paper-based devices)

due to soaking in chemical solutions [45, 46, 48, 49, 51, 52]; (8) compatibility with a wider range of chemicals due to the presence of a polymer sub-layer [47, 51, 52, 54], and (9) no need for customized equipment [45, 46, 48, 49, 51, 52].. A detailed comparison with previous methods is presented in table 3.2.

Table 3.2: Benefits of the proposed fabrication method compared to previously introduced methods to fabricate electrodes on flexible substrates

| **Advantages** | **Compared to** |
|---|---|
| Lower cost | Screen printing, Stencil printing, Inkjet printing, Micro-wire placement |
| Simpler and faster steps | Screen printing, Stencil printing, Inkjet printing, Micro-wire placement |
| Better reproducibility | Pen-on-paper (POP) |
| Easier to scale-up | Pen-on-paper (POP), Micro-wire placement |
| Better consistency | Pen-on-paper (POP), Inkjet printing |
| Better stability | Screen printing, Inkjet printing, Stencil printing |
| No substrate deformation | Screen printing, Stencil printing, Inkjet printing |
| Wider range of chemical compatibility | Pen-on-paper (POP), Inkjet printing |
| No need for customized equipment | Screen printing, Stencil printing, Inkjet printing |

Sixteen prevalent techniques in two categories (physical and chemical) were reported by researchers to selectively define hydrophobic/hydrophilic regions, including, wax patterning, flexographic printing, wax-screen printing, polydimethyl-siloxane (PDMS), ink stamping, subtractive laser treatment, inkjet etching, lacquer spraying, photolithography, chemical vapor deposition, plasma treatment, hand-held corona treatment, silane/UV-$O_3$ patterning, paper cutting and shaping, inkjet printing, and wet etching [69, 74, 75]. Compared to these techniques, the presented single-step

hydrophobic/hydrophilic contrast definition step (wax transferring) has the following advantages: (1) less number of manufacturing steps [56-67]; (2) no need for preparation of a medium layer [57, 67]; (3) faster hydrophobic/hydrophilic contrast definition (< 1 minute) [56-58, 60-67, 72]; (4) no need of customized specialty equipment and masks or modified printers [59, 60, 62, 64-66, 68, 70-73]; (5) compatibility with a wider range of substrates due to the use of lower temperature (< 110 °C) and faster heating time (< 25 seconds) [56, 73]; (6) higher repeatability, reliability, and controllability due to direct conversion of patterns from a digital file to a physical pattern and minimized manual steps [64, 66, 72]; (7) better flexibility [73], and (8) no need for further chemical treatment steps [56, 60, 65, 66, 70]. A detailed comparison with previous methods is presented in table 3.

Table 3.3: Benefits of the proposed fabrication method compared to previously introduced methods of hydrophobic/hydrophilic region definition

| Advantages | Compared to |
|---|---|
| Less fabrication steps | Wax patterning, Inkjet etching, Inkjet printing, Flexographic printing, Laser printing, Chemical vapor deposition, Plasma treatment, Hand-held corona treatment, Paper cutting and shaping, Wet etching, Polydimethyl-siloxane (PDMS) printing, silane/UV-O3 patterning |
| No need for a medium layer | Wax patterning, Wet etching |
| Faster manufacturing time | Wax patterning, Inkjet etching, Inkjet printing, Flexographic printing, Wax-screen printing, Laser printing, Chemical vapor deposition, Hand-held corona treatment, Paper cutting and shaping, Wet etching, Polydimethyl-siloxane (PDMS) printing, silane/UV-O3 patterning |
| No need for customized specialty equipment and mask | Inkjet etching, Inkjet printing, Flexographic printing, Wax-screen printing, Ink stamping, Subtractive laser treatment, Lacquer spraying, photolithography, Plasma treatment, Hand-held corona treatment, silane/UV-O3 patterning |
| Compatibility with wider range of substrates | Photolithography, Laser printing |
| Better repeatability, reliability, and controllability | Inkjet etching, Wax-screen printing, Hand-held corona treatment |
| Better flexibility | Photolithography |
| No need for further chemical treatment steps | Inkjet etching, Inkjet printing, Ink stamping, Laser printing, silane/UV-O3 patterning |

The proposed fabrication method is suitable for rapid prototyping devices, customized sensors, and scaled-up production. Fabrication costs of the presented devices in this study are just a few cents and initial equipment cost is minimal (< $250) since the listed office equipment is widely available as consumer products. In comparison

to 3D printing, a well-known decentralized fabrication method, this method may seem to require more equipment and steps; however, the equipment and supplies required for this method are far more accessible and much cheaper in terms of capital investment to acquire. Additionally, this method is more agile and adaptable in terms of the raw materials used and allows the user to choose from a wider range of easily accessible materials such as paper, cloth, metal sheets, and plastic films while also being robust and flexible in terms of the steps taken to fabricate the sensor/device. For example, the lamination step can be carried out using the thermal fuser of a laserjet printer rather than a laminator, and the cutting step can be carried out manually in place of a craft cutter. This flexibility also provides the user an advantage of creating sensors/devices customized to their individual needs cheaply and promptly.

Regarding the presence of silica, iron oxide, and PP wax in the printer toner [76, 104], no adverse effect was observed on the sensor's performance. Iron oxide remains within the printer cartridge after printing and silica is a chemically stable material, while the PP wax does not permeate the paper substrate laterally beyond the pre-cut boundary during the heating/lamination process at the given condition due to relatively low temperature. Additionally, utilizing polyester makes the fabricated components compatible with a wide range of detection experiments due to its physical robustness and chemical stability. Even though this study only presented sensors dependent on varying electrical resistance, fabrication of components that rely on other working principles, such as electrochemical sensors, is also feasible.

# CHAPTER 4: NANO-SORBENT DEVICE FABRICATION

Some of the materials used in this chapter have been previously published by IEEE:

A. Bamshad and H. J. Cho, "Digital microfabrication on paper and cloth For heavy metal detection and remediation." 2019 20th International Conference on Solid-State Sensors, Actuators and Microsystems & Eurosensors XXXIII (TRANSDUCERS & EUROSENSORS XXXIII). IEEE, 2019.

## 4.1 Introduction

In this chapter, the introduced method of fabrication devices is utilized to fabricate a nano absorbent cloth for removal of arsenic to explore the environmental applications of this method. For this purpose, a novel cloth-based DIY nano-sorbent filtration system to effectively remove As(III) from As-embedded wastewater was designed, fabricated, and studied. Cloth as a cheap, flexible, and porous material that is widely available all over the world is an excellent candidate to make such DIY water filtration systems. Adsorption as the removal mechanism and CuO nanostructures as the sorbent are utilized in filter layers. The CuO nanostructures were chemically grown on top of the transferred commercial copper leaf. A thin layer of polystyrene was used as the intermediate layer to transfer the copper leaf to cloth, due to its stability in contact with a wide range of chemicals. Simplicity, lower cost, faster filtration, and no power requirements are the main advantages of the proposed arsenic removal system compared to previous studies.

Arsenic is abundantly available in the earth`s crust [25, 105]. This element has a wide range of applications in the electronic industry, metal manufacturing, and agriculture

[25, 105]. Despite its industrial benefits, the toxicity to the human body of this metalloid element is well-documented [25]. Various human health problems such as cancer, skin lesions, and discoloration, carcinogenesis, kidney diseases, diabetes, and intestinal maladies have been reported as a result of long-term exposure to this heavy metal [25, 105-108]. Human exposure to this element mostly occurs through ingestion, although the other types of exposure, including inhalation and dermal absorption, were also reported [109]. Natural and anthropogenic activities are the main sources of this element in groundwaters [25, 105]. Dissolved inorganic arsenic in groundwater, consequently ingested by drinking or using the contaminated water is a serious problem, which can put the health of hundreds of millions of people at risk in developing countries [25, 106, 110].

Different arsenic removal techniques to remediate this pollutant from water resources and supplies have been studied by many researchers, such as adsorption using activated materials, coagulation, precipitation, nanofiltration, oxidation, reverse osmosis, and ion-exchange [111-114]. Among the prevalent arsenic removal techniques, adsorption is a popular method due to its simplicity and relatively low cost [107, 115]. Utilizing metal oxide nanostructures as nano-sorbents to remediate arsenic has been recently proposed [116, 117]. Its main advantages include high removal efficiency, rapid removal process, low fabrication cost originated from a large surface area compared to other techniques [115]. Iron, titanium, zirconium, and copper oxides (CuO) are the most common materials employed for this purpose [25]. CuO has been selected among these materials for this study due to its unique features. CuO can be made to produce a larger surface area and a higher number of active sites for the adsorption of arsenic [118]. In addition, copper is an inexpensive metal that is easily commercially available in the form

of a leaf. Transferring such copper leaf on flexible substrates and growing CuO nanostructure were demonstrated just by using a set of office equipment in our previous work [26, 119]. A filtration system can be made by the proposed method without incurring a high equipment cost.

The most prevalent forms of arsenic that exist in water are As(III) (known as arsenite) and As(V) (known as arsenate) [105, 107]. Arsenite, which is the predominant form of arsenic in drinking water, is generally uncharged; thus, it is more mobilized and harder to remove from water. It has also been reported to be about 25-60 times more toxic than arsenate to the human body [109, 120, 121]. Typically, a pre-treatment oxidation process to convert arsenite to arsenate is required before removing this pollutant from water in most of the filtering technologies [25]. Although, a few different methods independent of the pre-treatment step were already introduced; these techniques still require other extra steps [105, 106, 109, 118]. Dependence on expensive equipment such as furnaces, centrifuges, and vacuum pumps. as well as the requirement of complicated, additional steps are the major barriers to on-site applications, especially for resource-limited areas where residents are truly impacted by the exposure to these harmful substances [105-107, 109, 118, 120].

The World Health Organization (WHO) recommends 10 mg $L^{-1}$ of arsenic as the permissible limit in drinking water [25, 105, 106, 122]. Given the fact that most developing countries are struggling with this problem in their groundwater supplies (up to 100 mg $L^{-1}$), a simple, affordable, robust, one-step, environmentally friendly technology with no power requirement for arsenic removal to bring it down to less than 10 mg $L^{-1}$ has great importance for the affected communities. The concept of DIY to make simple devices has

been introduced already. Although industrial-scale water filtration systems are utilized in developed countries. The impoverished communities cannot afford such systems. Hence, decentralized DIY manufacturing methods can be an efficient and feasible solution to address the polluted water problem in the affected regions.

## 4.2 Material Synthesis

The cloth-based nano-sorbent devices were made by a two-step – pattern transfer and oxidation – fabrication technique, figure 4.1. A laser-jet printer was used to print out the filter patterns – designed by a CAD software – on cloth as shown in figure 4.1(a-b). During the metal transferring step, a thermal laminator was utilized for embedding toner particles into a fibrous matrix, which works as binding materials for selectively transferring the copper leaf sheet to the printed area. Finally, to emerge the final sorbent patterns as shown in figure 4.1(c), a brush was used to wipe out the surface and removing the residue of the copper leaf; the copper leaf was used to cover the printed area before the lamination step. Subsequently, a craft cutting machine was used to cut sorbent layers, figure 4.1(d). Before growing CuO nanostructures, a typical cleaning protocol to remove dust, impurities, and native CuO was used. For this purpose, the sorbent layers were washed with ethanol, rinsed with deionized water, washed with 2 M hydrochloric acid, and again rinsed with deionized water, respectively. Eventually, as illustrated in figure 4.1(e), the nanostructured CuO was grown at room temperature over the transferred copper layer by the following oxidation reaction [26, 123]:

$$Cu + 4NaOH + (NH_4)_2S_2O_8 \rightarrow CuO + 2Na_2SO_4 + 2NH_4OH + H_2O$$

To obtain different morphological shapes, the sorbent layers were soaked in a stock solution of 1 M sodium hydroxide and 35 mM ammonium persulfate for oxidation times ranging from 15 to 120 minutes. To have a uniform fluid flow and increase contact time during the filtration process, three different grades of filter paper (number 3, 1, 4, respectively) were used on top of the nanostructured CuO absorbent layers, figure 4.1(f); water-based acrylic paste was used to attach the layers. The uniform fluid flow could be formed through the constructed multiple layers, which have complementary patterns as shown in figure 4.1(g).

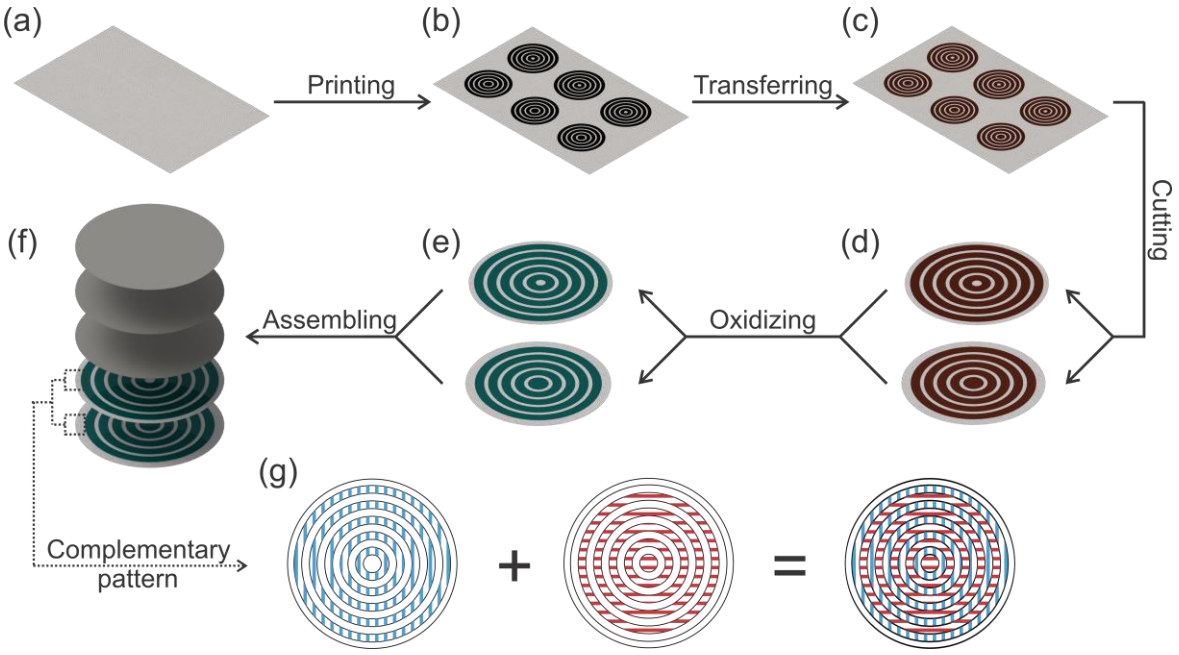


Figure 4.1: Fabrication steps of a nanostructured copper oxide double-layer filter on cloth for arsenic removal: (a-c) printing pattern and copper transferring; (d-f) cutting, oxidizing, and stacking filter layers, and (g) Complementary patterns used to cover the surface.

## 4.3 Design of Experiments

The arsenic adsorption mechanism was studied through XPS (Thermo Scientific ESCALAB XI+, USA) analysis. The batch experiment and kinetic studies were conducted to study the optimum CuO morphology, maximum adsorption capacity, kinetic modeling, and development of adsorption isotherms. Distilled water was spiked with As(III) standard solution to obtain 50 µg/L, 500 µg/L, and 1,100 µg/L arsenic-spiked water samples for the experiments. These concentrations represent samples of water with low, moderate, and high concentrations of pollutants, respectively. As(III) is the most dominant form of arsenic [107, 124]; it has a lower affinity for the surfaces of the various adsorbents and was employed in the studies due to its higher toxicity when compared to As (V) [125]. All the stock solutions were prepared under constant pH level. Also, the effect of different pH values (3 to 8) and competing anions on arsenic adsorption were investigated. All the experiments were conducted in triplicate at controlled room temperature (21 °C). Additionally, new materials and filters were used for each experiment. Blank experiments were conducted alongside all experiments to remove potential error sources.

Figure 4.2 shows the experimental setup used for the batch experiment and kinetic studies. Two complimentary cloth-based sorbent layers, three layers of filter paper, one layer of glass microfiber filter, two PVC unions (as supporting stand for filter layers), and one PVC pipe were used to complete this system. This system works with gravitational force and does not require auxiliary equipment and electricity, which can make it an appropriate remediation tool for resource-limited regions. The passage of the contaminated water through this connection, with multi-layer construction, is shown in figure 4.2. This system consisted of three major processing units, arsenic removal by CuO

nanostructures, CuO removal by silicon dioxide ($SiO_2$), and $SiO_2$ particle captured by a glass microfiber filter, respectively. $SiO_2$ has been used due to its ability to remove copper nanoparticles [105, 106]. A water-based acrylic paste was used to attach layers; also, plastic O-rings were used to seal PVC unions.

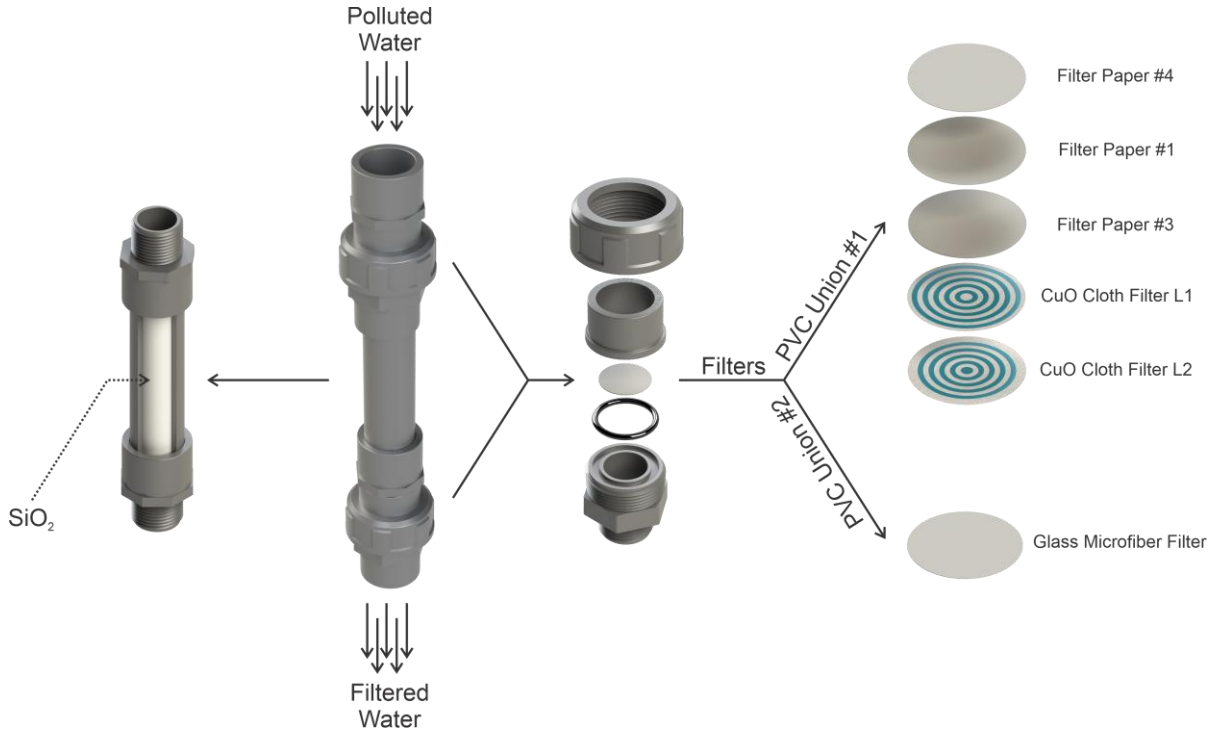


Figure 4.2: Schematic image of arsenic remediation system used; PVC unions, pipe, silicon dioxide, filter papers, cloth-based sorbent layers, and glass microfiber filter are shown.

## 4.4 Adsorption Mechanism

The XPS analysis was conducted on the surface of the copper leaf after the oxidation step. It investigates the presence of grown copper oxide, the chemical state of elements, and the adsorption mechanism of arsenic. This analysis was performed on five different samples. Figure 4.3 shows XPS surveys of the grown CuO on the top of a cloth filter layer (90 minutes oxidation duration), before and after passing the As(III) polluted water

through. The samples were rinsed with distilled water before XPS analysis to wash out unattached chemicals. The XPS survey scan reveals the presence of oxygen and copper on the adsorbent layer. Additionally, the presence of arsenic was confirmed by observing the peaks of this element (As 3d, As 3p, As 3s, As LMM, and As $2p_{1/2}$) on the adsorbent surface after polluted water passage. This confirms the adsorption of arsenic on the grown metal oxide on top of the cloth.

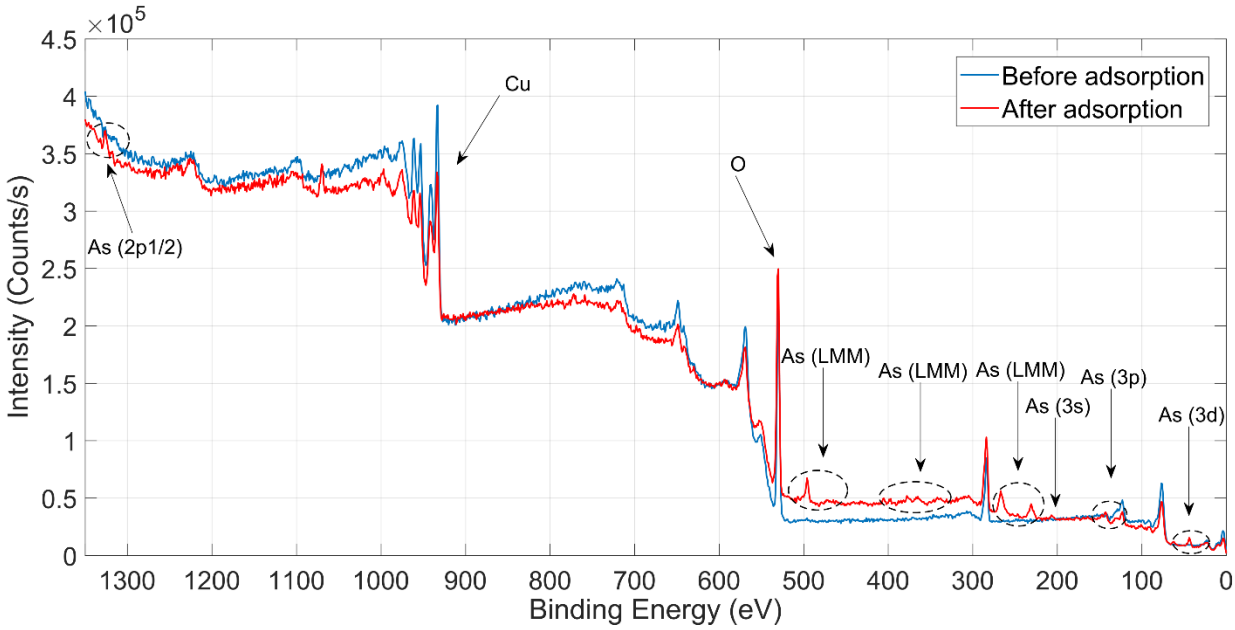


Figure 4.3: XPS survey scan of the surface of nano-sorbent filters before and after the pollutant adsorption.

Figure 4.4 shows the spectra for the Cu 2p region core levels and shake-up satellites. It shows the main peaks of Cu $2p_{3/2}$ and Cu $2p_{1/2}$ appear around 934.4 eV and 954.0 eV, respectively, which are associated with $Cu^{2+}$ species. The other peaks for the core levels are observed around 932.8 eV and 952.6 eV, which are assigned to $Cu^{+}$ species.

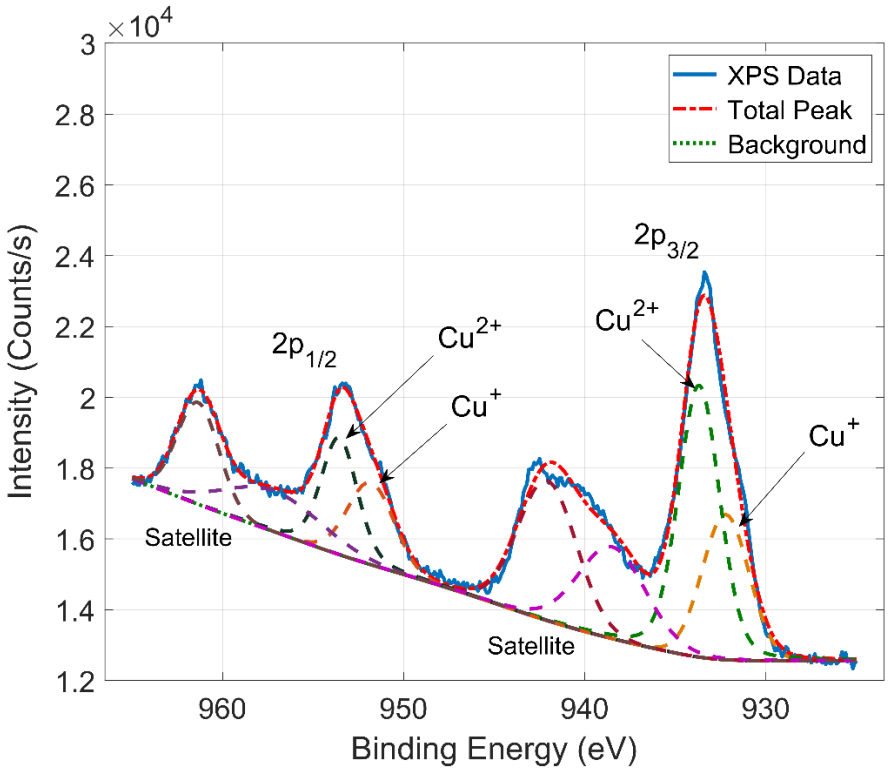


Figure 4.4: High-resolution spectra of the grown copper oxide nanostructures.

Figure 4.5 shows the fitted spectra for the O1s; two peaks at 530.2 eV and 531.4 eV are respectively assigned to CuO and $Cu_2O$ species. The obtained peak level confirms the presence of CuO as the main compound after oxidation. The reduction of CuO to $Cu_2O$ can explain the presence of $Cu^+$ (cuprous oxide) in this analysis. However, further investigation on arsenic spectra is required to validate this assumption.

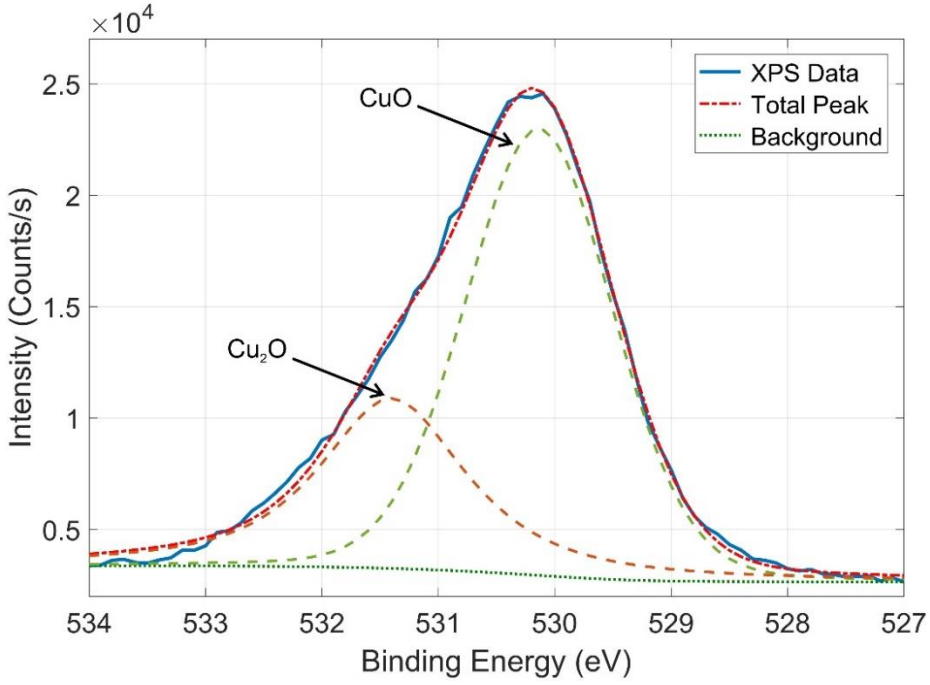


Figure 4.5: High-resolution spectra of oxygen on the grown copper oxide nanostructures after adsorption of As(III).

Figure 4.6 shows the spectra for the As 3d. This spectrum exhibits two peaks at 43.5 eV and 44.2 eV, which are assigned to As(III) and As(V), respectively. The presence of As(V) while As(III) was the only form of the pollutant in the aqueous solution concludes the oxidation of As(III) to As(v) on the surface of CuO. The oxidation occurred through electron transfer near the surface of CuO before the adsorption. This electron transfer ultimately results in the reduction of CuO to $Cu_2O$. Similar results have been reported in many other studies [105, 126]. The adsorption of both forms of arsenic on the surface of CuO nanostructures previously was reported [118]. Additionally, the presence of hydroxyl groups on the surface of CuO explains the adsorption affinity for arsenic [107, 127]. Therefore, the adsorption of arsenic on the surface of CuO that is immobilized on the fabric surface is the adsorption mechanism of the filter.

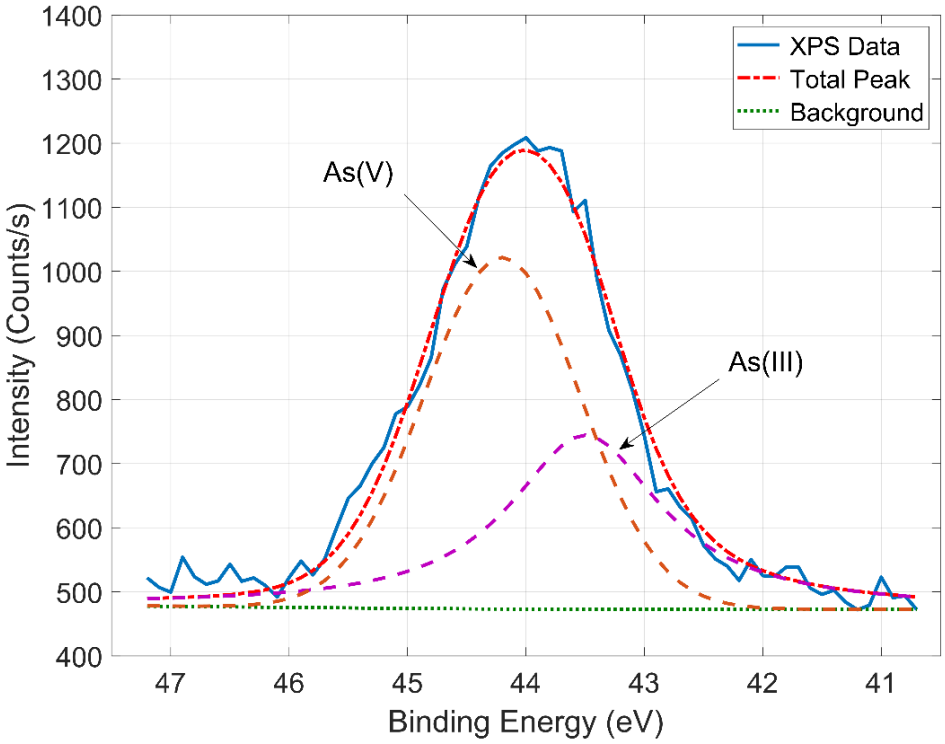


Figure 4.6: High-resolution spectra of arsenic on the grown copper oxide nanostructures after adsorption of As.

## 4.5 Morphological Study

The morphology study was conducted to investigate the morphological evolution of CuO over prolonged oxidation time and its impact on arsenic removal efficiency. Various CuO samples were prepared on cloth by increasing the duration of oxidation from 15 minutes to 120 minutes, figure 4.7. The progress of oxidation was indicated by color changes from shining opaque red (15 minutes) to matte light green (30 minutes), matte dark blue (45 minutes), and matte dark black (120 minutes) at room temperature subsequently.

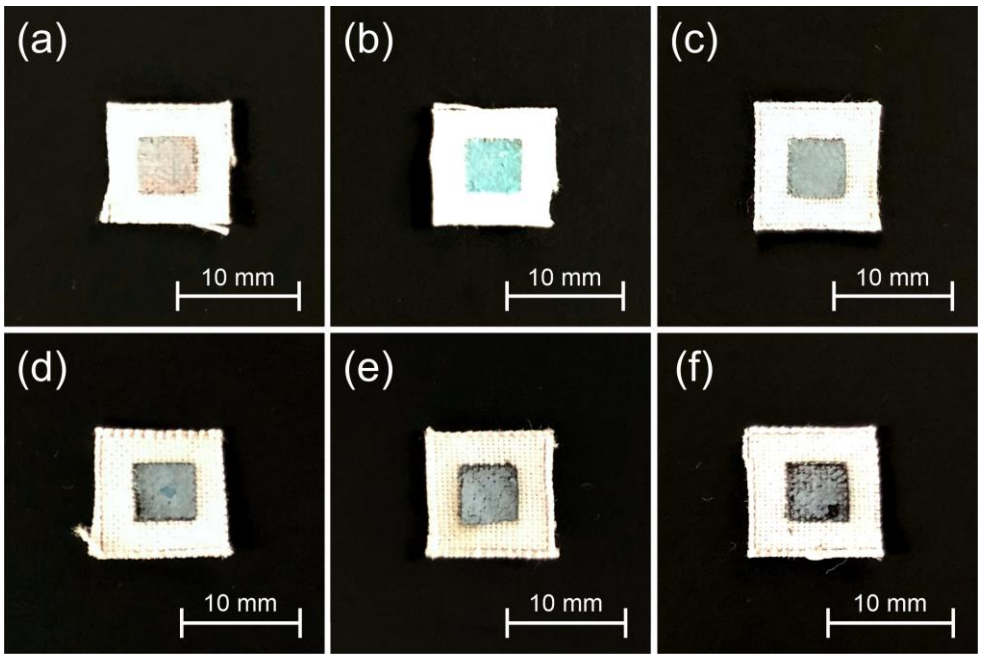


Figure 4. 7: Color changes of transferred copper leaf on top of cloth after oxidation for: (a) 15 minutes; (b) 30 minutes; (c) 45 minutes; (d) 60 minutes; (e) 90 minutes, and (f) 120 minutes.

The examination of synthesized CuO products by SEM (FEG-SEM, Zeiss Ultra-55, Germany) shows nanowires with 80-100 nm diameters and 6 µm length were obtained during the early stages (15 minutes) of oxidation, figure 4.8(a). Increasing oxidation time to 30-45 minutes results in forming bundles of nanowires of the same length, figure 4.8(b-c). An increase in the density and length (≈8-10 µm) of the nanowires bundles was observed by increasing the oxidation time to 60-90 minutes, figure 4.8(d-e). Finally, the tip of some nanowires bundles has grown bigger and formed nanoflowers of 400-500 nm diameter, figure 4.8(f). This phenomenon is accompanied by a decrease in the number of smaller nanowires. Although the emergence of nanoflowers increases the surface area, increasing the diameter of the nanowires can reduce the overall surface area and subsequently active sites for adsorption of arsenic. The effect of this phenomenon was

determined by examining the efficiency of arsenic removal. Increasing the oxidation time to more than 120 minutes results in the emergence of nanoflakes (100 nm thickness – 750 nm length) and nanoflakes-flowers (2 μm diameter) [119]. The low adhesion of these nanostructures to the surface of the melted toner on top of the fabric, which is due to their high weight, is the reason for not studying samples with an oxidation time higher than 120 minutes.

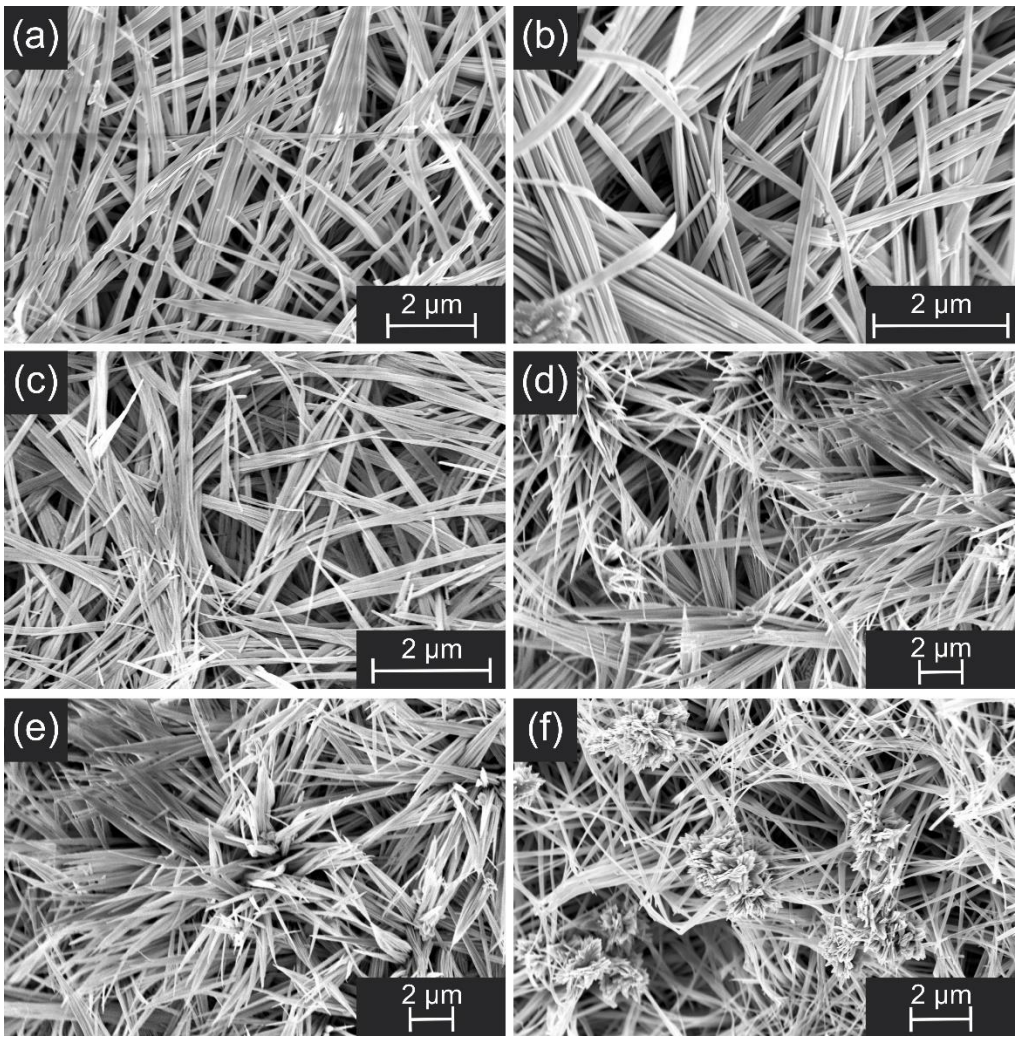


Figure 4.8: SEM images of different morphologies of nanostructured CuO immobilized on cloth after oxidation for: (a) 15 minutes; (b) 30 minutes; (c) 45 minutes; (d) 60 minutes; (e) 90 minutes, and (f) 120 minutes.

## 4.6 The Batch Adsorption Study

The removal efficiency of each morphology was individually investigated through the batch adsorption experiment. For this purpose, 50 ml of polluted water with three different concentrations of As(III) solution were passed through the filtration system with various oxidation times. Figure 4.9 shows the nano-sorbent filter layers with various oxidation times that was used in this study. The concentration of arsenic was measured using ICP-MS (Thermo Scientific iCAP Qc, USA) before and after the filtering process.

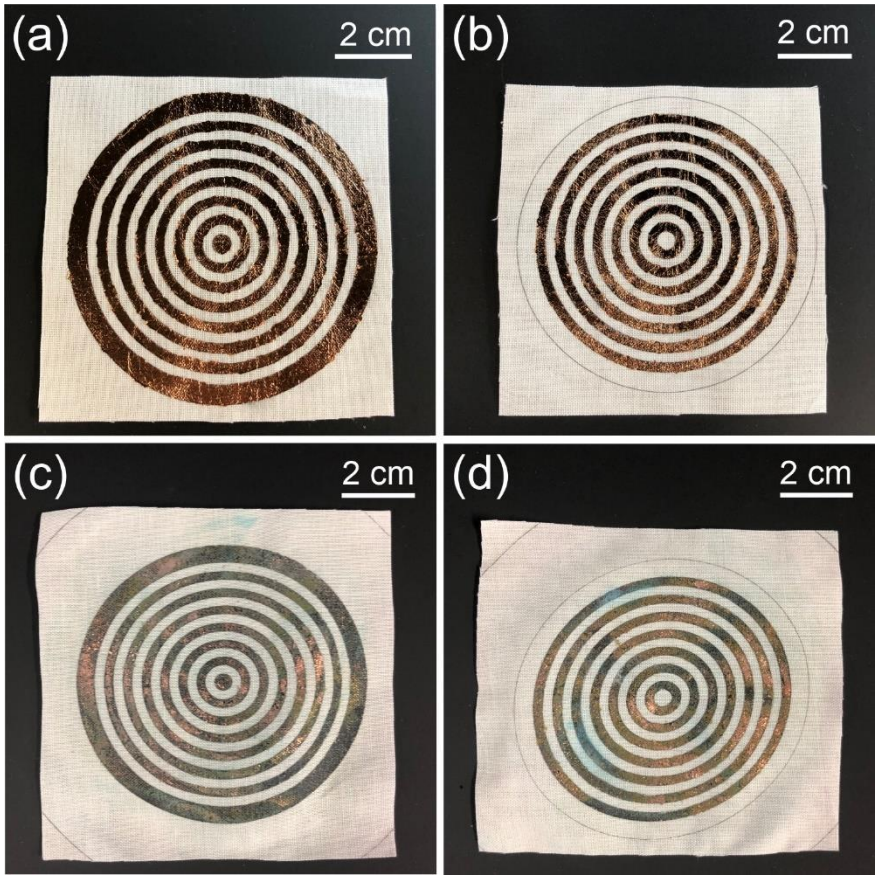


Figure 4.9: Filter ring patterns on cloth; images of top and bottom layers: (a-b) after copper leaf transfer, and (c-d) after oxidation for 15 minutes.

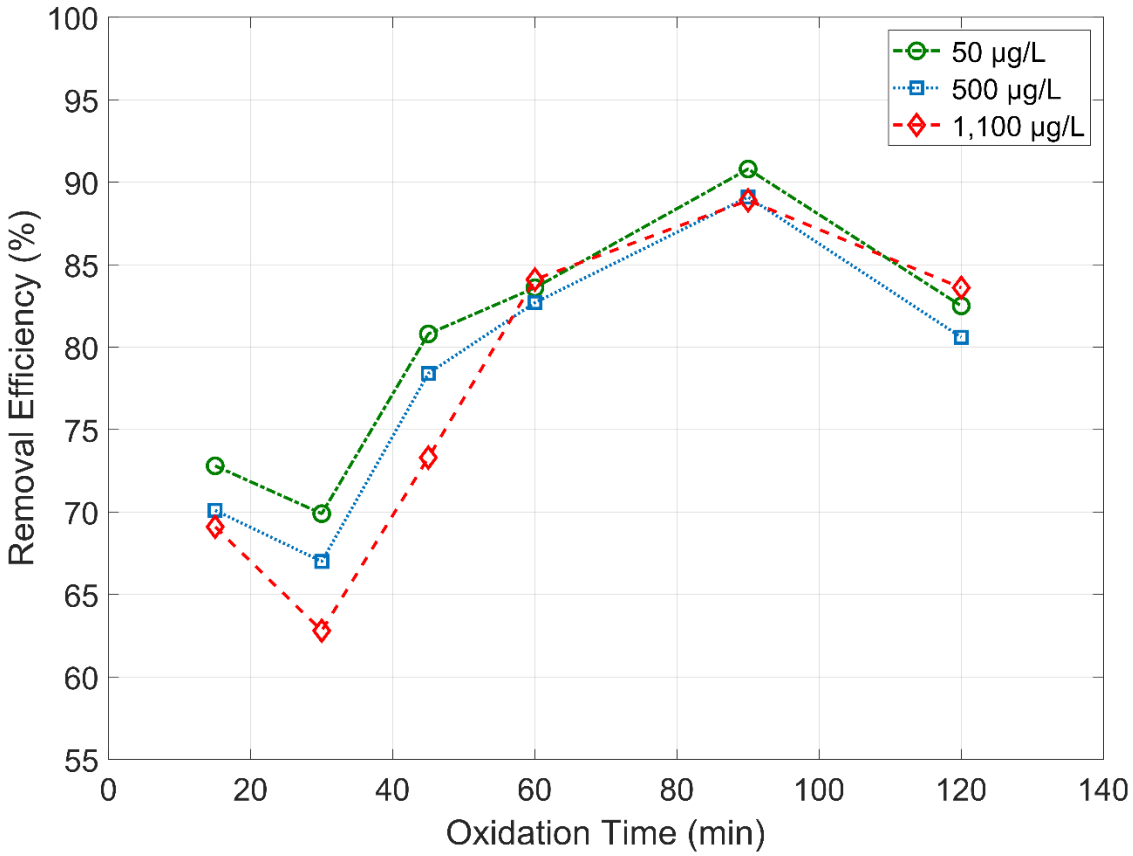


Figure 4. 10: The arsenic removal efficiency of the filter with different nanostructure morphologies in contact with various concentrations of arsenic-spiked water (a) 50 µg $L^{-1}$; (b) 100 µg $L^{-1}$, and 500 µg $L^{-1}$.

Figure 4.10 shows the removal efficiency for each level of concentrations versus oxidation times. Similar removal performance in contact with various concentrations of arsenic was observed. The best performance in arsenic removal was observed in the filters created by the 90-minute oxidation process. The second-best performance was observed in the filters created by the 60-minute oxidation process, which has similar nanostructured CuO morphology. This agrees with the SEM morphological observations that demonstrate the nanowire bundles possess the most active sites for adsorption.

The utilized filtration system consists of different parts that could be a source of interference in the adsorption of arsenic. These include cellulose fibers in the filter papers, borosilicate fibers in the glass fiber filter, mixed cellulose/polymers fibers in the fabric, polystyrene particles in the laserjet toner [26, 76, 119]. To validate the lack of interference from the components other than the CuO in the adsorption of the arsenic blank experiment was conducted. In the blank experiment, the amount of arsenic removed after passing through the experimental setup without copper oxide was investigated. No change in the arsenic level was observed, demonstrating that the adsorption mechanism is solely dependent on the nanostructured CuO.

The possible breakage/detachment of CuO nanoparticles with attached arsenic may end up carrying arsenic into the filtered water, which causes a decrease in the arsenic removal efficiency. To capture possibly detached nanoparticles, $SiO_2$ was utilized after the cloth filter layers. The ability of $SiO_2$ to capture such nanoparticles already has been reported [105, 106]. Additionally, this ability was utilized to confirm the source of the detected arsenic after the second PVC union and was done by measuring the concentration of copper in water before and after passing through the $SiO_2$ layer. Traces of copper were detected after the CuO cloth filters; however, no significant traces of copper were observed after the $SiO_2$. This shows the source of the detected arsenic at the outlet was solely the unfiltered polluted water, which was not bound to detached nanoparticles. It was observed that this can be resolved by adding extra CuO filter layers to increase contacting time.

## 4.7 The Effect of Co-Existing Anions and pH

There are several co-existing anions such as nitrate, chloride, sulfate, and phosphate in natural water along with arsenic, which may interfere with the adsorption process [128]. To investigate the selective removal of anionic arsenic compared to these anions, the removal efficiency of identical filters (90 minutes oxidation time) in the presence of these anions was investigated. The concentrations of arsenic and co-existing anions were maintained at 100 mg l-1 for this study. Except for phosphate, no significant effect was observed on the efficiency of arsenic removal due to the presence of these anions. Consistent with prior research, it demonstrates that nanostructured CuO has a stronger affinity for arsenic than other anions commonly found in natural water [109]. Similar interference of phosphate on arsenic removal has been discovered in previous studies, which can be explained by the chemical similarities between these two elements that are classified in the same group of the periodic table [128, 129].

It has been reported that the initial pH of water influences the adsorption of heavy metals for most adsorbents [117, 130]. To study this, arsenic removal was studied for 50 ml arsenic-spiked water samples at pH ranging from 3 to 8. The nano-sorbent cloth filter was found to be effective at removing arsenic in this pH range. The As(V) removal for pH values greater than 8 is lower compared to lower pH values. Also, As(V) removal considerably decreased at pH 11. This abrupt decrease in adsorption efficiency could be caused by an increase in the production of hydroxyl ions ($OH^-$), which begin competing with the arsenic ions [122, 131]. The findings show that such nanowire bundle morphologies are well suited for usage in a wide range of pH environments for arsenic removal.

## 4.8 Summary

In this chapter incorporating nanostructures via a metal transfer process for functionalization and embedding on a cloth medium was shown to be efficient as well as novel. The data obtained indicate that the arsenic contamination was reduced by an order of magnitude in a matter of minutes. Increasing the number of sorbent layers may result in an increase in the removal efficiency and total removal capacity. The laserjet toner works as an active binding material to transfer the copper leaf to the fabric. This material mostly consists of polystyrene particles [76]. No evidence of intervention was observed upon an investigation of the effect of the toner on arsenic removal efficiency carried out by passing the contaminant through the same fabric filters in the absence of Cu/CuO. The use of fabric to settle copper oxide and prevent the penetration of these particles into clean water was accompanied by the addition of protection by a glass filter.

Compared to earlier copper oxide nanoparticle-based methods, the proposed system has several advantages, including: 1) better removal efficiency [107, 122]; 2) lower overall cost [105, 107, 132]; 3) real-time and robust filtration without taking extra and time-consuming steps that required around 24 hours [105, 106, 109, 133]; 4) independence from auxiliary equipment (i.e. external pumps, centrifuge, etc.) for water filtration [105, 106, 133]; 5) simplicity and fast fabrication process [132, 134, 135]; 6) no need for pre and post treatment steps such as elevating temperature during fabrication of CuO nanostructures or filtration of arsenic [109, 133-135], and 7) filter fabrication solely based on widely available office-grade equipment (laserjet printer, thermal laminator, metal leaf) [106, 107, 122].

# CHAPTER 5: MICROPLASTIC FABRICATION

Some of the materials used in this chapter have been previously published by Elsevier:

A. Bamshad and H. J. Cho, "A novel print-and-release method to prepare microplastics using an office-grade laserjet printer; a low-cost solution for preliminary studies." Marine Pollution Bulletin 170 (2021): 112601.

## 5.1 Introduction

In this chapter, first, a novel print-and-release technique to prepare color-tagged microplastic (polystyrene) particles is introduced. Printing the laserjet toner on a water-soluble receptive/sacrificial layer is the working principle of the proposed method. Preparation of microplastics via this protocol is inexpensive, simple, rapid, robust, and fully controllable, without requiring any special equipment except an office-grade laserjet printer. Visibility of the colored particles (bigger than 100 μm) with unaided eyes is another advantage of this method. Therefore, the consistency and accessibility of the proposed microplastics preparation protocol are significantly useful for designing experiments that require multitudes of microplastic samples with desired sizes and shapes. In order to demonstrate the applicability of the fabricated microplastics to a designed experiment, the microplastic samples were removed and collected successfully by a newly proposed antibiotic binding and magnetic separation.

The unrelenting increase of non-biodegradable plastic wastes during the recent century has become one of the major environmental threats [136, 137]. The presence

and harmful effects of plastic debris in water resources such as rivers, lakes, seas, and oceans have been well documented [138-140]. The trace of floating plastic particles in the atmosphere has also been observed [138-141]. It is estimated that more than 5.25 trillion particles weighing at least 243,948 tonnes are floating in the oceans and this number is continuously increasing [142]. It was observed, during an only one-year time period in 2010, between 4.8-12.7 million tonnes of plastics entered into oceans across the globe [142, 143]. As a result, microscopic plastic particles (known as microplastic) are considered among the most widespread modern pollutants [144]. Their persistent presence and propagation in aquatic ecosystems pose a potential threat to all living creatures on this planet [108, 145].

Various aspects of long-term exposure of this pollutant on living tissues are not still completely understood [146]. This pollutant can directly enter our bodies through respiratory or digestion systems [140, 141]. The presence of this contaminant in filtered water, liquors, etc. already has been reported [147, 148]. Microplastics can also enter our diets, indirectly, by the consumption of contaminated seafood as well [149, 150]. Additionally, microplastics can serve as carriers for other harmful chemicals and toxins that can pass through prevalent industrial filtration systems and cause health hazards [137, 151]. In order to fully grasp the risk of microplastics, it is necessary to conduct more well-designed experiments in this area.

According to previous studies, polystyrene (PS), polyamide (PA), polyvinyl chloride (PVC), polyethylene (PE), and polypropylene (PP) are the most commonly found microplastic particles in aquatic environments [152, 153]. Among these polymers, PS, PE, and PP have higher transportability – in other words, these polymers will not settle

down in aquatic environments due to their lower density compared to seawater [154-156]. Recently the presence of theese microplastics in returnable and single-use water bottles has been also discovered [140]. Direct and indirect use of polluted water resources in agriculture and fish farming as well as abundant consumption of bottled water that is highly prone to microplastic contamination prompts the urgency of determining unknown aspects and human health implications of microplastics.

Difficulties to conduct laboratory studies on microplastics stem from two aspects – preparation and detection. A lack of reliable methods to replicate the microplastic samples is one of the main challenges in the design of experiments for systematic studies. The existing methods have relied on special equipment (e.g. ultra-low temperature freezer, cryostat microtome, etc.) to produce samples, which is costly but inconsistent in controlling the particle size due to non-automated procedures, e.g., manual fiber alignment, coffee grinder cutting, etc. [146, 157] In the field of detection, dependency on special detection instruments (e.g. μ-FTIR, μ-Raman, etc.) restricts easy access to setting up even preliminary experiments [138, 140]. Hence, it is imperative to secure a replicable, consistent, on-demand method, which can produce optically discernable microplastics with various shapes and a wide range of dimensions suitable for the targeted study.

## 5.2 Fabrication Method of Microplastics

Figure 5.1 illustrates the microplastic sample preparation steps. A printable transparent film was first covered with a thin layer of the water-soluble receptive/sacrificial layer (clear gloss precoat), which is mostly used to improve the quality of printing on glossy surfaces, figure 5.1(a-b). This step was performed through a three-step spin-

coating step – 300 RPM for 20 seconds, 1000 RPM for 50 seconds, and 300 RPM for 20 seconds – to create a uniform thickness over the entire surface of the substrate, which ultimately provides uniform contact with the OPC drum, and minimizes thickness error of particle printing. The microscopic plastic pattern with the desired geometry was first designed in CAD software and then printed on top of the coated layer by using a laserjet printer after drying the receptive/sacrificial layer at room temperature, figure 5.1(c-d). Two blank sheets were printed before microplastic printing with the same printer, to remove any residue from previous printings and clean the OPC drum with the wiper blade. Neutralization of the heating effect in the printing process was performed by considering a one-minute time delay between printing a new sheet. Plastic particles were printed with a resolution of 1200 dpi (dot per inch), no geometry line thickness (after filling inside the patterns), and a halftone of smoothing.

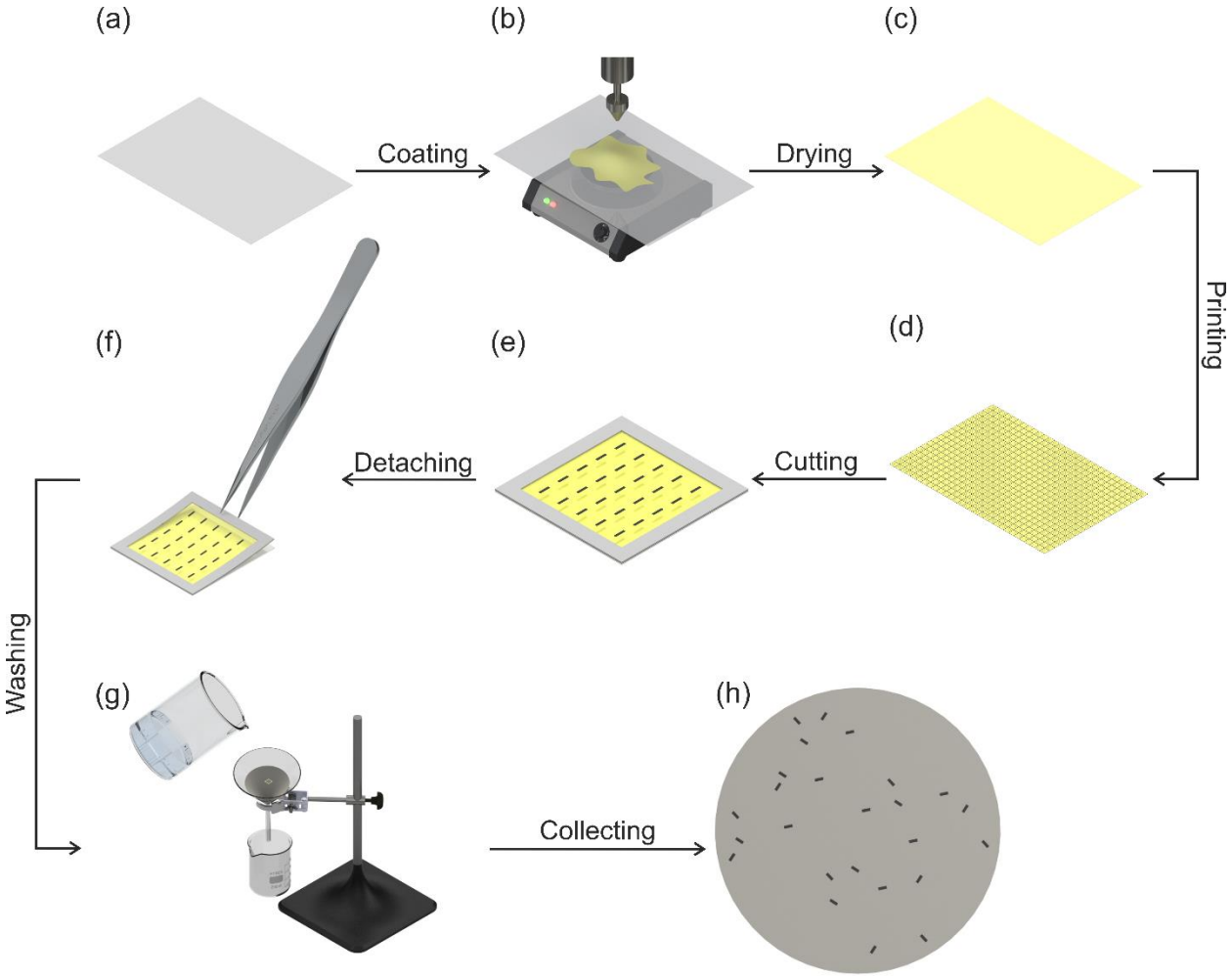


Figure 5.1: Microplastic preparation steps: (a-b) coating the receptive layer on a printable transparent plastic film; (c-d) drying the receptive layer and printing the microplastic on top of it; (e-f) cutting and framing a certain segment of the printed microplastics, followed by removal the receptive layer, and (g-h) filtering, washing, and rinsing the microplastic samples followed by collection from the top of a glass fiber filter.

A segment of the printed film containing the desired number of plastic particles required for the experiment was cut, then framed with a border of scotch tape, figure 5.1(e). This creates a supportive frame around the segment, which allows for easier removal of the receptive layer from the surface using a pair of tweezers, figure 5.1(f). The thin layer was transferred on top of a glass fiber filter, which was placed inside a

borosilicate glass funnel, accompanied by rinsing with ethanol, isopropyl alcohol, and distilled water, respectively, figure 5.1(g). Unlike regular filter papers, glass fiber filters take significantly more time for the filtration process; however, regular filter papers result in cellulose fibers binding to the plastic particles whereas the glass fiber filters prevent this occurrence (ATR-FTIR study). Ultimately, the microplastic particles were collected directly from the unfolded glass fiber filter followed by a drying step at room temperature, figure 5.1(h). The thickness of the printed and collected particles without further changes in the laserjet cartridge was measured 6 µm. This thickness can be adjusted according to the desired thickness of particles needed by changing the distance between the wiper blade and the OPC drum in the cartridge of the printer.

## 5.3 Physical Analysis

Particle size analysis was performed to characterize and evaluate the effectiveness of the proposed print-and-release method through physical studies. Particle size analysis was conducted to evaluate repeatability/production error and investigate the minimum achievable particle size. The dimensions and quality of plastic particles were investigated with scanning electron microscopy (10 keV). An open-source software (ImageJ) was used to process SEM images.

Microplastics in different geometries (circular, rectangular, and triangular) with dimensions from 100 µm to 500 µm were designed (in CAD software) and printed for this study. This range was selected due to the resolution limit of office-grade printers, which is 100 µm. Figure 5.2(a-c) shows the fabrication of microplastic particles utilized for particle size analysis study. Figure 5.2(a) shows printed circular particles with 500 µm

diameter. This particle size was selected for better visualization. Figure 5.2(b) shows the cutting/detachment processes of the printed microplastics. Figure 5.2(c) shows the collected microplastics after the washing step. The microplastics were successfully printed in the desired geometry with no significant difference in their size. This demonstrates the ability to fabricate microplastics with various transportabilities. Inability to make specimens consistently, with a feature size of less than 100 µm was observed. The sharp corners in designed microplastic with a feature size of less than 150 µm were observed as round corners after the printing step. These can be explained by the limitations of lasers used in the printer. Reconfiguration of the laser structure in laserjet printers can help to overcome this limitation. Figure 5.2(d-f) shows SEM images of printed microplastics in different geometries. An identical thickness (6 µm ± 1 µm) was observed for the collected samples. This thickness was obtained without providing any changes in the distance between the wiper blade and the OPC drum in the cartridge of the printer.

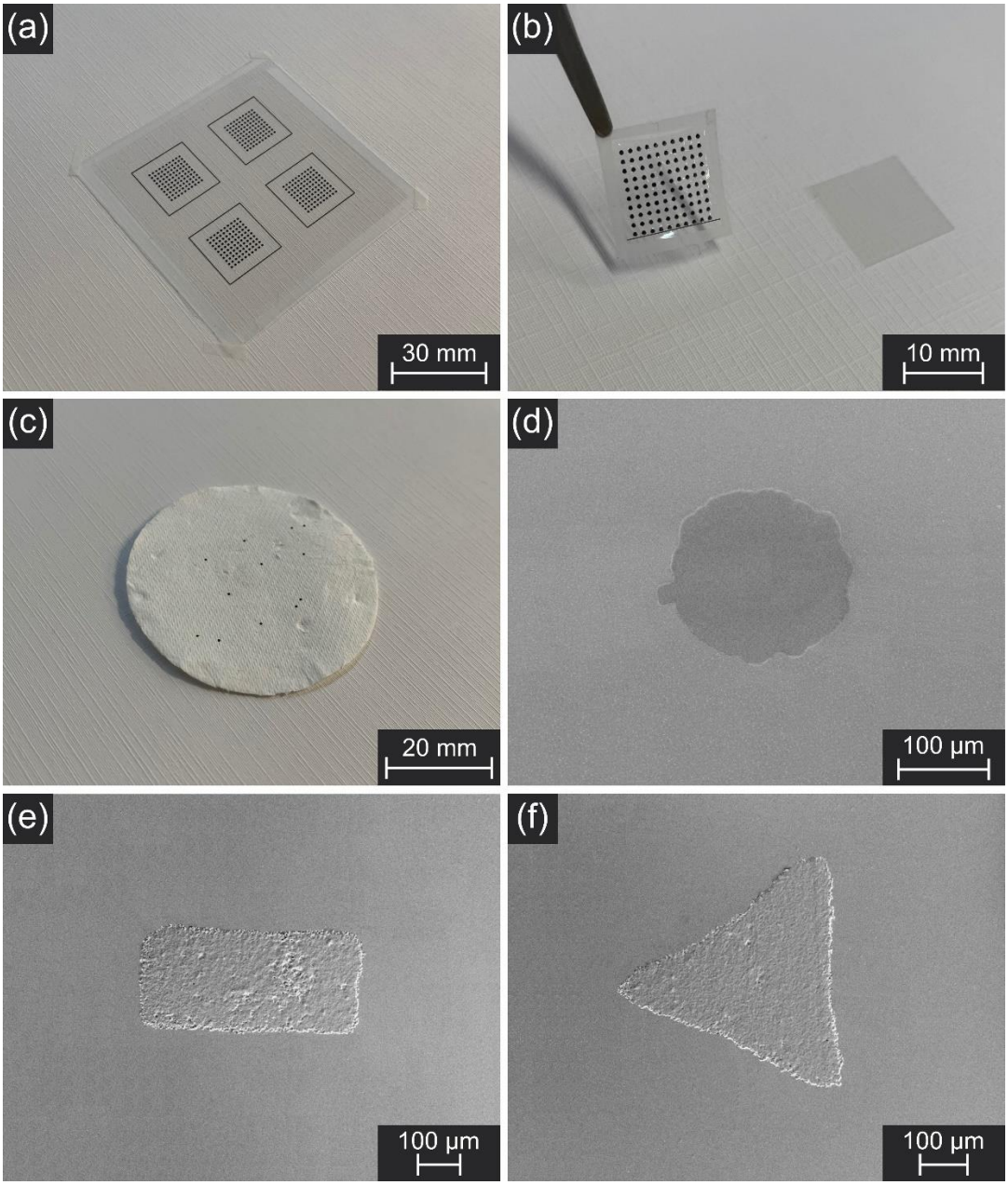


Figure 5.2: (a) Printed circular microplastics; (b) detaching the receptive layer with printed microplastic on it; (c) collection of microplastics on top of a glass fiber filter after the washing step; (d) SEM image of a printed circular microplastic with 175 µm diameter; (e) SEM image of a printed rectangular microplastic with 500 µm width and 200 µm height, and (f) SEM image of a printed triangular microplastic with sides of 500 µm.

The patterns with sharp corners were avoided in dimensional error study specimens due to the inherent resolution limit of the laserjet printer for sharp corners <150 μm. This provides a wider range of dimensions to be studied. Fifty particles of circular microplastics (for each size) were collected for the measurements. Figure 5.3 shows particle size analysis results for the plastic particles in the form of a box plot. The x- and y- axes represent the calculated equivalent diameter through image processing and the ideal particle diameter drawn with CAD software, respectively. The equivalent diameter ($D_{equivalent}$) was calculated by measuring the surface of each particle, equation (5.1).

$$D_{equivalent} = \sqrt{\frac{4 \times Area}{\pi}} \tag{5.1}$$

Average error ($E_{ave}$) was calculated individually for each sample by averaging the errors of specimens. The average of these values was 5.1 % in 100 μm to 500 μm diameter samples. However, this average was less than 3.9 % in 125 μm to 500 μm diameter samples. According to this experiment, the dimensional errors tend to decrease as the size increases. The maximum error was observed for samples with dimensions of 100 μm. Similar results were observed for other geometries` microplastics for the range of 150 μm to 500 μm.

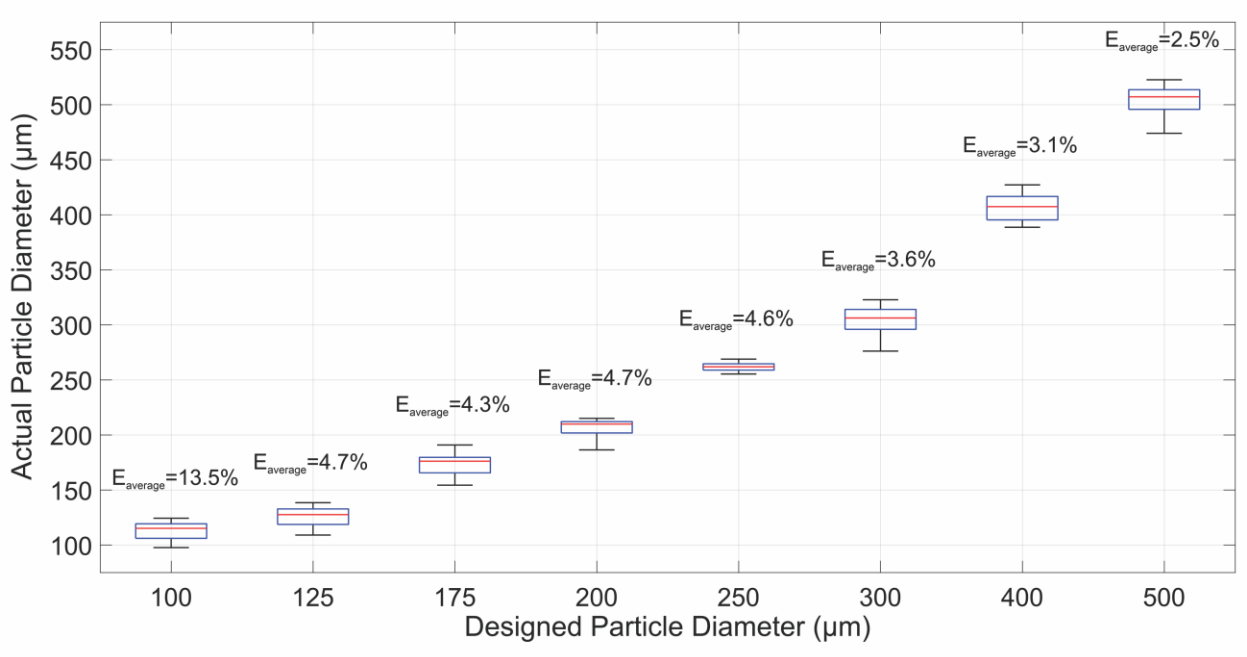


Figure 5.3: Particle size analysis of circular printed microplastics with 100 µm – 500 µm diameter.

## 5.4 Chemical Analysis

Chemical analysis through XPS and ATR-FTIR (Spectrum 100 Series, PerkinElmer Co., USA) studies was performed to characterize and evaluate the chemical composition of the fabricated microplastics. Laserjet toners typically consist of various chemicals including a specific polymer (>75%), polypropylene (pp) wax, a ferromagnetic material (iron oxide or titanium dioxide), silicon dioxide ($SiO_2$) [158]. The amount and type of the polymer used in the toner may be different, depending on the manufacturer [159]. Styrene-co-acrylate, polystyrene, polystyrene-co-acrylate, polystyrene-co-acrylate, polyethylene, etc., have been reported as the most widely used polymers in different toners [158, 159]. ATR-FTIR analysis was conducted to investigate the chemical composition of printed microplastic particles. Figure 5.4 shows this spectrum with out-of-plane deformation substitution bands between 730 $cm^{-1}$ to 825 $cm^{-1}$, and the

characteristic C-H stretching bands about 2,900 $cm^{-1}$, which are indicative of polystyrene. Additionally, simultaneous observation of a peak at 1,715 $cm^{-1}$, which identifies ester carbonyl band, and C-O-C stretch near 1,100 $cm^{-1}$, indicate the presence of polystyrene-co-acrylate as the chemical composition of the printed microplastics. The smaller peaks around 1,100 $cm^{-1}$ may indicate the presence of $SiO_2$; however, an XPS study must be conducted for confirmation.

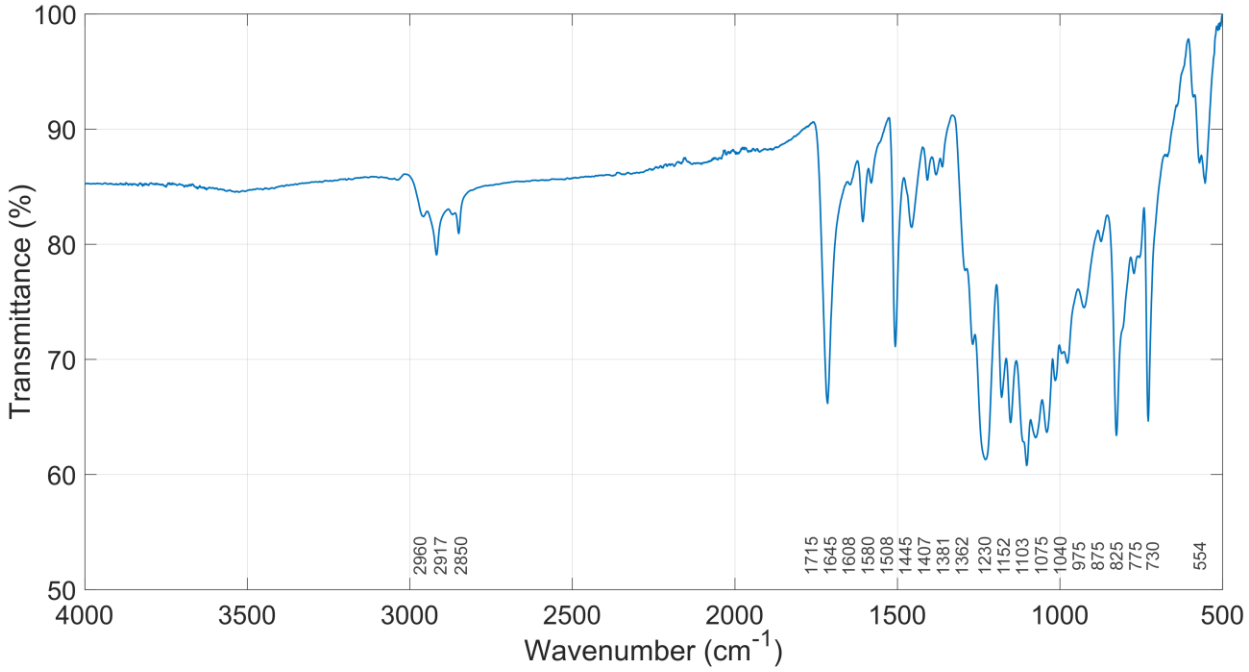


Figure 5.4: FTIR spectra of microplastic particles prepared by the introduced print-and-release method.

An XPS study was conducted to investigate traces of the ferromagnetic components possibly transferred from the OPC drum during the printing step, identify other possible elements that were not observed through FTIR analysis, and confirm the presence of $SiO_2$ on the released and cleaned microplastic particle. Figure 5.5 shows survey spectra from XPS analysis on a printed microplastic sample. The presence of carbon, oxygen,

and silicon was confirmed in the printed particles. However, the presence of the ferromagnetic material was not observed in the microplastic.

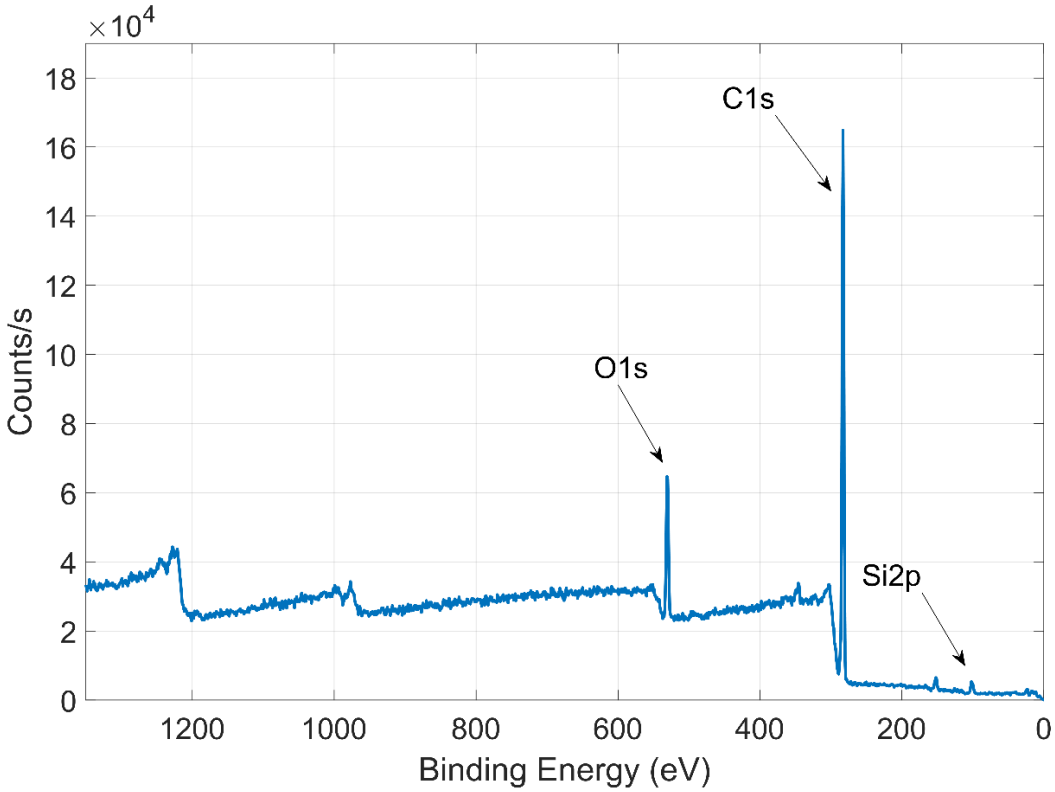


Figure 5.5: XPS survey of a printed microplastic – the presence of carbon, oxygen, and silicon is observable.

The presence of silicon in form of silicon dioxide ($SiO_2$) and silicon carbide (SiC) was confirmed, figure 5.6 which are typically used in toner mixture to improve printing quality. The presence of additive chemicals as colorants, fillers, and stabilizers has already been reported in microplastics found in aquatic environments [160]. For this reason, the microplastic samples produced and collected by the proposed method are relevant and applicable to any subsequent studies.

Adding an extra rinsing step (five seconds) with ferric chloride resulted in the removal of traceable silicon content from the microplastic particles, which was confirmed by the XPS analysis, figures 5.7 – 5.8.

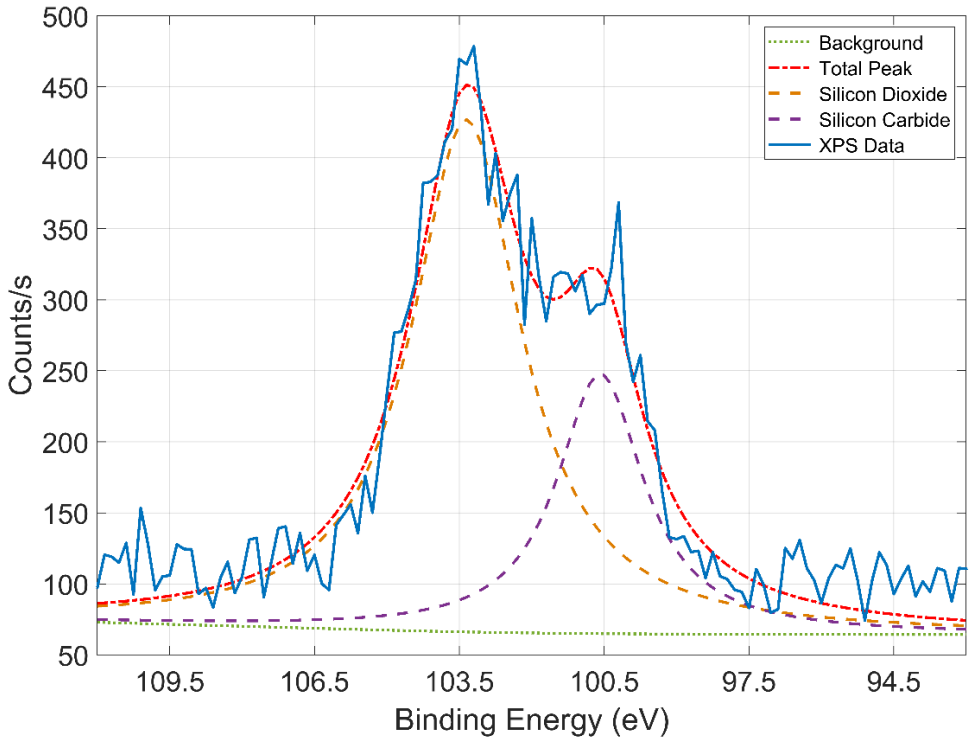


Figure 5.6: High-resolution Si2p spectra of the microplastic with curve fitting in XPS analysis.

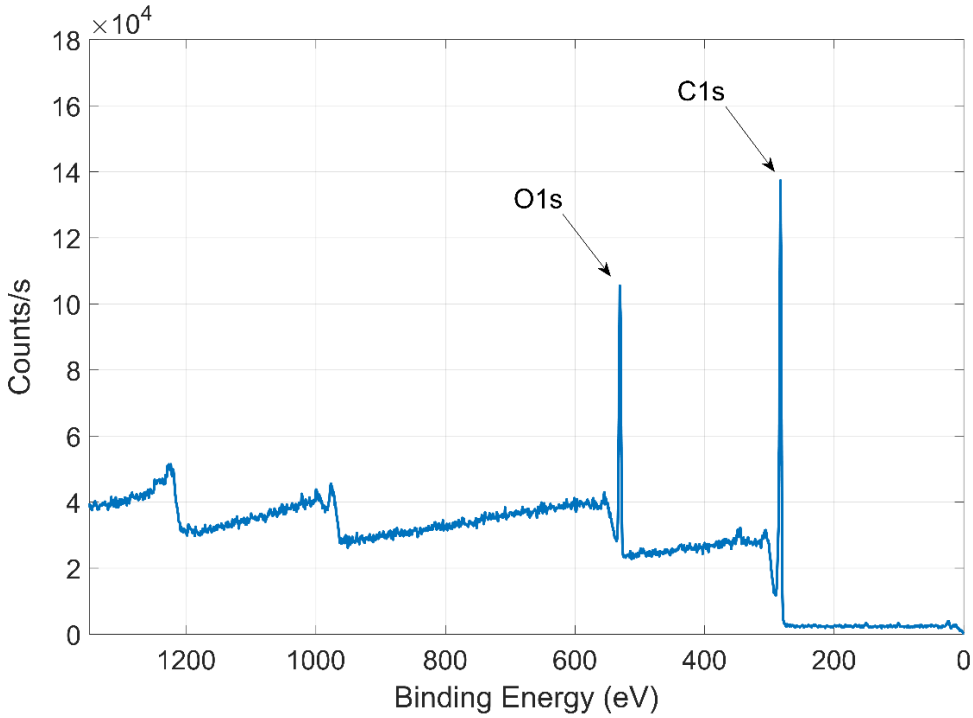


Figure 5.7: XPS survey of the microplastic after rinsing with ferric chloride – the presence of carbon and oxygen is observable.

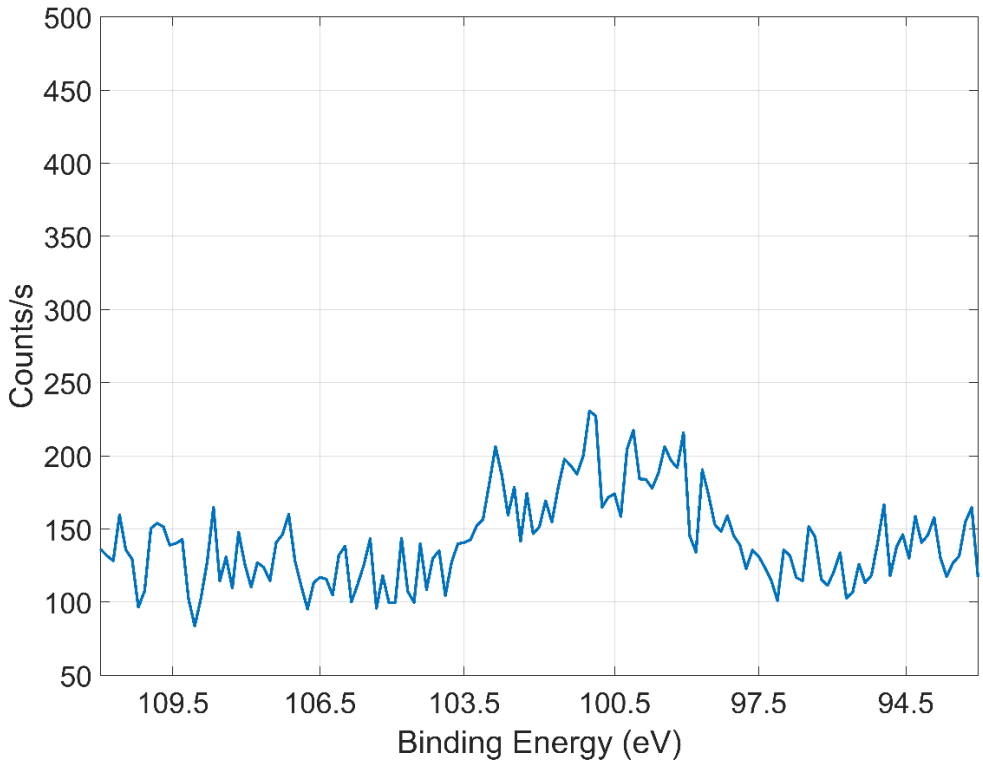


Figure 5.8: High-resolution Si2p spectra of the microplastic after rinsing with ferric chloride.

## 5.5 Microplastic Remediation

Taking advantage of the ideas presented in the previous chapters, a device for microplastic remediation was conceived. In order to emulate a water body that contains microplastic, a suspension of microplastics was prepared by dispersing the collected particles in water. An experiment was designed to demonstrate the removal and collection of microplastics from a water body based on a newly proposed antibiotic binding and magnetic separation. Figure 5.9 shows a device that separates and collects polystyrene microplastics from a water stream. This two-layer filtration system is located inside a PVC union and is consisted of a neodymium magnetic disc and a felt fabric that is drop-cast by 100 mg of doxycycline from the top and 300 mg of iron (III) oxide from the bottom.

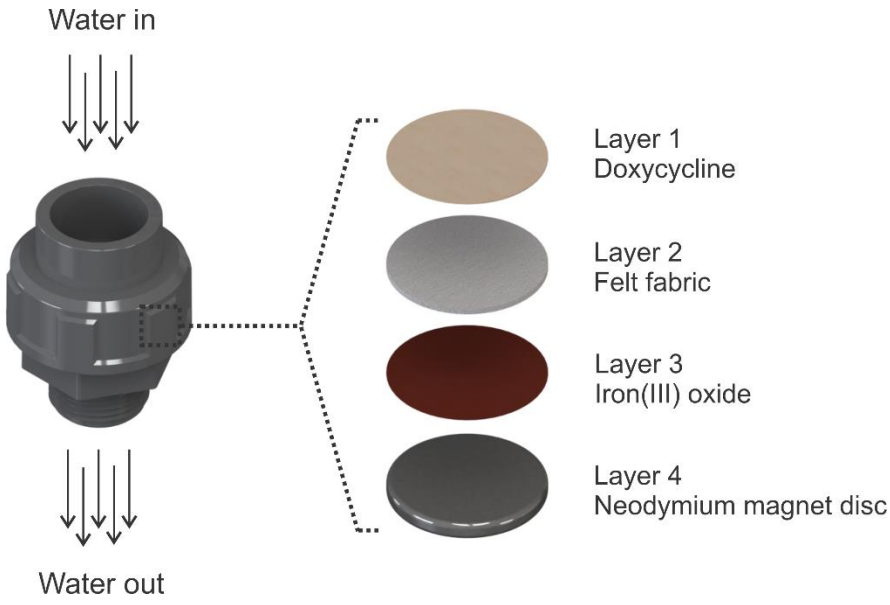


Figure 5.9: Schematic image of antibiotic-based microplastic removal and collection filtration system.

The working principle of the proposed removal and collection concept is based on the binding of polystyrene particles to the antibiotic (doxycycline) and the binding of this antibiotic to the iron (III) oxide, which is ferromagnetic [137, 161], figure 5.10. The hydrogen bonding between the amide group of polystyrene and the carbonyl group of doxycycline is the underlying adsorption mechanism of the antibiotic binding method [137]. This enables the magnetic separation of polystyrene particles in the presence of a magnetic field.

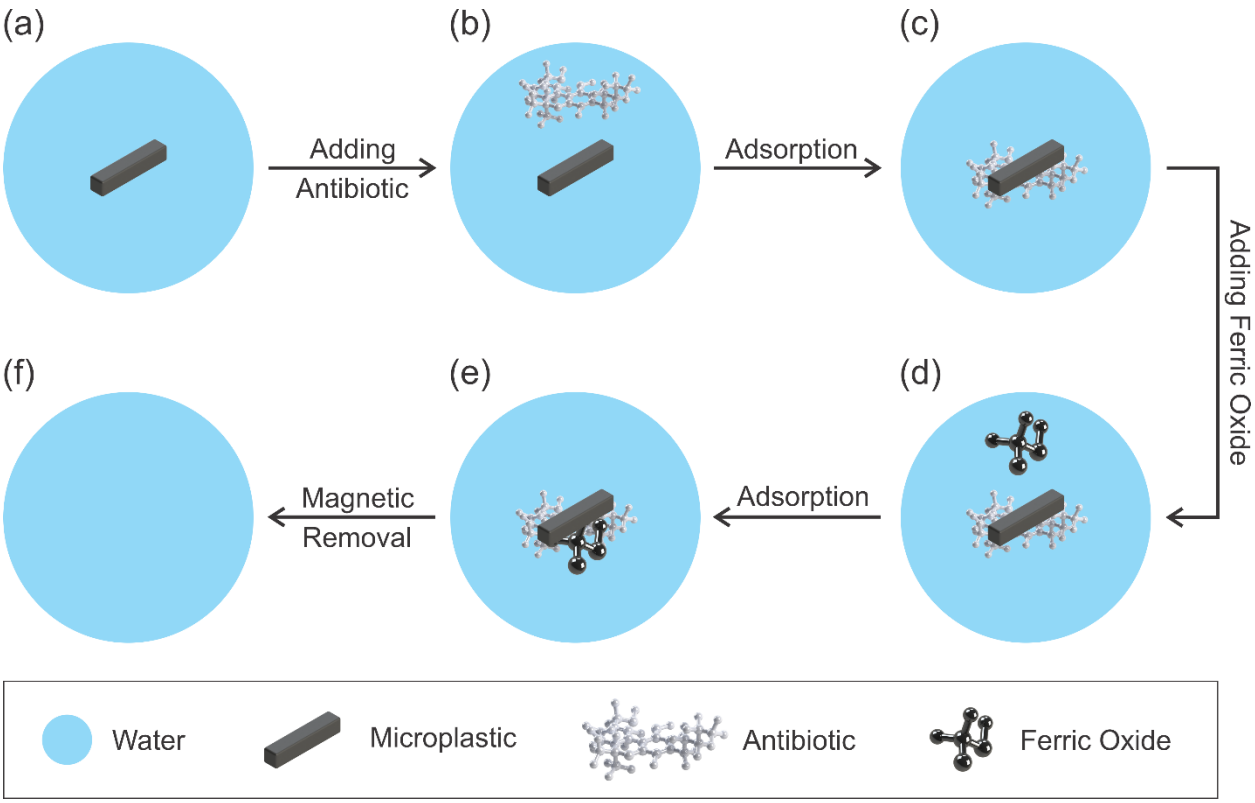


Figure 5.10: Schematic illustration of antibiotic-based microplastic removal and collection filtration system, (a) polystyrene microparticle floated in water; (b) adding doxycycline to water; (c) adsorbing polystyrene microparticle to doxycycline; (d) adding Iron (III) oxide to the water mixture; (e) adsorbing doxycycline bound with plastic particle to Iron (III) oxide, and (f) removing Iron (III) oxide bound to other particles by applying magnetic force.

Figure 5.11 shows the microplastic removal process using a permanent magnet, which demonstrates the working principle of this newly proposed method. The removal efficiency study was conducted by passing 500 particles through the removal/collection device and measuring the number of particles passing through the device. This experiment was repeated using microplastics with two different geometries (circular and square) and various sizes (200 µm, 300 µm, 400 µm, 500 µm)

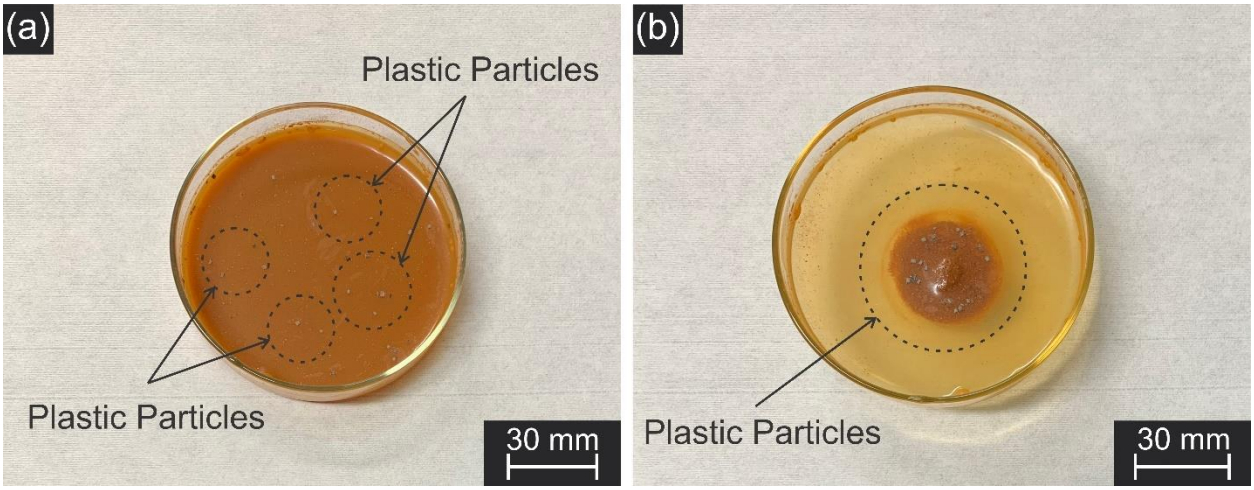


Figure 5.11: Polystyrene particles in presence of doxycycline and iron (III) oxide (a) before and (b) after applying a magnetic field.

Table 5.1 indicates the removal efficiency of the antibiotic-based microplastic removal method. The efficiency was obtained by comparing the number of captured particles with the total number of particles passing through the device. Hence, the fabricated microplastic could successfully remediate with an efficiency of 100 % for all of the samples regardless of their size and geometry.

Table 5.1: Removal efficiency of the filtration system for elimination of polystyrene particles

| Size (µm) | Geometry | Efficiency |
|---|---|---|
| 200 | Circular | 100 |
| | Square | 100 |
| 300 | Circular | 100 |
| | Square | 100 |
| 400 | Circular | 100 |
| | Square | 100 |
| 500 | Circular | 100 |
| | Square | 100 |

## 5.6 Summary

Multitudes of identical microplastic particles were fabricated with high speed and low cost utilizing an office-grade laserjet printer as compared to the preexisting methods that required specialty instruments (e.g. ultra-low temperature freezer, cryostat microtome, cryogenic-grinder) [146, 157, 162]. Besides, the black color of the printed microplastics facilitates detection and tracing of these particles without the utilization of prevalent detection instruments required for microplastics such as µ-FTIR and µ-Raman [138, 140, 160]. A commercial toner that only contains one specific type of polymer (polystyrene) was intentionally utilized for the initial validation study and to demonstrate the concept. However, customized toners which are made of other polymers powder in the presence of similar additive materials may be used to print-and-release a wider range of microplastics such as PE, PP, PA, and PVC. Considering the working principle of laserjet printers and usage of static electricity to form plastic particles in a desired shape, the customized toner can easily be replaced in commercial cartridges while maintaining the performance of the printer. The quality of printed patterns can also be improved by the use of high-resolution printers. From the perspective of remediation, a continuous

collection and removal method based on binding of microplastics to antibiotic and antibiotic to ferromagnetic particles was newly proposed and demonstrated using the microplastic suspension prepared by the facile fabrication method.

# CHAPTER 6: CONCLUSIONS

In this dissertation, a new facile fabrication technique for a wide range of micro/nano sensors, nano-sorbent devices, microplastic samples, and microfluidic systems was presented. The proposed method takes advantage of unique characteristics of a laser printing process. Many MEMS and NEMS devices were successfully fabricated outside of the cleanroom environment without customizing the laserjet printer. In comparison with existing fabrication techniques, low fabrication cost (<10 US cents), utilization of desktop office equipment, simple and rapid fabrication process (<5 minutes), portability, reproducibility, decentralization, and applicability to a vast range of devices on various flexible substrates are the main advantages of this technology.

The validity of this technology was successfully demonstrated in three forms of applications: sensors, nano-sorbent water filters, and microplastics. First, four different types of sensors were fabricated and tested: leakage, heavy metal, glucose, and gas sensors. The functional units in these sensors range from several nanometers to several centimeters and the viability of this technology in sensor fabrication was demonstrated by acquiring electrochemical, conductometric, colorimetric, biochemical, and chemoresistive detections with an accuracy similar to that of cleanroom fabricated sensors. Secondly, a CuO nano-sorbent cloth-based filter for real-time arsenic removal from polluted water was fabricated and tested. The arsenic was removed through a one-step adsorption process by immobilized CuO nanostructures on cloth with 90 % removal efficiency. Finally, color-tagged microplastic particles with desired geometry and dimensions (> 100 µm) were fabricated with < 5 % error, which is beneficial for conducting designed experiments for studying the environmental impacts of microplastics.

The outcome of this work implicates the removal of technological barriers and the creation of new opportunities for scientists in underdeveloped countries who do not have access to sophosticated and expensive instruments in a cleanroom envrionment.. This research presented a pathway to a more robust, decentralized alternative to the traditional manufacturing system which exposed its vulnerability during the pandemic. With the proposed method, various devices can be distributed in the form of digital files and produced using readily available office equipment and supplies.

# APPENDIX A: FABRICATION STEPS OF A PAPER-BASED FLUIDIC DEVICE WITH INTERDIGITATED ELECTRODES

**Electrode fabrication**

1. Designing the electrode patterns using CAD software (SolidWorks).
2. Importing the electrode patterns from CAD software to CorelDraw.
3. Changing the line thickness to “none” in CorelDraw.
4. Exporting the electrode patterns as a PDF file.
5. Printing the electrode patterns using a laserjet printer on a filter paper that is previously taped to a US letter size paper.
6. Covering the filter paper with a metal leaf followed by a taping step on the edges.
7. Covering the metal leaf with a regular paper followed by taping step to stick layers together.
8. Laminating the papers using a thermal laminator with 5 seconds delay to increase the heating time.
9. Detaching the top layer (paper).
10. Wiping the surface of metal leaf with a brush (or tip of a razor) to remove residue. Electrode`s pattern appears in this step.
11. Cutting each individual device using scissors or a craft cutting machine.

**Hydrophobic/hydrophilic definition**

12. Designing the channel patterns using CAD software (SolidWorks).
13. Importing the patterns from the CAD software to Silhouette Studio.

14. Covering one side of the wax paper with scotch tape completely (to improve cutting quality and preventing jamming the wax paper in the cutting step).
15. Adjusting the wax paper and cutter on the craft cutter machine (Silhouette Curio).
16. Cutting the wax paper to create two samples of the channel patterns on wax paper.
17. Taping one of the cut wax papers on a regular paper.
18. Adjusting the filter paper on the wax paper and covering it with the other cut wax paper.
19. Covering these papers with a regular US letter size paper.
20. Laminating the papers using a thermal laminator.
21. Removing layers, the final device is ready (created on a filter paper).

# APPENDIX B: PAPER-BASED ELECTRODE FABRICATION STEPS

**Electrode fabrication**

1. Designing electrode patterns using CAD software (SolidWorks).
2. Importing electrode patterns from CAD software to CorelDraw.
3. Changing the line thickness to “none” in CorelDraw.
4. Exporting the electrode patterns as a PDF file.
5. Printing the electrode patterns using a laserjet printer on a filter paper that is previously taped to a US letter size paper.
6. Covering the filter paper with a metal leaf followed by taping the edges.
7. Covering the metal leaf with regular paper followed by taping layers together.
8. Laminating the papers using a thermal laminator with 5 seconds delay (to increase the heating time).
9. Detaching the top layer (paper).
10. Wiping the surface of the metal leaf with a brush (or tip of a razor) to remove residue. Electrode`s pattern appears in this step.
11. Cutting each device using scissors or a craft cutting machine.

**Hydrophobic definition**

12. Cutting wax paper to completely cover the paper-based device.
13. Taping one of the wax papers on a regular paper.
14. Adjusting the filter paper on the wax paper and covering them with the other wax paper.
15. Covering these papers with a US letter size paper.
16. Laminating the papers using a thermal laminator.

17. Removing layers, the final device is ready (created on filter paper).

# APPENDIX C: FLEXIBLE CONNECTORS FABRICATION STEPS

**Metal transferring**

1. Designing connector patterns using CAD software (SolidWorks).
2. Exporting the connector patterns as a PDF file.
3. Cutting cloth and taping it to a US letter paper.
4. Printing the connector patterns using a laserjet printer on cloth.
5. Covering cloth with a metal leaf followed by taping the edges.
6. Cover the metal leaf with a regular paper followed by a taping step to stick layers together.
7. Laminating the papers using a thermal laminator with 5 seconds delay (to increase the heating time).
8. Detaching the top layer (paper).
9. Wiping the surface of the metal leaf with a brush (or tip of a razor) to remove residue. The connector`s pattern appears in this step.
10. Cutting each device using scissors.
11. Use tape to cover the electrodes on cloth followed by a peeling step to transfer the connectors to the scotch tape and form the connectors.
12. The final device is ready (created on a Scotch tape).

# APPENDIX D: FABRICATION STEPS OF A MULTILAYER PAPER-BASED ANALYTICAL DEVICE

**Electrode fabrication**

1. Designing electrode patterns using CAD software (SolidWorks).
2. Importing electrode patterns from CAD software to CorelDraw.
3. Changing the line thickness to “none” in CorelDraw.
4. Exporting the electrode patterns as a PDF file.
5. Printing the electrode patterns using a laserjet printer on a filter paper that is previously taped on a US letter size paper.
6. Cover the filter paper with a metal leaf followed by taping on the edges.
7. Cover the metal leaf with a regular paper followed by a taping step to stick layers together.
8. Laminating the papers using a thermal laminator with 5 seconds delay (to increase the heating time).
9. Detaching the top layer (paper).
10. Wiping the surface of the metal leaf with a brush (or tip of a razor) to remove residue. Electrode`s pattern appears in this step.
11. Cut each device using scissors or a craft cutting machine.

**Hydrophobic/hydrophilic definition**

12. Designing the channel patterns using CAD software (SolidWorks).
13. Importing the patterns from the CAD software to Silhouette Studio.
14. Covering one side of the wax paper with scotch tape completely (to improve the cutting quality and prevent the wax paper from jamming in the cutting step).
15. Adjusting the wax paper and cutter on the craft cutter machine (Silhouette Curio).

16. Cutting the wax paper to create two samples of the channel patterns on wax paper.
17. Taping one of the cut wax papers on a regular paper.
18. Adjust the filter paper on the wax paper and cover it with the other cut wax paper.
19. Cover these papers with a sheet of regular paper.
20. Laminating the papers using a thermal laminator.
21. After detaching extra layers, the final device (created on filter paper) is ready.

# APPENDIX E: FABRICATION STEPS OF A 3D ANALYTICAL DEVICE

**Region definition**

1. Designing the regions/channels patterns using CAD software (SolidWorks).
2. Exporting the CAD file as a PDF file.
3. Printing the patterns using a laserjet printer on a filter paper that is previously taped to a US letter size paper.
4. Cut each device using scissors or a craft cutting machine.

**Hydrophobic/hydrophilic definition**

5. Designing channel patterns using CAD software (SolidWorks).
6. Importing the patterns from the CAD software to Silhouette Studio.
7. Covering one side of the wax paper with scotch tape completely (to improve the cutting quality and prevent jamming the wax paper in the cutting step).
8. Adjusting the wax paper and cutter on the craft cutter machine (Silhouette Curio).
9. Cutting the wax paper to create two samples of the channel patterns on wax paper.
10. Taping one of the cut wax papers to a regular paper.
11. Adjusting the filter paper on the wax paper and covering it with the other cut wax paper.
12. Covering these papers with another sheet of regular paper.
13. Laminating the papers using a thermal laminator.
14. After removing layers, the final device (created on a filter paper) is ready.

# APPENDIX F: FABRICATION STEPS OF A PAPER-BASED HEAVY METAL SENSOR (COBALT MEASUREMENT)

**Region definition**

1. Designing the regions/channels patterns using CAD software (SolidWorks).
2. Exporting the CAD file as a PDF file.
3. Printing the patterns using a laserjet printer on a filter paper that is previously taped on a US letter size paper.
4. Cut each device using scissors or a craft cutting machine.

**Hydrophobic/hydrophilic definition**

5. Designing the channel patterns using CAD software (SolidWorks).
6. Importing the patterns from the CAD software to Silhouette Studio.
7. Covering one side of the wax paper with scotch tape completely (to improve the cutting quality and prevent the wax paper from jamming in the cutting step).
8. Adjusting the wax paper and cutter on the craft cutter machine (Silhouette Curio).
9. Cutting the wax paper to create two samples of the channel patterns on wax paper.
10. Taping one of the cut wax papers a regular paper.
11. Adjust the filter paper on the wax paper and covering it with the other cut wax paper.
12. Covering these papers with a sheet of regular paper.
13. Laminating the papers using a thermal laminator.
14. Removing layers and drop-casting APTES into the confinement areas (the final device).

# APPENDIX G: FABRICATION STEPS OF A PAPER-BASED GLUCOSE SENSOR

**Electrode fabrication**

1. Designing electrode patterns using CAD software (SolidWorks).
2. Importing electrode patterns from CAD software to CorelDraw.
3. Changing the line thickness to “none” in CorelDraw.
4. Exporting the electrode patterns as a PDF file.
5. Printing the electrode patterns using a laserjet printer on a filter paper that is previously taped on a US letter size paper.
6. Covering the filter paper with a metal leaf followed by taping on the edges.
7. Covering the metal leaf with a regular paper followed by a taping step to stick layers together.
8. Laminating the papers using a thermal laminator with 5 seconds delay to increase the heating time.
9. Detaching the top layer (paper).
10. Wiping the surface of the metal leaf with a brush (or tip of a razor) to remove residue. Electrode`s pattern appears in this step.
11. Cutting each device using scissors or a craft cutting machine.

**Hydrophobic/hydrophilic definition**

12. Designing the channel patterns using CAD software (SolidWorks).
13. Importing the patterns from the CAD software to Silhouette Studio.
14. Covering one side of the wax paper with scotch tape completely (to improve the cutting quality and prevent jamming the wax paper in the cutting step).
15. Adjusting the wax paper and cutter on the craft cutter machine (Silhouette Curio).

16. Cutting the wax paper to create two samples of the channel patterns on wax paper.
17. Taping one of the cut wax papers to a regular paper.
18. Adjusting the filter paper on the wax paper and covering it with the other cut wax paper.
19. Covering these papers with a regular US letter size paper.
20. Laminating the papers using a thermal laminator.
21. Removing layers and drop-casting GOx in the detection (hydrophilic) zone (the final device).

# APPENDIX H: FABRICATION STEPS OF A FLEXIBLE GAS SENSOR

**Electrode fabrication**

1. Cutting plastic film into the size of sensor.
2. Designing a fully black square (the sensor base) in DorelDraw.
3. Exporting the file into a PDF file.
4. Taping the plastic film on top of a US letter size paper.
5. Printing the black square using a laserjet printer on the plastic film.
6. Covering the plastic film with a copper leaf followed by taping the edges.
7. Covering the metal leaf with a regular paper followed by taping step on edges of the paper.
8. Laminating the papers using a thermal laminator with 5 seconds delay to increase the heating time.
9. Detaching the top layer (paper).
10. Using surface plasma (Corona surface treater) for 20 seconds on the surface of transferred copper.
11. Designing the electrode patterns using CAD software (SolidWorks).
12. Importing the electrode patterns from CAD software to CorelDraw.
13. Changing the line thickness to “none” in CorelDraw.
14. Exporting the electrode patterns as a PDF file.
15. Printing the electrode patterns using a laserjet printer on top of transferred copper after surface treatment.

**Nanostructure formation**

16. Covering the connection pads and sensing area with S1813 (Shipley) photoresist (insulin syringe) and leaving at room temperature for drying step for 6 hours.
17. Etching the uncovered parts of copper by soaking the device in copper etchant (ferric chloride solutions) for 5 seconds.
18. Washing and rinsing the device with acetone and DI water (3 times) to wash S1813.
19. Soaking the device in 4 M HCl for 2 seconds to remove the naturally grown CuO on the surface of copper leaf.
20. Rinsing the device with DI water (5 times).
21. Soaking only the sensing area (the electrodes) in a solution of 1 M sodium hydroxide and 35 mM ammonium persulfate for desired oxidation time (based on the desired nanostructure morphology).
22. Rinsing the sample with DI water (5 times).
23. Drying at room temperature for 6 hours.

# APPENDIX I: FABRICATION STEPS OF A NANOSTRUCTURED COPPER OXIDE DOUBLE-LAYER FILTER ON CLOTH FOR ARSENIC REMOVAL

**Metal transferring**

1. Cutting cloth and taping it to a US letter paper.
2. Designing the filter patterns using CAD software (SolidWorks).
3. Importing the filter patterns from CAD software to CorelDraw.
4. Changing the line thickness to “none” in CorelDraw.
5. Exporting the filter patterns as a PDF file.
6. Printing the filter patterns using a laserjet printer on the cloth.
7. Covering the filter patterns with a metal leaf followed by taping the edges.
8. Covering the metal leaf with a regular paper followed by tapingon the edges.
9. Laminating the papers using a thermal laminator with 5 seconds delay to increase the heating time.
10. Detaching the top layer (paper).
11. Wiping the surface of metal leaf with a brush (or tip of a razor) to remove residue.
12. Cutting each individual layer using scissors.

**Nanostructure formation**

13. Soaking filter layers in 4 M HCl for 2 seconds to remove the naturally grown CuO on the surface of copper leaf.
14. Rinsing the device with DI water (5 times).
15. Soaking filter layers in DI water for 2 minutes.
16. Soaking the filter layers in a solution of 1 M sodium hydroxide and 35 mM ammonium persulfate for desired oxidation time (based on the desired nanostructure morphology).

17. Rinsing filter layers gently with DI water (5 times).
24. Drying filters at room temperature for 6 hours.

**Assembling layers**

25. Drawing circles (filter`s diameter) using CAD software (SolidWorks).
26. Importing the file from the CAD software to Silhouette Studio.
27. Cutting filter papers (grades: 1, 3, and 4) using a craft cutter machine (Silhouette Curio).
28. Putting water-based acrylic adhesive on the edges of filter papers and filter layers.
29. Assembling the filter layers by gently putting filter layers together (final device).

# APPENDIX J: FABRICATION STEPS OF MICROPLASTIC PARTICLES

1. Designing the desired geometries of microplastic particles using CAD software (SolidWorks).
2. Importing the microplastic particle CAD file to CorelDraw.
3. Using smart fill to make particles fully black and changing the line thickness to “none” in CorelDraw.
4. Exporting the filter patterns as a PDF file.
5. Cutting plastic film into square shapes with 6” length.
6. Coating the water-soluble receptive/sacrificial layer (clear gloss precoat) through a three-step spin-coating step – 300 RPM for 20 seconds, 1000 RPM for 50 seconds, and 300 RPM for 20 seconds.
7. Drying the plastic films by leaving at room temperature for 5 minutes.
8. Taping the dried plastic films to a US letter size paper.
9. Printing the microplastic patterns (the PDF file) on taped plastic films using a laserjet printer.
10. Cutting a segment of microplastic particles based on a desired application.
11. Using tape on the border of the plastic film to form a frame.
12. Removing the taped frame using a tweezer. It peels off the water-soluble part.
13. Placing the detached layer on a glass fiber filter in a funnel.
14. Gently adding ethanol and DI water to the opposite side of the glass fiber filter.
15. Rinsing the released microplastic by gently passing DI water.
16. Drying the glass fiber filter at room temperature.
17. Dried microplastics will be on top of the filter paper. These particles can easily be released from the surface of the filter paper by adding DI water.

# REFERENCES


1. Madou, M.J., *Fundamentals of microfabrication: the science of miniaturization*. 2018: CRC press.
2. Hayat, A. and J.L. Marty, *Disposable screen printed electrochemical sensors: Tools for environmental monitoring.* Sensors, 2014. **14**(6): p. 10432-10453.
3. Lin, Y., et al., *Detection of heavy metal by paper-based microfluidics.* Biosensors and Bioelectronics, 2016. **83**: p. 256-266.
4. Eyvazi Hesar, M., et al., *Contactless, battery-free, and stretchable wearable for continuous recording of seismocardiograms.* ACS Applied Electronic Materials, 2020. **3**(1): p. 11-20.
5. Hajikhani, A., et al., *Experimental characterization and computational modeling of hydrogel cross-linking for bioprinting applications.* The International journal of artificial organs, 2019. **42**(10): p. 548-557.
6. Hajikhani, A., P. Wriggers, and M. Marino, *Chemo-mechanical modelling of swelling and crosslinking reaction kinetics in alginate hydrogels: A novel theory and its numerical implementation.* Journal of the Mechanics and Physics of Solids, 2021. **153**: p. 104476.
7. Shahriyari, F., et al., *Effect of cell imprinting on viability and drug susceptibility of breast cancer cells to doxorubicin.* Acta Biomaterialia, 2020. **113**: p. 119-129.
8. Zhang, H., et al., *Microfluidic ionic liquid dye laser.* IEEE Photonics Journal, 2020. **13**(1): p. 1-8.

9. Biswas, P., et al., *A Portable Micro-Gas Chromatography with Integrated Photonic Crystal Slab Sensors on Chip.* Biosensors, 2021. **11**(9): p. 326.

10. Pishbin, E., et al., *Frequency dependent multiphase flows on centrifugal microfluidics.* Lab on a Chip, 2020. **20**(3): p. 514-524.

11. Moghaddam, A.S., et al., *Review of Bioprinting in Regenerative Medicine: Naturally Derived Bioinks and Stem Cells.* ACS Applied Bio Materials, 2021. **4**(5): p. 4049-4070.

12. Ko, Y.H., et al., *Perfectly-reflecting guided-mode-resonant photonic lattices possessing Mie modal memory.* Optics Express, 2021. **29**(17): p. 26971-26982.

13. Razmjooei, N., et al., *Resonant reflection by microsphere arrays with AR-quenched Mie scattering.* Optics Express, 2021. **29**(12): p. 19183-19192.

14. Karbalaei, A. and H.J. Cho, *Microfluidic devices developed for and inspired by thermotaxis and chemotaxis.* Micromachines, 2018. **9**(4): p. 149.

15. Karbalaei, A., R. Kumar, and H.J. Cho, *Thermocapillarity in microfluidics—A review.* Micromachines, 2016. **7**(1): p. 13.

16. Nayebzadeh, A., H. Tabkhi, and Y. Peles, *Hydrodynamic Cavitation Downstream a Micropillar Entrained Inside a Microchannel—A Parametric Study.* Journal of Fluids Engineering, 2019. **141**(1).

17. Nayebzadeh, A., et al., *Cavitation behind a circular micro pillar.* International Journal of Multiphase Flow, 2018. **98**: p. 67-78.

18. Tabkhi, H., A. Nayebzadeh, and Y. Peles, *Experimental and numerical local heat transfer study on micro pin fin with tip clearance.* Applied Thermal Engineering, 2020. **179**: p. 115756.

19. Bamshad, A., A. Nikfarjam, and H. Khaleghi, *A new simple and fast thermally-solvent assisted method to bond PMMA–PMMA in micro-fluidics devices.* Journal of Micromechanics and Microengineering, 2016. **26**(6): p. 065017.

20. Bamshad, A., et al. *Theoretical and numerical investigation of liquid-gas interface location of capillary driven flow during the time throughout circular microchannels*. in *2017 5th RSI International Conference on Robotics and Mechatronics (ICRoM)*. 2017. IEEE.

21. Bongaarts, J., *Human population growth and the demographic transition.* Philosophical Transactions of the Royal Society B: Biological Sciences, 2009. **364**(1532): p. 2985-2990.

22. Lutz, W. and S. KC, *Dimensions of global population projections: what do we know about future population trends and structures?* Philosophical Transactions of the Royal Society B: Biological Sciences, 2010. **365**(1554): p. 2779-2791.

23. Blackstone, E.A., J.P. Fuhr Jr, and S. Pociask, *The health and economic effects of counterfeit drugs.* American health & drug benefits, 2014. **7**(4): p. 216.

24. Driggin, E., et al., *Cardiovascular considerations for patients, health care workers, and health systems during the COVID-19 pandemic.* Journal of the American College of Cardiology, 2020. **75**(18): p. 2352-2371.

25. Wong, W., et al., *Recent advances in exploitation of nanomaterial for arsenic removal from water: a review.* Nanotechnology, 2016. **28**(4): p. 042001.

26. Bamshad, A. and H.J. Cho. *Digital microfabrication on paper and cloth For heavy metal detection and remediation*. in *2019 20th International Conference on Solid-*

*State Sensors, Actuators and Microsystems & Eurosensors XXXIII (TRANSDUCERS & EUROSENSORS XXXIII)*. 2019. IEEE.

27. Mehrpouya, M., et al., *The potential of additive manufacturing in the smart factory industrial 4.0: A review.* Applied Sciences, 2019. **9**(18): p. 3865.
28. Siow, W.T., et al., *Managing COVID-19 in resource-limited settings: critical care considerations*. 2020, Springer.
29. Tayyab, M., et al., *Potential microfluidic devices for COVID-19 Antibody detection at Point-of-Care (POC): A Review.* IEEE Sensors Journal, 2020.
30. St John, A. and C.P. Price, *Existing and emerging technologies for point-of-care testing.* The Clinical Biochemist Reviews, 2014. **35**(3): p. 155.
31. Silveira, C.M., T. Monteiro, and M.G. Almeida, *Biosensing with paper-based miniaturized printed electrodes–a modern trend.* Biosensors, 2016. **6**(4): p. 51.
32. Almeida, M.I.G., et al., *Developments of microfluidic paper-based analytical devices (μPADs) for water analysis: A review.* Talanta, 2018. **177**: p. 176-190.
33. Schumacher, S., et al., *Platform technologies for molecular diagnostics near the patient's bedside*, in *Molecular Diagnostics*. 2012, Springer. p. 75-87.
34. Bamshad, A., A. Nikfarjam, and M.H. Sabour, *Capillary-based micro-optofluidic viscometer.* Measurement Science and Technology, 2018. **29**(9): p. 095901.
35. Ciuti, G., et al., *MEMS sensor technologies for human centred applications in healthcare, physical activities, safety and environmental sensing: a review on research activities in Italy.* Sensors, 2015. **15**(3): p. 6441-6468.

36. Xia, Y., J. Si, and Z. Li, *Fabrication techniques for microfluidic paper-based analytical devices and their applications for biological testing: A review.* Biosensors and Bioelectronics, 2016. **77**: p. 774-789.

37. Zhang, H., et al., *Reconfigurable Integrated Optofluidic Droplet Laser Arrays.* ACS Applied Materials & Interfaces, 2020. **12**(24): p. 26936-26942.

38. Karbalaei, A. and H.J. Cho, *Passive mixing rate of trapped squeezed nanodroplets—A time scale analysis.* Experimental and Computational Multiphase Flow, 2020. **2**(3): p. 135-141.

39. Lee, M., et al., *How to respond to the fourth industrial revolution, or the second information technology revolution? Dynamic new combinations between technology, market, and society through open innovation.* Journal of Open Innovation: Technology, Market, and Complexity, 2018. **4**(3): p. 21.

40. Berman, B., *3-D printing: The new industrial revolution.* Business horizons, 2012. **55**(2): p. 155-162.

41. Abramovici, M., J.C. Göbel, and M. Neges, *Smart engineering as enabler for the 4th industrial revolution*, in *Integrated systems: Innovations and applications*. 2015, Springer. p. 163-170.

42. Liao, Y., et al., *Past, present and future of Industry 4.0-a systematic literature review and research agenda proposal.* International journal of production research, 2017. **55**(12): p. 3609-3629.

43. Liana, D.D., et al., *Recent advances in paper-based sensors.* Sensors, 2012. **12**(9): p. 11505-11526.

44. Li, X., D.R. Ballerini, and W. Shen, *A perspective on paper-based microfluidics: Current status and future trends.* Biomicrofluidics, 2012. **6**(1): p. 011301.

45. Pathak, P., S. Park, and H.J. Cho, *A Carbon Nanotube–Metal Oxide Hybrid Material for Visible-Blind Flexible UV-Sensor.* Micromachines, 2020. **11**(4): p. 368.

46. Devarakonda, S., et al., *Cost-effective and handmade paper-based immunosensing device for electrochemical detection of influenza virus.* Sensors, 2017. **17**(11): p. 2597.

47. Li, Z., et al., *Direct writing electrodes using a ball pen for paper-based point-of-care testing.* Analyst, 2015. **140**(16): p. 5526-5535.

48. Downs, C., A. Nejely, and E. Fu, *Disposable fabric-based electrochemical sensors fabricated from wax-transfer-printed fluidic cells and stencil-printed electrodes.* Analytical methods, 2018. **10**(29): p. 3696-3703.

49. Medina-Sánchez, M., et al., *Eco-friendly electrochemical lab-on-paper for heavy metal detection.* Analytical and bioanalytical chemistry, 2015. **407**(28): p. 8445-8449.

50. Adkins, J.A. and C.S. Henry, *Electrochemical detection in paper-based analytical devices using microwire electrodes.* Analytica chimica acta, 2015. **891**: p. 247-254.

51. Hu, C., et al., *Inkjet printing of nanoporous gold electrode arrays on cellulose membranes for high-sensitive paper-like electrochemical oxygen sensors using ionic liquid electrolytes.* Analytical chemistry, 2012. **84**(8): p. 3745-3750.

52. da Costa, T.H., et al., *A paper-based electrochemical sensor using inkjet-printed carbon nanotube electrodes.* ECS Journal of Solid State Science and Technology, 2015. **4**(10): p. S3044.

53. Gebretsadik, T., et al., *Recent advances in and potential utilities of paper-based electrochemical sensors: beyond qualitative analysis.* Analyst, 2019. **144**(8): p. 2467-2479.

54. Dossi, N., et al., *Simple pencil-drawn paper-based devices for one-spot electrochemical detection of electroactive species in oil samples.* Electrophoresis, 2015. **36**(16): p. 1830-1836.

55. Fosdick, S.E., et al., *Wire, mesh, and fiber electrodes for paper-based electroanalytical devices.* Analytical chemistry, 2014. **86**(7): p. 3659-3666.

56. Ghosh, R., et al., *Fabrication of laser printed microfluidic paper-based analytical devices (LP-μPADs) for point-of-care applications.* Scientific reports, 2019. **9**(1): p. 1-11.

57. Cai, L., et al., *A simple paper-based sensor fabricated by selective wet etching of silanized filter paper using a paper mask.* Biomicrofluidics, 2014. **8**(5): p. 056504.

58. Fang, X., S. Wei, and J. Kong, *Paper-based microfluidics with high resolution, cut on a glass fiber membrane for bioassays.* Lab on a Chip, 2014. **14**(5): p. 911-915.

59. Li, X., et al., *Paper-based microfluidic devices by plasma treatment.* Analytical chemistry, 2008. **80**(23): p. 9131-9134.

60. He, Q., et al., *Method for fabrication of paper-based microfluidic devices by alkylsilane self-assembling and UV/O3-patterning.* Analytical chemistry, 2013. **85**(3): p. 1327-1331.

61. Bruzewicz, D.A., M. Reches, and G.M. Whitesides, *Low-cost printing of poly (dimethylsiloxane) barriers to define microchannels in paper.* Analytical chemistry, 2008. **80**(9): p. 3387-3392.

62. Olkkonen, J., K. Lehtinen, and T. Erho, *Flexographically printed fluidic structures in paper.* Analytical chemistry, 2010. **82**(24): p. 10246-10250.

63. Lam, T., et al., *A chemically patterned microfluidic paper-based analytical device (C-µPAD) for point-of-care diagnostics.* Scientific reports, 2017. **7**(1): p. 1-10.

64. Jiang, Y., et al., *A simple method for fabrication of microfluidic paper-based analytical devices and on-device fluid control with a portable corona generator.* RSC advances, 2016. **6**(4): p. 2888-2894.

65. Xu, C., et al., *Low-cost and rapid prototyping of microfluidic paper-based analytical devices by inkjet printing of permanent marker ink.* Rsc Advances, 2015. **5**(7): p. 4770-4773.

66. Abe, K., et al., *Inkjet-printed paperfluidic immuno-chemical sensing device.* Analytical and bioanalytical chemistry, 2010. **398**(2): p. 885-893.

67. Songjaroen, T., et al., *Blood separation on microfluidic paper-based analytical devices.* Lab on a Chip, 2012. **12**(18): p. 3392-3398.

68. Yu, P., et al., *3D Microfluidic Devices in a Single Piece of Paper for the Simultaneous Determination of Nitrite and Thiocyanate.* Sensors, 2020. **20**(15): p. 4118.

69. Yetisen, A.K., M.S. Akram, and C.R. Lowe, *Paper-based microfluidic point-of-care diagnostic devices.* Lab on a Chip, 2013. **13**(12): p. 2210-2251.

70. Akyazi, T., et al., *Fluidic flow delay by ionogel passive pumps in microfluidic paper-based analytical devices.* Sensors and Actuators B: Chemical, 2016. **233**: p. 402-408.

71. Chitnis, G., et al., *Laser-treated hydrophobic paper: an inexpensive microfluidic platform.* Lab on a Chip, 2011. **11**(6): p. 1161-1165.

72. Sameenoi, Y., et al., *One-step polymer screen-printing for microfluidic paper-based analytical device (μPAD) fabrication.* Analyst, 2014. **139**(24): p. 6580-6588.

73. He, Y., W.-b. Wu, and J.-z. Fu, *Rapid fabrication of paper-based microfluidic analytical devices with desktop stereolithography 3D printer.* RSC advances, 2015. **5**(4): p. 2694-2701.

74. Cate, D.M., et al., *Recent developments in paper-based microfluidic devices.* Analytical chemistry, 2015. **87**(1): p. 19-41.

75. Akyazi, T., L. Basabe-Desmonts, and F. Benito-Lopez, *Review on microfluidic paper-based analytical devices towards commercialisation.* Analytica chimica acta, 2018. **1001**: p. 1-17.

76. Bamshad, A. and H.J. Cho, *A novel print-and-release method to prepare microplastics using an office-grade laserjet printer; a low-cost solution for preliminary studies.* Marine Pollution Bulletin, 2021. **170**: p. 112601.

77. Schilling, K.M., et al., *Fully enclosed microfluidic paper-based analytical devices.* Analytical chemistry, 2012. **84**(3): p. 1579-1585.

78. Zikulnig, J., et al., *Low-Cost Inkjet-Printed Temperature Sensors on Paper Substrate for the Integration into Natural Fiber-Reinforced Lightweight Components.* Chemosensors, 2021. **9**(5): p. 95.

79. Yuen, P.K. and V.N. Goral, *Low-cost rapid prototyping of flexible microfluidic devices using a desktop digital craft cutter.* Lab on a Chip, 2010. **10**(3): p. 384-387.

80. Chowdhury, S.A., et al., *Highly conductive polydimethylsiloxane/carbon nanofiber composites for flexible sensor applications.* Advanced Materials Technologies, 2019. **4**(1): p. 1800398.

81. Thuo, M.M., et al., *Fabrication of low-cost paper-based microfluidic devices by embossing or cut-and-stack methods.* Chemistry of Materials, 2014. **26**(14): p. 4230-4237.

82. Yang, Y., et al., *Paper-based microfluidic devices: Emerging themes and applications.* Analytical chemistry, 2017. **89**(1): p. 71-91.

83. Nomura, K.-i., et al., *Fabrication of a textile-based wearable blood leakage sensor using screen-offset printing.* Sensors, 2018. **18**(1): p. 240.

84. Adegboye, M.A., W.-K. Fung, and A. Karnik, *Recent advances in pipeline monitoring and oil leakage detection technologies: Principles and approaches.* Sensors, 2019. **19**(11): p. 2548.

85. McDonald, K.J., B. Reynolds, and K. Reddy, *Intrinsic properties of cupric oxide nanoparticles enable effective filtration of arsenic from water.* Scientific reports, 2015. **5**(1): p. 1-10.

86. Jeong, U. and Y. Kim, *Colorimetric detection of heavy metal ions using aminosilane.* Journal of Industrial and Engineering Chemistry, 2015. **31**: p. 393-396.

87. Sung, H.K., et al., *Colorimetric detection of Co2+ ion using silver nanoparticles with spherical, plate, and rod shapes.* Langmuir, 2013. **29**(28): p. 8978-8982.

88. Strakosas, X., et al., *A non-enzymatic glucose sensor enabled by bioelectronic pH control.* Scientific reports, 2019. **9**(1): p. 1-7.

89. Maddah, E. and B. Beigzadeh, *Use of a smartphone thermometer to monitor thermal conductivity changes in diabetic foot ulcers: a pilot study.* Journal of Wound Care, 2020. **29**(1): p. 61-66.

90. Yoo, E.-H. and S.-Y. Lee, *Glucose biosensors: an overview of use in clinical practice.* Sensors, 2010. **10**(5): p. 4558-4576.

91. Juska, V.B. and M.E. Pemble, *A critical review of electrochemical glucose sensing: evolution of biosensor platforms based on advanced nanosystems.* Sensors, 2020. **20**(21): p. 6013.

92. Hwang, D.-W., et al., *Recent advances in electrochemical non-enzymatic glucose sensors–a review.* Analytica chimica acta, 2018. **1033**: p. 1-34.

93. Kangkamano, T., et al., *Chitosan cryogel with embedded gold nanoparticles decorated multiwalled carbon nanotubes modified electrode for highly sensitive flow based non-enzymatic glucose sensor.* Sensors and Actuators B: Chemical, 2017. **246**: p. 854-863.

94. Nazemi, H., et al., *Advanced micro-and nano-gas sensor technology: A review.* Sensors, 2019. **19**(6): p. 1285.

95. Lin, T., et al., *Semiconductor metal oxides as chemoresistive sensors for detecting volatile organic compounds.* Sensors, 2019. **19**(2): p. 233.

96. Dey, A., *Semiconductor metal oxide gas sensors: A review.* Materials Science and Engineering: B, 2018. **229**: p. 206-217.

97. Yoo, R., et al., *Highly selective detection of dimethyl methylphosphonate (DMMP) using CuO nanoparticles/ZnO flowers heterojunction.* Sensors and Actuators B: Chemical, 2017. **240**: p. 1099-1105.

98. Deore, M.K., V.B. Gaikwad, and G.H. Jain, *Role of CuO-ZnO Heterojunctions in Gas Sensing Response of CuO-ZnO Thick Films.* Journal of Physical Science and Application, 2016. **6**(2): p. 51-60.

99. Nandy, T., R.A. Coutu, and C. Ababei, *Carbon monoxide sensing technologies for next-generation cyber-physical systems.* Sensors, 2018. **18**(10): p. 3443.

100. Krcmar, P., et al., *Fully inkjet-printed CuO sensor on flexible polymer substrate for alcohol vapours and humidity sensing at room temperature.* Sensors, 2019. **19**(14): p. 3068.

101. Yan, H., et al., *Enhanced sensing properties of CuO nanosheets for volatile organic compounds detection.* Journal of Materials Science: Materials in Electronics, 2015. **26**(1): p. 280-287.

102. Rydosz, A., *The use of copper oxide thin films in gas-sensing applications.* Coatings, 2018. **8**(12): p. 425.

103. Steinhauer, S., *Gas Sensors Based on Copper Oxide Nanomaterials: A Review.* Chemosensors, 2021. **9**(3): p. 51.

104. Bamshad, A. and H.J. Cho. *Disposable Sensor Devices Fabricated by Paper Crafting Tools*. in *2020 IEEE Sensors Applications Symposium (SAS)*. 2020. IEEE.

105. McDonald, K.J., B. Reynolds, and K. Reddy, *Intrinsic properties of cupric oxide nanoparticles enable effective filtration of arsenic from water.* Scientific reports, 2015. **5**: p. 11110.

106. Reddy, K., K. McDonald, and H. King, *A novel arsenic removal process for water using cupric oxide nanoparticles.* Journal of colloid and interface science, 2013. **397**: p. 96-102.

107. Yu, X.-Y., et al., *Novel 3D hierarchical cotton-candy-like CuO: surfactant-free solvothermal synthesis and application in As (III) removal.* ACS applied materials & interfaces, 2012. **4**(4): p. 1954-1962.

108. Hwang, J.-H., et al., *A novel Fe-Chitosan-coated carbon electrode sensor for in situ As (III) detection in mining wastewater and soil leachate.* Sensors and Actuators B: Chemical, 2019. **294**: p. 89-97.

109. Pillewan, P., et al., *Removal of As (III) and As (V) from water by copper oxide incorporated mesoporous alumina.* Journal of hazardous materials, 2011. **186**(1): p. 367-375.

110. Mukherjee, S., et al., *Sustainable and affordable composites built using microstructures performing better than nanostructures for arsenic removal.* ACS Sustainable Chemistry & Engineering, 2018.

111. Ali, I., *New generation adsorbents for water treatment.* Chemical reviews, 2012. **112**(10): p. 5073-5091.

112. Qu, X., P.J. Alvarez, and Q. Li, *Applications of nanotechnology in water and wastewater treatment.* Water research, 2013. **47**(12): p. 3931-3946.

113. Mohan, D. and C.U. Pittman Jr, *Arsenic removal from water/wastewater using adsorbents—a critical review.* Journal of hazardous materials, 2007. **142**(1-2): p. 1-53.

114. Ali, I., M. Asim, and T.A. Khan, *Low cost adsorbents for the removal of organic pollutants from wastewater.* Journal of environmental management, 2012. **113**: p. 170-183.

115. Zhang, Q., et al., *CuO nanostructures: synthesis, characterization, growth mechanisms, fundamental properties, and applications.* Progress in Materials Science, 2014. **60**: p. 208-337.

116. Maiti, A., S. Mishra, and M. Chaudhary, *Nanoscale materials for arsenic removal from water*, in *Nanoscale materials in water purification*. 2019, Elsevier. p. 707-733.

117. Maity, J.P., et al., *Advanced application of nano-technological and biological processes as well as mitigation options for arsenic removal.* Journal of Hazardous Materials, 2021. **405**: p. 123885.

118. Martinson, C.A. and K. Reddy, *Adsorption of arsenic (III) and arsenic (V) by cupric oxide nanoparticles.* Journal of Colloid and Interface Science, 2009. **336**(2): p. 406-411.

119. Bamshad, A. and H.J. Cho, *Laserjet Printed Micro/Nano Sensors and Microfluidic Systems: A Simple and Facile Digital Platform for Inexpensive, Flexible, and Low-Volume Devices.* Advanced Materials Technologies, 2021. **n/a**(n/a): p. 2100401.

120. Zhang, G., et al., *Nanostructured iron (III)-copper (II) binary oxide: a novel adsorbent for enhanced arsenic removal from aqueous solutions.* Water Research, 2013. **47**(12): p. 4022-4031.

121. Cui, H.-J., et al., *Fabrication of magnetic porous Fe–Mn binary oxide nanowires with superior capability for removal of As (III) from water.* Journal of hazardous materials, 2014. **279**: p. 26-31.

122. Malwal, D. and P. Gopinath, *Rapid and efficient removal of arsenic from water using electrospun CuO–ZnO composite nanofibers.* RSC Advances, 2016. **6**(116): p. 115021-115028.

123. Momeni, M., et al., *Preparation of CuO nanostructures coating on copper as supercapacitor materials.* Surface Engineering, 2014. **30**(11): p. 775-778.

124. Zhi, B., et al., *Ordered mesoporous MnO 2 as a synergetic adsorbent for effective arsenic (III) removal.* Journal of Materials Chemistry A, 2014. **2**(7): p. 2374-2382.

125. De Gisi, S., et al., *Characteristics and adsorption capacities of low-cost sorbents for wastewater treatment: A review.* Sustainable Materials and Technologies, 2016. **9**: p. 10-40.

126. Zhang, G.-S., et al., *Removal mechanism of As (III) by a novel Fe− Mn binary oxide adsorbent: oxidation and sorption.* Environmental Science & Technology, 2007. **41**(13): p. 4613-4619.

127. Xu, Z., et al., *As (III) removal by hydrous titanium dioxide prepared from one-step hydrolysis of aqueous TiCl4 solution.* water research, 2010. **44**(19): p. 5713-5721.

128. Maliyekkal, S.M., L. Philip, and T. Pradeep, *As(III) removal from drinking water using manganese oxide-coated-alumina: Performance evaluation and mechanistic details of surface binding.* Chemical Engineering Journal, 2009. **153**(1): p. 101-107.

129. Tripathy, S.S. and A.M. Raichur, *Enhanced adsorption capacity of activated alumina by impregnation with alum for removal of As (V) from water.* Chemical Engineering Journal, 2008. **138**(1-3): p. 179-186.

130. Siddique, T., N.K. Dutta, and N. Roy Choudhury, *Nanofiltration for arsenic removal: challenges, recent developments, and perspectives.* Nanomaterials, 2020. **10**(7): p. 1323.

131. Li, W., et al., *Extremely high arsenic removal capacity for mesoporous aluminium magnesium oxide composites.* Environmental Science: Nano, 2016. **3**(1): p. 94-106.

132. Goswami, A., P. Raul, and M. Purkait, *Arsenic adsorption using copper (II) oxide nanoparticles.* Chemical Engineering Research and Design, 2012. **90**(9): p. 1387-1396.

133. Brockgreitens, J.W., F. Heidari, and A. Abbas, *Versatile Process for the Preparation of Nanocomposite Sorbents: Phosphorus and Arsenic Removal.* Environmental science & technology, 2020. **54**(14): p. 9034-9043.

134. Priyadarshni, N., P. Nath, and N. Chanda, *Sustainable removal of arsenate, arsenite and bacterial contamination from water using biochar stabilized iron and copper oxide nanoparticles and associated mechanism of the remediation process.* Journal of Water Process Engineering, 2020. **37**: p. 101495.

135. Cao, A.-m., et al., *Hierarchical nanostructured copper oxide and its application in arsenic removal.* The journal of physical chemistry C, 2007. **111**(50): p. 18624-18628.

136. Browne, M.A., et al., *Accumulation of microplastic on shorelines woldwide: sources and sinks.* Environmental science & technology, 2011. **45**(21): p. 9175-9179.

137. Li, J., K. Zhang, and H. Zhang, *Adsorption of antibiotics on microplastics.* Environmental Pollution, 2018. **237**: p. 460-467.

138. Ivleva, N.P., A.C. Wiesheu, and R. Niessner, *Microplastic in aquatic ecosystems.* Angewandte Chemie International Edition, 2017. **56**(7): p. 1720-1739.

139. McCormick, A.R., et al., *Microplastic in surface waters of urban rivers: concentration, sources, and associated bacterial assemblages.* Ecosphere, 2016. **7**(11): p. e01556.

140. Schymanski, D., et al., *Analysis of microplastics in water by micro-Raman spectroscopy: release of plastic particles from different packaging into mineral water.* Water Research, 2018. **129**: p. 154-162.

141. Dris, R., et al., *Synthetic fibers in atmospheric fallout: a source of microplastics in the environment?* Marine pollution bulletin, 2016. **104**(1-2): p. 290-293.

142. Eriksen, M., et al., *Plastic pollution in the world's oceans: more than 5 trillion plastic pieces weighing over 250,000 tons afloat at sea.* PloS one, 2014. **9**(12): p. e111913.

143. Jambeck, J.R., et al., *Plastic waste inputs from land into the ocean.* Science, 2015. **347**(6223): p. 768-771.

144. Wang, X., et al., *Polystyrene microplastics impaired the feeding and swimming behavior of mysid shrimp Neomysis japonica.* Marine pollution bulletin, 2020. **150**: p. 110660.

145. Cózar, A., et al., *Plastic debris in the open ocean.* Proceedings of the National Academy of Sciences, 2014. **111**(28): p. 10239-10244.

146. Cole, M., *A novel method for preparing microplastic fibers.* Scientific reports, 2016. **6**: p. 34519.

147. Kosuth, M., S.A. Mason, and E.V. Wattenberg, *Anthropogenic contamination of tap water, beer, and sea salt.* PloS one, 2018. **13**(4).

148. Koelmans, A.A., et al., *Microplastics in freshwaters and drinking water: Critical review and assessment of data quality.* Water research, 2019. **155**: p. 410-422.

149. Cole, M., et al., *Microplastic ingestion by zooplankton.* Environmental science & technology, 2013. **47**(12): p. 6646-6655.

150. Barboza, L.G.A., et al., *Marine microplastic debris: An emerging issue for food security, food safety and human health.* Marine pollution bulletin, 2018. **133**: p. 336-348.

151. Hüffer, T. and T. Hofmann, *Sorption of non-polar organic compounds by micro-sized plastic particles in aqueous solution.* Environmental pollution, 2016. **214**: p. 194-201.

152. Hidalgo-Ruz, V., et al., *Microplastics in the marine environment: a review of the methods used for identification and quantification.* Environmental science & technology, 2012. **46**(6): p. 3060-3075.

153. Fok, L., et al., *Size distribution of stranded small plastic debris on the coast of Guangdong, South China.* Environmental Pollution, 2017. **220**: p. 407-412.

154. Erni-Cassola, G., et al., *Lost, but found with Nile Red: a novel method for detecting and quantifying small microplastics (1 mm to 20 μm) in environmental samples.* Environmental science & technology, 2017. **51**(23): p. 13641-13648.

155. Jang, M., et al., *Formation of microplastics by polychaetes (Marphysa sanguinea) inhabiting expanded polystyrene marine debris.* Marine pollution bulletin, 2018. **131**: p. 365-369.

156. Zhou, W., et al., *Fine polystyrene microplastics render immune responses more vulnerable to two veterinary antibiotics in a bivalve species.* Marine Pollution Bulletin, 2021. **164**: p. 111995.

157. Watts, A.J., et al., *Ingestion of plastic microfibers by the crab Carcinus maenas and its effect on food consumption and energy balance.* Environmental Science & Technology, 2015. **49**(24): p. 14597-14604.

158. Tănase, I.G., et al., *Infrared spectroscopy in qualitative analysis of laser printer and photocopy toner on questioned documents.* Instrumentation Science and Technology, 2009. **37**(1): p. 30-39.

159. Merrill, R.A., E.G. Bartick, and J.H. Taylor III, *Forensic discrimination of photocopy and printer toners I. The development of an infrared spectral library.* Analytical and bioanalytical chemistry, 2003. **376**(8): p. 1272-1278.

160. Kühn, S., et al., *Marine microplastic: Preparation of relevant test materials for laboratory assessment of ecosystem impacts.* Chemosphere, 2018. **213**: p. 103-113.

161. Dobretsov, K., S. Stolyar, and A. Lopatin, *Magnetic nanoparticles: a new tool for antibiotic delivery to sinonasal tissues. Results of preliminary studies.* Acta Otorhinolaryngologica Italica, 2015. **35**(2): p. 97.

162. Coppock, R.L., et al., *A small-scale, portable method for extracting microplastics from marine sediments.* Environmental Pollution, 2017. **230**: p. 829-837.